Wen Chen

Zhuo-Jia Fu

C.S. Chen

Recent Advances in Radial Basis Function Collocation Methods

Springer

SpringerBriefs in Applied Sciences and Technology

Wen Chen · Zhuo-Jia Fu · C. S. Chen

Recent Advances in Radial Basis Function Collocation Methods

Wen Chen
College of Mechanics and Materials
Hohai University
Nanjing
People's Republic of China

C. S. Chen
University of Southern Mississippi
Hattiesburg
USA

Zhuo-Jia Fu
College of Mechanics and Materials
Hohai University
Nanjing
People's Republic of China

Preface

Function approximation and interpolation play an essential role in most fields of computational sciences and engineering, such as data processing and numerical solution of partial differential equations (PDEs), in which the interpolation basis function is a key component. The traditional basis functions are mostly coordinate functions, such as polynomial and trigonometric functions, which are computationally expensive in dealing with high-dimensional problems due to their dependency on geometric complexity. Instead, radial basis functions (RBFs) are constructed in terms of a one-dimension distance variable, irrespective of dimensionality of problems, and appear to have a clear edge over the traditional polynomial basis functions.

RBFs were originally introduced in the early 1970s to multivariate scattered data approximations and function interpolations. Now, it is broadly employed in the neural network and machine learning, multivariate scattered data processing, and in the recent two decades, the fast emerging applications in numerical PDEs. Notably, in contrast to the traditional meshed-based methods such as finite difference, finite element, and boundary element methods, the RBF collocation methods are mathematically simple and truly meshless, which avoid troublesome mesh generation for high-dimensional problems involving irregular or moving boundary. In general, the RBF collocation methods can be classified into domain- and boundary-type categories. For instance, the Kansa method and its variants are of a classical domain-type scheme, while the boundary-type RBF collocation methods are usually involved in the fundamental solutions or general solutions of the governing equation of interest, such as the method of fundamental solutions, boundary knot method, regularized meshless method, singular boundary method, and boundary particle method, just to mention a few. Hence, the basis function of the boundary-type RBF collocation methods is basically satisfied by the governed equation while the domain-type RBF collocation methods are not.

Despite excellent performances in some numerical experiments, the reported work has been mostly based on intuitions and the RBF methods still encounter some notable challenges, such as time-consuming evaluation of large dense RBF interpolation matrix, the efficient solution of such large-scale matrix equations, and constructing efficient and reliable basis functions.

This book is aimed at making a comprehensive survey of the latest advances on radial basis function (RBF) collocation methods. The content of the book is focused on basic concepts, numerical algorithms, and engineering applications. This book is intended to provide a wide selection of RBF collocation methods for scientists, engineers, and graduate students who are interest to apply the state-of-the-art RBF meshless techniques for solving real-life problems.

Some useful supplements and computer codes, based on the RBF collocation methods described in this monograph, are provided from the following websites:

http://em.hhu.edu.cn/chenwen/html/distance.htm
http://em.hhu.edu.cn/ccms/fuzj/rbfe.html
http://em.hhu.edu.cn/ccms/fuzj/BPM.htm.

June 2013   Wen Chen
                                                                                            Zhuo-Jia Fu
                                                                                            C. S. Chen

Acknowledgments

Contents

Chapter 1
Introduction

Abstract Radial basis functions (RBFs) are constructed in terms of one-dimensional distance variable and appear to have certain advantages over the traditional coordinates-based functions. In contrast to the traditional meshed-based methods, the RBF collocation methods are mathematically simple and truly meshless, which avoid troublesome mesh generation for high-dimensional problems involving irregular or moving boundary. This opening chapter begins with the introduction to RBF history and its applications in numerical solution of partial differential equations and then gives a general overview of the book.

Keywords Radial basis functions · Collocation method · Meshless · Partial differential equation

The functions expressed in the distance variable are usually termed as radial basis functions (RBFs) in the literature. The strengths of the RBFs are easy-to-implement and independent of dimensionality and geometric complicity. In recent decades, various RBF-based methods have gained fast growing attention from a broad range of scientific computing and engineering applications, such as multivariate scattered data processing [1], numerical solutions of partial differential equations (PDEs), neural networks [2], and machine learning [3, 4], just to mention a few. This book focuses on the latest advances of the RBF collocation solution of PDEs, which has become a hot research topic since the early 1990s.

The history of RBFs goes back to 1971. Hardy [5] innovated probably the most famous RBF, multi-quadrics (MQ) function, to deal with surface fitting on topography and irregular surfaces, and later considered the MQ as a consistent solution of biharmonic solution [6] to give a physical interpretation of its prowess. In 1975, Duchon [7] proposed another famous RBF, thin-plate splines (TPS), by employing the minimum bending energy theory of the surface of a thin plate. In 1982, Franke [8] extensively tested 29 different algorithms on the typical benchmark function interpolation problems, and ranked the MQ-RBF and TPS-RBF as two of the best candidates based on the following criteria: timing, storage, accuracy, visual pleasantness of the surface, and ease of implementation. Since then,

the RBFs have become popular in the scientific computing community, such as computer graphics, data processing [9], and economics [10].

In 1990, Kansa [11, 12] first developed an RBF collocation scheme for solving PDEs of elliptic, parabolic, and hyperbolic types, in particular, using the MQ. The methodology is now often called the Kansa method. This pioneering work kicks off a research boom in the RBFs and their applications to numerical PDEs. The Kansa method is meshless and has distinct advantages compared with the classical methods, such as superior convergence, integration-free, and easy implementation.

It is interesting to point out that, prior to Kansa's pioneer work, Nardini and Brebbia [13] in the early 1980s, without knowing the RBFs, applied the function $1 + r$, an ad hoc RBF, as the basis function in the dual reciprocity method (DRM) for effectively eliminating domain integral in the context of the boundary element methods (BEM). This original work gives rise to currently popular dual reciprocity BEM (DR-BEM).

On the other hand, the method of fundamental solutions (MFS) was first proposed by Kupradze and Aleksidze [14], also known as the regular BEM, the superposition method [15], desingularized method [16], the charge simulation method [17], etc. The MFS uses the fundamental solutions of the governing equation of interest as the basis functions. It is noted that fundamental solutions of radially invariant differential operators, like the Laplace or the Helmholtz operator, have radial form with respect to origin and appear like the RBFs. Thus, we can consider the fundamental solutions as a special type of the RBFs. Unlike the Kansa method, the MFS only requires the discretization at boundary nodes to solve the homogeneous problems. Hence the MFS is classified as a boundary-type RBF collocation method.

For nonhomogeneous problems, the MFS should be combined with additional techniques to evaluate the particular solution, i.e., Monte Carlo method [18], radial integration method [19], dual reciprocity method (DRM) [20], and multiple reciprocity method (MRM) [21], and so on. In the past decade, the DRM and the MRM have emerged as two promising techniques to handle nonhomogeneous term. For instance, the so-called DR-BEM and MR-BEM are very popular in the BEM community.

Being meshless and dimensionality-independent, quite a few RBF-based schemes for numerical solutions of PDEs have been developed in the last two decades. In contrast to the traditional meshed-based methods such as finite difference, finite element, and boundary element methods, the RBF collocation methods are mathematically very simple to implement and truly meshless, which avoid troublesome mesh generation for high-dimensional problems involving irregular or moving boundary. In general, the RBF-based methods can be classified into domain-type and boundary-type categories, such as the above-mentioned Kansa method and the MFS.

Despite numerous successful applications in a wide range of fields, the traditional RBFs still encounter some disadvantages compared with the other numerical techniques. In implementation, the construction and the use of efficient and stable

distance functions are often intuitive and largely based on experiences. For instance, although the MQ enjoys the reputation of spectral accuracy, the determination of its optimal shape parameter is often problem-dependent and remains an open issue, and no mature mathematical theory and methodology are so far available for its applications to various problems. The compactly supported RBFs (CS-RBFs) are a recent class of potentially important RBFs. Although in theory the CS-RBFs can result in a sparse interpolation matrix, their lower order of accuracy causes some concern to its practical use. Recently, the Green second identity was found to be a powerful alternative tool to create and analyze the kernel-based RBFs. In addition, one can find several books [22–24] on the mathematical analysis of the RBFs.

In the recent two decades, the RBF collocation methods have gained considerable attention in engineering and applied mathematics. Based on the above-mentioned pioneer works, various improved RBF collocation methods have been proposed and applied to scientific computing and engineering simulation. This book makes the first attempt to survey the latest advances on RBF collocation methods for numerical solutions of PDEs. In Chap. 2, we start with an introduction of traditional RBFs, such as globally supported RBFs and compactly-supported RBFs. Following this, several operator-dependent RBFs, such as fundamental solutions, general solutions, harmonic functions, and particular solutions, are presented. After that, based on the second Green identity, the kernel RBFs are introduced to construct the appropriate problem-dependent RBFs. In Chap. 3, the basic procedure of the Kansa method is described in detail, followed by its improved formulations, such as the Hermite collocation method, the modified Kansa method, the method of particular solutions, the method of approximate particular solutions, and the localized RBF methods. In Chap. 4 we introduce the basic concepts of the method of fundamental solutions and the other novel boundary-type RBF collocation schemes. The latter ones are presented to avoid the fictitious boundary outside the physical domain, a perplexing drawback of the MFS. Such new techniques include the boundary knot method, the regularized meshless method, the singular boundary method, just to mention a few here. To evaluate the particular solution in the boundary-type RBF collocation methods, the recursive composite multiple reciprocity method (RC-MRM) is introduced for solving nonhomogeneous problems. The RC-MRM is an improved MRM and has great flexibility to handle a variety of nonhomogeneous terms without requiring inner nodes. In the conclusion, Chap. 5 discusses some open issues and perspectives on RBF collocation methods.

At the end of this introduction we would like to remind readers that everything presented here is the result of a selection, not comprehensive, of course, from our personal point of view. It is inevitable that some relevant materials will be left out as a consequence.

References

1. A. Iske, Scattered data modelling using radial basis functions. In: Tutorials on Multiresolution in Geometric Modelling, eds. by A. Iske, E. Quak, M.S. Floater (Springer-Verlag, Heidelberg, 2002), pp. 205–242
2. S. Chen, C.F.N. Cowan, P.M. Grant, Orthogonal least-squares learning algorithm for radial basis function networks. IEEE Trans. Neural Netw. **2**(2), 302–309 (1991)
3. C. Cortes, V. Vapnik, Support-vector networks. Mach. Learn. **20**(3), 273–297 (1995)
4. C.J.C. Burges, A tutorial on support vector machines for pattern recognition. Data Min. Knowl. Disc. **2**(2), 121–167 (1998)
5. R.L. Hardy, Multiquadric equations of topography and other irregular surfaces. J. Geophys. Res. **76**, 1905–1915 (1971)
6. R.L. Hardy, Theory and applications of the multiquadric-biharmonic method 20 years of discovery 1968–1988. Comput. Math. Appl. **19**(8–9), 163–208 (1990)
7. J. Duchon, Splines minimizing rotation-invariant semi-norms in Sobolev spaces, in constructive theory of functions of several variables (Springer, Berlin, 1977), pp. 85–100
8. R. Franke, Scattered data interpolation: tests of some method. Math. Comput. **38**(157), 181–200 (1982)
9. B. Zitova, J. Flusser, Image registration methods: A survey. Image Vis. Comput. **21**(11), 977–1000 (2003)
10. C.C. Tsai, D.L. Young, J.H. Chiang, D.C. Lo, The method of fundamental solutions for solving options pricing models. Appl. Math. Comput. **181**(1), 390–401 (2006)
11. E.J. Kansa, Multiquadrics–a scattered data approximation scheme with applications to computational fluid-dynamics–II solutions to parabolic, hyperbolic and elliptic partial differential equations. Comput. Math. Appl. **19**(8–9), 147–161 (1990)
12. E.J. Kansa, Multiquadrics–a scattered data approximation scheme with applications to computational fluid-dynamics–I surface approximations and partial derivative estimates. Comput. Math. Appl. **19**(8–9), 127–145 (1990)
13. D. Nardini, C.A. Brebbia, A new approach to free vibration analysis using boundary elements. Appl. Math. Model. **7**(3), 157–162 (1983)
14. V.D. Kupradze, M.A. Aleksidze, The method of functional equations for the approximate solution of certain boundary value problems. USSR Comput. Math. Math. Phys. **4**(4), 82–126 (1964)
15. G.H. Koopmann, L. Song, J.B. Fahnline, A method for computing acoustic fields based on the principle of wave superposition. J. Acoust. Soc. Am. **86**(6), 2433–2438 (1989)
16. C. Yusong, W.S. William, F.B. Robert, Three-dimensional desingularized boundary integral methods for potential problems. Int. J. Numer. Meth. Fluids **12**(8), 785–803 (1991)
17. K. Amano, A charge simulation method for the numerical conformal mapping of interior, exterior and doubly-connected domains. J. Comput. Appl. Math. **53**(3), 353–370 (1994)
18. C.S. Chen, M.A. Golberg, Y.C. Hon, The method of fundamental solutions and quasi-Monte-Carlo method for diffusion equations. Int. J. Numer. Meth. Eng. **43**(8), 1421–1435 (1998)
19. X.W. Gao, A meshless BEM for isotropic heat conduction problems with heat generation and spatially varying conductivity. Int. J. Numer. Meth. Eng. **66**(9), 1411–1431 (2006)
20. P.W. Partridge, C.A. Brebbia, L.C. Wrobel, The dual reciprocity boundary element method (Computational Mechanics Publications, Southampton, 1992)
21. A.J. Nowak, P.W. Partridge, Comparison of the dual reciprocity and the multiple reciprocity methods. Eng. Anal. Boundary Elem. **10**(2), 155–160 (1992)
22. M.D. Buhmann, Radial basis functions, theory and implementations (Cambridge University Press, New York, 2003)
23. G.E. Fasshauer, Meshfree approximation methods with MATLAB (World Scientific Publishers, Singapore, 2007)
24. C.S. Chen , Y.C. Hon, R.S. Schaback, Radial basis functions with scientific computation (Department of Mathematics, University of Southern Mississippi, Hattiesburg, 2007)

Chapter 2
Radial Basis Functions

Abstract The traditional basis functions in numerical PDEs are mostly coordinate functions, such as polynomial and trigonometric functions, which are computationally expensive in dealing with high dimensional problems due to their dependency on geometric complexity. Alternatively, radial basis functions (RBFs) are constructed in terms of one-dimensional distance variable irrespective of dimensionality of problems and appear to have a clear edge over the traditional basis functions directly in terms of coordinates. In the first part of this chapter, we introduces classical RBFs, such as globally-supported RBFs (Polyharmonic splines, Multiquadratics, Gaussian, etc.), and recently developed RBFs, such as compactly-supported RBFs. Following this, several problem-dependent RBFs, such as fundamental solutions, general solutions, harmonic functions, and particular solutions, are presented. Based on the second Green identity, we propose the kernel RBF-creating strategy to construct the appropriate RBFs.

The functions expressed in the Euclidean distance variable are usually termed as the radial basis functions (RBFs) in literatures. This is due to the fact that all such RBFs are radially isotropic due to the rotational invariant, and have become de facto the conventional distance functions of the widest use today. However, there do exist some quite important anisotropic and inhomogeneous RBFs, for instance, the spherical RBFs in handling geodesic problems and the so-called time–space RBFs. It is obvious that all these so-called anisotropic RBFs are not radially isotropic.

In terms of PDE kernel solutions, we have distance functions using three kinds of distance variables underlying (1) rotational invariant, (2) translation invariant, and (3) a scalar product of two vectors with the ridge function. The traditional rotational invariant RBFs do not cover the latter two. In addition, there are many other distance variables in the area of neural network and machine learning.

In most literature, the term "RBF" is, however, often simply used indiscriminatingly for the rotational and translation invariants distance variables and functions. Thus, this book extends the definition of RBF to general distance functions.

This chapter begins with an introduction of traditional RBFs for multivariate data interpolation, such as globally-supported RBFs and compactly-supported RBFs. In addition, several problem-dependent RBFs, such as fundamental solutions, general solutions, harmonic functions, and particular solutions, are also presented for the use in the following chapters. In the end, we introduce the kernel RBF-creating strategy.

2.1 Traditional RBFs

2.1.1 Globally-Supported RBFs

RBFs are mostly multivariate functions, and their values depend only on the distance from the origin, so that $\phi(\mathbf{x}) = \phi(r) \in R$, $\mathbf{x} \in R^n$, $r \in R$; or alternatively on the distance from a point of a given set $\{\mathbf{x}_j\}$, and $\phi(\mathbf{x} - \mathbf{x}_j) = \phi(r_j) \in R$. Any function ϕ satisfying the property $\phi(\mathbf{x}) = \phi(||\mathbf{x}||_2)$ is a radial function. The norm $r_j = ||\mathbf{x} - \mathbf{x}_j||_2$ is usually the Euclidean distance. Certainly, the other distance functions [1] are also possible. Some commonly used globally-supported RBFs are shown in Table 2.1.

Our interest lies in the RBF interpolation of a continuous multivariate function, $f(\mathbf{x}), \mathbf{x} \in \Omega \subset R^n$, where Ω is a bounded domain. Given N interpolation function values $\{y_i\}_{i=1}^N \in R$ at data location $\{\mathbf{x}_i\}_{i=1}^N \in \Omega \subset R^n$, then $f(\mathbf{x})$ can be approximated by a linear combination of RBFs, namely,

$$f(\mathbf{x}) \approx \sum_{j=1}^N \alpha_j \phi\left(||\mathbf{x} - \mathbf{x}_j||_2 \right), \ \mathbf{x} \in \Omega, \tag{2.1}$$

Table 2.1 Commonly used globally-supported RBFs

RBFs	$\phi(\mathbf{x})$	CPD order (m)
Polyharmonic spline	$\begin{cases} r^{2k-1}, k \in \mathbb{N} \\ r^{2k} \ln(r), k \in \mathbb{N} \end{cases}$	$[k/2] + 1$
Thin plate splines (TPS)	$r^2 \ln(r)$	2
MQ	$(r^2 + c^2)^k, k > 0, k \notin \mathbb{N}$	$[k] + 1$
IMQ	$(r^2 + c^2)^{-k}, k > 0, k \notin \mathbb{N}$	0
Gaussian	$e^{-(r^2/c^2)}$	0

$[k]$ denotes the nearest integers less than or equal to k, and $\mathbb{N}$ the natural number, c a positive constant which is known as the shape parameter, and CPD denotes the m-order conditionally positive definite functions [2]

where $\{\alpha_j\}$ are the unknown coefficients to be determined. By the collocation method, we have

$$y_i = f(\mathbf{x}_i) = \sum_{j=1}^{N} \alpha_j \phi \left(\left\| \mathbf{x}_i - \mathbf{x}_j \right\|_2 \right), \ i = 1, \cdots, N. \tag{2.2}$$

The above linear system of equations can be expressed in the following matrix form

$$\mathbf{A}\alpha = \mathbf{b}, \tag{2.3}$$

in which $\boldsymbol{\alpha} = (\alpha_1, \alpha_2, \ldots, \alpha_N)^T$ is an unknown coefficient vector to be determined, $\mathbf{b} = (y_1, y_2, \ldots, y_N)^T$ is the right-hand side vector, and the RBF interpolation matrix is given by

$$\mathbf{A} = [\Phi_{ij}] = [\phi(\|\mathbf{x}_i - \mathbf{x}_j\|_2)]_{1 \le i,j \le N}. \tag{2.4}$$

However, some RBFs are conditionally positive definite functions as listed in Table 2.1, such as MQ and TPS. Hence polynomials are augmented to Eq. (2.1) to guarantee that the resultant interpolation matrix is invertible. Such a formulation is expressed as follows

$$f(\mathbf{x}) = \sum_{j=1}^{N} \alpha_j \phi(\|\mathbf{x} - \mathbf{x}_j\|_2) + \sum_{i=1}^{M} \alpha_{N+i} p_i(\mathbf{x}), \tag{2.5}$$

with constraints

$$\sum_{j=1}^{N} \alpha_j p_i(\mathbf{x}_j) = 0, \ i = 1, 2, \cdots, M, \tag{2.6}$$

in which $p_i \in \Pi_{m-1}, i = 1, 2, \cdots, M$, where Π_m represents the polynomial space that all polynomials of total degree less than m in n variables, $M = \begin{pmatrix} N + m - 1 \\ m - 1 \end{pmatrix}$.

Then, Eqs. (2.5) and (2.6) yield a matrix system of $(M + N) \times (M + N)$

$$\begin{bmatrix} \mathbf{A} & P \\ P^T & \mathbf{0} \end{bmatrix} [\boldsymbol{\alpha}] = \begin{bmatrix} \mathbf{b} \\ \mathbf{0} \end{bmatrix}. \tag{2.7}$$

To illustrate the stability and efficiency of the RBF interpolation, without loss of generality, we consider the following test functions on the 2D unit square domain

$$f_1 = f_a + f_b, \tag{2.8}$$

$$f_2 = \sin\left(\frac{\pi x}{6}\right) \sin\left(\frac{7\pi x}{4}\right) \cos\left(\frac{3\pi y}{4}\right) \cos\left(\frac{5\pi y}{4}\right), \tag{2.9}$$

Fig. 2.1 Profiles of test functions **a** Eq. (2.8), **b** Eq. (2.9)

where

$$f_a = \frac{3}{4}\exp\left(\frac{-(9x-2)^2}{4} - \frac{(9y-2)^2}{4}\right) + \frac{3}{4}\exp\left(\frac{-(9x+1)^2}{49} - \frac{(9y+1)^2}{10}\right), \quad (2.10)$$

$$f_b = \frac{1}{2}\exp\left(\frac{-(9x-7)^2}{4} - \frac{(9y-3)^2}{4}\right) - \frac{1}{5}\exp\left(-(9x-4)^2-(9y-7)^2\right). \quad (2.11)$$

Figure 2.1 shows the profiles of these two test functions. Note that f_1 is the well-known Franke's function [3]. We conduct numerical experiments via the MQ. This study defines the normalized root-mean-square error (Rerr) and the normalized maximum error (Mrerr) as

$$\text{Rerr} = \frac{1}{\max_{1 \le i \le \text{NT}} |f_e(\mathbf{x}_i)|} \sqrt{\frac{1}{\text{NT}} \sum_{i=1}^{\text{NT}} |f(\mathbf{x}_i) - f_e(\mathbf{x}_i)|^2}, \quad (2.12)$$

$$\text{Mrerr} = \frac{1}{\max_{1 \le i \le \text{NT}} |f_e(\mathbf{x}_i)|} \max_{1 \le i \le \text{NT}} |f(\mathbf{x}_i) - f_e(\mathbf{x}_i)|, \quad (2.13)$$

where $f_e(\mathbf{x}_i)$ and $f(\mathbf{x}_i)$ are the analytical and numerical solutions evaluated at $\mathbf{x}_i$, respectively, and $\text{NT} = 10,201$ is the total number of 101×101 uniformly distributed test points in a unit square domain.

In this study, we place the interpolation points with uniform spacing, h, for easy comparisons. From the numerical errors presented in Table 2.2, one can observe that

(a) The error decreases with the grid refinement.
(b) The condition number of RBF interpolation matrix increases with the grid refinement.
(c) The shape parameter c is very sensitive to the test functions and the grid size.

Table 2.2 Numerical errors using MQ RBF based on grid size $h = 0.1$ and $h = 0.05$

Functions	Grid size (h)	Optimal shape parameter (c)	Condition number	Mrerr	Rerr
f_1	0.1	0.16	3.4e + 05	1.2e−02	1.4e−03
f_1	0.05	0.31	3.8e + 14	2.8e−05	3.1e−06
f_2	0.1	1.16	3.2e + 17	8.5e−05	1.1e−05
f_2	0.05	0.78	6.6e + 19	3.4e−06	4.7e−07

Table 2.3 Error estimates of different RBFs with respect to grid size h

RBFs	$\phi(\mathbf{x})$	Error estimate
Polyharmonic spline	$\begin{cases} r^{2k-1}, k \in \mathbb{N} \\ r^{2k} \ln(r), k \in \mathbb{N} \end{cases}$	h^k
Thin plate splines (TPS)	$r^2 \ln(r)$	h^2
MQ	$(r^2 + c^2)^k, k > 0, k \notin \mathbb{N}$	$e^{-a/h}$
IMQ	$(r^2 + c^2)^{-k}, k > 0, k \notin \mathbb{N}$	$e^{-a/h}$
Gaussian	$e^{-(r^2/c^2)}$	$e^{-a \ln h/h}$

(d) The accuracy in function f_1, with the grid size $h = 0.1$, is poor because the grid is too coarse to perform a more accurate solution.

From the above numerical experiments, we observe that the numerical accuracy depends on the grid size, the shape parameter, the complexity of the given functions, and the other potential factors. Great efforts have been made to find the relationship between the RBF interpolation's accuracy and that of various influential factors [4–8]. Duchon [9], Madych and Nelson [10–12], Wu and Schaback [13], and Cheng [14] made contributions to estimate the error of RBF interpolation. Wendland [15] made a summary of these estimates for different RBFs with respect to grid size h, which is presented in Table 2.3.

Theoretical analysis and empirical formulas for RBF interpolation are also proposed in literature but remain underdeveloped. Based on Madych's theoretical analysis [16], the error estimates of MQ, IMQ, and Gaussian RBFs are made up of the product of two rival terms. Namely, one part grows exponentially, and the other decays exponentially as the shape parameter c increases

$$\varepsilon \sim O\left(e^{ac} \lambda^{c/h}\right), \, 0 < \lambda < 1, a > 0, \tag{2.14}$$

or

$$\varepsilon \sim O\left(e^{ac^2} \lambda^{c/h}\right), \, 0 < \lambda < 1, a > 0. \tag{2.15}$$

Huang et al. [6] proposed an empirical error estimate for the IMQ RBF

$$\varepsilon \sim O\left(e^{ac^{3/2}} \lambda^{c^{1/2}/h}\right), \, 0 < \lambda < 1, a > 0. \tag{2.16}$$

Following Madych's formula, Cheng [14] established the following estimate for the Gaussian RBF

$$\varepsilon \sim O\left(e^{ac^4}\lambda^{c/h}\right), \ 0 < \lambda < 1, a > 0. \tag{2.17}$$

From the above-mentioned error estimates, one can derive different explicit formulas for the optimal c. According to Eq. (2.15), the optimal c can be approximated by

$$c_{\mathrm{opt}} \sim O(-\ln\lambda/2ah). \tag{2.18}$$

Similar to Eq. (2.18), the optimal c for IMQ RBF in terms of Eq. (2.16) is

$$c_{\mathrm{opt}} \sim O(-\ln\lambda/3ah). \tag{2.19}$$

The optimal c for Gaussian RBF can also be obtained from Eq. (2.17)

$$c_{\mathrm{opt}} \sim O\left((-\ln\lambda)^{1/3}\Big/\left(2^{2/3}a^{1/3}h^{1/3}\right)\right). \tag{2.20}$$

In recent years, we have witnessed the continued efforts of many to establish the theory of evaluating the optimal shape parameter c in the MQ interpolation. However, such an explicit formula is only available in special cases. Consequently, numerically determining the optimal c proves to be essential. And numerical experiments find that the best c, via a numerical scheme, may not be theoretically optimal.

Since the condition number of the MQ interpolation matrix grows rapidly as c increases, the optimal c is the largest value at which it can be utilized before the instability of matrix calculation occurs due to the machine precision. We draw the following conclusions upon the above discussions.

Among the advantages of Globally-supported RBFs are

(a) Highly accurate and often converge exponentially.
(b) Easy to apply to high dimensional problems.
(c) Meshless in the approximation of multivariate scattered data, and easy to improve the numerical accuracy by adding more points around large gradient regions.

On the other hand, the downside is that the interpolation matrix is fully populated and ill-conditioned, and thus sensitive to shape parameter. As a result, it is computationally very expensive to apply the traditional RBF interpolation to large-scale problems.

Table 2.4 Wendland's CS-RBFs

Dimension	$\phi(\mathbf{x})$	Continuity of function
$d = 1$	$(1 - r)_+$	C^0
	$(1 - r)_+^3 (3r + 1)$	C^2
	$(1 - r)_+^5 (8r^2 + 5r + 1)$	C^4
$d = 2, 3$	$(1 - r)_+^2$	C^0
	$(1 - r)_+^4 (4r + 1)$	C^2
	$(1 - r)_+^6 (35r^2 + 18r + 3)$	C^4
	$(1 - r)_+^8 (32r^3 + 25r^2 + 8r + 1)$	C^6

2.1.2 Compactly-Supported RBFs

Following a similar methodology in the corrected reproducing kernel approximation [17], Wu [18] and Wendland [19] proposed a new type of RBFs to make the interpolation matrix sparse, which is defined as compactly-supported positive definite RBFs (CS-RBFs). The popular Wendland's CS-RBFs [19] are listed below in Table 2.4.

Note that the cut-off function $(r)_+$ is defined to be r if $0 \leq r \leq 1$ and to be zero elsewhere. Furthermore, another class of CS-RBFs constructed by Buhmann [20] is reminiscent of the popular thin plate splines. Three examples of these CS-RBFs are given below

$$\phi(\mathbf{x}) = \left(2r^4 \log(r) - 7r^4/2 + 16r^3/3 - 2r^2 + 1/6\right)_+, \mathbf{x} \in R^3, \qquad (2.21)$$

$$\phi(\mathbf{x}) = \left(112r^{9/2}/45 + 16r^{7/2}/3 - 7r^4 - 14r^2/15 + 1/9\right)_+, \mathbf{x} \in R^2, \qquad (2.22)$$

$$\phi(\mathbf{x}) = \left(1/18 - r^2 + 4r^3/9 + r^4/2 - 4r^3 \log(r)/3\right)_+, \mathbf{x} \in R^2. \qquad (2.23)$$

Wu employs convolution to construct another kind of CS-RBFs as shown in Table 2.5. Wu's functions can be derived by the following formula

$$\varphi_{k,s} = D^k(\varphi_s), d \leq 2k+1, \qquad (2.24)$$

where differential operator D is defined as

Table 2.5 Wu's CS-RBFs

k	$\varphi_{k,3}(\mathbf{x})$	Continuity of function
0	$(1 - r)_+^7 (5r^6 + 35r^5 + 101r^4 + 147r^3 + 101r^2 + 35r + 5)$	C^6
1	$(1 - r)_+^6 (5r^5 + 30r^4 + 72r^3 + 82r^2 + 36r + 6)$	C^4
2	$(1 - r)_+^5 (5r^4 + 25r^3 + 48r^2 + 40r + 8)$	C^2
3	$(1 - r)_+^4 (5r^3 + 20r^2 + 29r + 16)$	C^0

$$(D\varphi)(r) = -\varphi'(r)/r, r \geq 0, \tag{2.25}$$

and the strictly positive definite function $\varphi_s(r)$ is stated as

$$\varphi_s(r) = (\varphi * \varphi)(2r) = \int_{-\infty}^{\infty} \left(1 - t^2\right)_+^s \left(1 - (2r - t)^2\right)_+^s dt. \tag{2.26}$$

The CS-RBFs can result in a sparse banded interpolation matrix and effectively avoids the ill-conditioned and dense matrix in the classical RBF interpolation and consequently reduces computational costs. However, the discouraging lower order of accuracy causes a major impediment to its practical use. To overcome the ill-conditioned problems and reduce the computational costs without loss of accuracy, several alternative localized approaches have been proposed and will be introduced in Chap. 3.

2.2 Problem-Dependent RBFs

As the RBF collocation methods attract growing attention in the field of numerical PDEs in the recent two decades, various solutions of PDEs and their variants emerge to be a powerful approach in the construction of the problem-dependent RBFs. This section introduces several problem-dependent RBFs. Consider the following elliptic PDEs

$$\begin{aligned} \Re u &= f(\mathbf{x}), \ \mathbf{x} \in \Omega, \\ Bu &= g(\mathbf{x}), \ \mathbf{x} \in \Gamma, \end{aligned} \tag{2.27}$$

where $\Re$ and B denote the linear partial differential operator and boundary operators. $\Omega \subset R^n$ is a bounded domain, and Γ denotes its boundary.

2.2.1 Fundamental Solutions

The fundamental solutions of radially invariant differential operator have the radial form with respect to origin and are of a radial function. The fundamental solution ϕ_F satisfies the governing differential equation of interest

$$\Re\{\phi_F\} = -\delta_i, \tag{2.28}$$

where δ_i is the Dirac delta function.

The fundamental solutions of commonly used differential operators are listed in Table 2.6 [21], where Δ denotes the Laplace operator, ∇ the gradient operator, D the diffusivity coefficient, λ a real number known as the wave number, $\mathbf{v}$ and $\mathbf{r}$ the velocity vector and distance vector, $\mu = \sqrt{(|\mathbf{v}|/2D)^2 + \lambda/D}$, κ foundation stiffness,

Table 2.6 Fundamental solutions to commonly used differential operators of two and three dimensions

$\Re$	2D	3D
Δ	$\ln(r)/(2\pi)$	$1/(4\pi r)$
$\Delta + \lambda^2$	$Y_0(\lambda r)/(2\pi)$	$\cos \lambda r/(4\pi r)$
$\Delta - \lambda^2$	$K_0(\lambda r)/(2\pi)$	$e^{-\lambda r}/(4\pi r)$
$D\Delta + \mathbf{v} \bullet \nabla - \lambda^2$	$K_0(\mu r)e^{-\frac{\mathbf{v} \bullet r}{2D}}/(2\pi)$	$e^{-\mu r - \frac{\mathbf{v} \bullet r}{2D}}/(4\pi r)$
$\Delta^2 - \lambda^4$	$(Y_0(\lambda r) + K_0(\lambda r))/(2\pi)$	$\left(e^{-\lambda r} + \cos \lambda r\right)/(4\pi r)$
$\Delta^2 + \kappa^2$	$Kei(\sqrt{\kappa}r) + Ber(\sqrt{\kappa}r)$	$Kei_{3/2}(\sqrt{\kappa}r) + Ber_{3/2}(\sqrt{\kappa}r)$
$\Delta^2 - \lambda^2\Delta$	$(K_0(\lambda r) + \ln(r))/(2\pi\lambda^2)$	$\left(e^{-\lambda r} + 1\right)/(4\pi\lambda^2 r)$

and r the Euclidean norm between the point $\mathbf{x}$ and the origin. Y_0 and K_0 are the Bessel and modified Bessel functions of the second kind of order zero, respectively. We can see that the two Kelvin functions are the component functions of the fundamental solutions of the Winkler operator, where Kei represents the modified Kelvin functions of the second kind, and Ber denotes the Kelvin functions of the first kind. It is worthy noting that the fundamental solutions to a differential operator may not be unique. For the Laplace operator, a constant may be included in its fundamental solution.

By utilizing Green second identity, the high-order fundamental solutions of the Laplace operator Δ^m [22] can be derived by

$$\phi_F^m(\mathbf{x}) = \begin{cases} \dfrac{r^{2m}}{2\pi}(C_m \ln r - B_m), & \mathbf{x} \in R^2 \\ \dfrac{1}{(2m)!}\dfrac{r^{2m-1}}{4\pi}, & \mathbf{x} \in R^3 \end{cases}, \tag{2.29}$$

where

$$C_0 = 1, \; B_0 = 0, \; C_{m+1} = \frac{C_m}{4(m+1)^2}, \; B_{m+1} = \frac{1}{4(m+1)^2}\left(\frac{C_m}{m+1} + B_m\right).$$

Itagaki [23] and Chen [24] derived the explicit expressions of high-order fundamental solutions of Helmholtz, modified Helmholtz, and steady convection–diffusion operators. The high-order fundamental solutions of Helmholtz-type operator $\left(\Delta + \lambda^2\right)^m$ [23, 24] are given by

$$\phi_F^m(\mathbf{x}) = A_m(\lambda r)^{m+1-n/2}Y_{m-1+n/2}(\lambda r), \quad \mathbf{x} \in R^n, \tag{2.30}$$

where $A_m = A_{m-1}/2m\lambda^2, A_0 = 1$, m is the order of operator of interest, and n denotes dimensionality.

The high-order fundamental solutions of modified Helmholtz-type operator $\left(\Delta - \lambda^2\right)^m$ [23, 24] are given by

$$\phi_F^m(\mathbf{x}) = A_m(\lambda r)^{m+1-n/2} K_{m-1+n/2}(\lambda r), \quad \mathbf{x} \in R^n. \tag{2.31}$$

The high-order fundamental solutions of modified convection–diffusion-type operator $\left(D\Delta + \mathbf{v} \bullet \nabla - \lambda^2\right)^m$ [24] are given by

$$\phi_F^m(\mathbf{x}) = A_m(\mu r)^{m+1-n/2} e^{-\frac{\mathbf{v} \bullet \mathbf{r}}{2D}} K_{m-1+n/2}(\mu r), \quad \mathbf{x} \in R^n. \tag{2.32}$$

Furthermore, the high-order composite operator is the product of different types of commonly used differential operators. For instance, the thin plate vibration operator is the product of the Laplace and the Helmholtz operators, and the Berger operator is a composite operator of the Laplace and the modified Helmholtz operators. And their fundamental solutions of orders are a sum of the solutions of the corresponding component operators. Recently, Chen [24] derived the high-order fundamental solutions of thin plate vibration, Berger plate, and Winkler plate. The high-order fundamental solutions of thin plate vibration-type operator $\left(\nabla^4 - \lambda^4\right)^m$ are given by

$$\phi_F^m(\mathbf{x}) = A_m(\lambda r)^{m+1-n/2} \left(Y_{m-1+n/2}(\lambda r) + K_{m-1+n/2}(\lambda r)\right), \quad \mathbf{x} \in R^n. \tag{2.33}$$

The high-order fundamental solutions of Berger plate-type operator $\left(\nabla^4 - \lambda^2\nabla^2\right)^m$ are given by

$$\phi_F^m(\mathbf{x}) = \begin{cases} \dfrac{r^{2m}}{2\pi}(C_m \ln r - B_m) + A_m(\lambda r)^m K_m(\lambda r), & \mathbf{x} \in R^2 \\ \dfrac{1}{(2m)!}\dfrac{r^{2m-1}}{4\pi} + A_m(\lambda r)^{m-1/2} K_{m-1/2}(\lambda r), & \mathbf{x} \in R^3 \end{cases}. \tag{2.34}$$

The high-order fundamental solutions of Winkler plate-type operator $\left(\nabla^4 + \kappa^2\right)^m$ are given by

$$\phi_F^m(\mathbf{x}) = A_m\left(\sqrt{\kappa}r\right)^{m+1-n/2} \left(\mathrm{Kei}_{n/2}\left(\sqrt{\kappa}r\right) + \mathrm{Ber}_{n/2}\left(\sqrt{\kappa}r\right)\right), \quad \mathbf{x} \in R^n, \tag{2.35}$$

where m is an odd-integer order of operator, and

$$\phi_F^m(\mathbf{x}) = A_m\left(\sqrt{\kappa}r\right)^{m+1-n/2} \left(\mathrm{Kei}_{n/2-1}\left(\sqrt{\kappa}r\right) + \mathrm{Ber}_{n/2-1}\left(\sqrt{\kappa}r\right)\right), \quad \mathbf{x} \in R^n, \tag{2.36}$$

where m is an even-integer order. Note that we cannot verify the high-order Winkler plate-type fundamental solutions for more than 5-dimensions ($n > 5$) because of the following reasons:

(a) Equations (2.35) and (2.36) are not applicable for the Winkler operator of more than 5-dimensions.
(b) The solutions of the Winkler operator of more than 5-dimensions do not exist.

Table 2.7 Nonsingular RBF general solutions to commonly used differential operators

$\Re$	2D	3D
Δ	/	/
$\Delta + \lambda^2$	$J_0(\lambda r)/(2\pi)$	$\sin(\lambda r)/(4\pi r)$
$\Delta - \lambda^2$	$I_0(\lambda r)/(2\pi)$	$\sinh(\lambda r)/(4\pi r)$
$D\Delta + \mathbf{v} \bullet \nabla - \lambda^2$	$I_0(\mu r)e^{-\frac{\mathbf{v}\cdot\mathbf{r}}{2D}}/(2\pi)$	$e^{-\frac{\mathbf{v}\cdot\mathbf{r}}{2D}}\sinh(\mu r)/(4\pi r)$
$\nabla^4 - \lambda^4$	$(J_0(\lambda r) + I_0(\lambda r))/(2\pi)$	$(\sin(\lambda r) + \sinh(\lambda r))/(4\pi r)$
$\nabla^4 + \kappa^2$	$\mathrm{Bei}(\sqrt{\kappa}r) + \mathrm{Ber}(\sqrt{\kappa}r)$	$\mathrm{Bei}_{3/2}(\sqrt{\kappa}r) + \mathrm{Ber}_{3/2}(\sqrt{\kappa}r)$
$\nabla^4 - \lambda^2\nabla^2$	$(I_0(\lambda r) + 1)/(2\pi\lambda^2)$	$(\sinh(\lambda r) + r)/(4\pi\lambda^2 r)$

2.2.2 General Solutions

It is well known that the fundamental solutions have singularities at origin. Thereby, the special treatment of these singularities should be handled numerically. In contrast, Chen [24, 25] proposed the general solutions ϕ_G, which are nonsingular radial functions satisfying the corresponding governing differential equations in the manner

$$\Re\{\phi_G\} = 0. \tag{2.37}$$

It is seen from Eq. (2.37) that the general solutions at origin have a bounded value rather than infinity as in the fundamental solution case. The general solutions of differential operator differ essentially from the corresponding fundamental solutions in that the former are nonsingular, while the latter are singular at origin.

Similarly, the nonsingular general solutions are also one kind of radial functions. Some useful general solutions [24] are listed in Table 2.7, where I_0 and J_0 represent the Bessel and modified Bessel functions of the first kind of order zero, respectively, and two Kelvin functions are the component functions of the general solutions of the Winkler operator, *Ber* and *Bei* denote the Kelvin functions of the first and second kind, respectively. It is noted that the RBF general solution of Laplace equation is a constant and is not suitable as a basis function. This issue will be further discussed in the next section.

We can also obtain the high-order RBF general solutions of Helmholtz-type operator $(\Delta + \lambda^2)^m$ [24]

$$\phi_G^m(\mathbf{x}) = A_m(\lambda r)^{m+1-n/2}J_{m-1+n/2}(\lambda r), \quad \mathbf{x} \in R^n, \tag{2.38}$$

where $A_m = A_{m-1}/2m\lambda^2, A_0 = 1$, m denotes the order of operator, and n represents the dimensionality.

The high-order RBF general solutions of modified Helmholtz-type operator $(\Delta - \lambda^2)^m$ [24] are given by

$$\phi_G^m(\mathbf{x}) = A_m(\lambda r)^{m+1-n/2}I_{m-1+n/2}(\lambda r), \quad \mathbf{x} \in R^n. \tag{2.39}$$

The high-order RBF general solutions of modified convection–diffusion-type operator $\left(D\Delta + \mathbf{v} \bullet \nabla - \lambda^2\right)^m$ [24] are represented by

$$\phi_G^m(\mathbf{x}) = A_m(\mu r)^{m+1-n/2} e^{-\frac{\mathbf{v} \bullet r}{2D}} I_{m-1+n/2}(\mu r), \quad \mathbf{x} \in R^n. \tag{2.40}$$

The high-order RBF general solutions of thin plate vibration-type operator $\left(\nabla^4 - \lambda^4\right)^m$ are expressed as

$$\phi_G^m(\mathbf{x}) = A_m(\lambda r)^{m+1-n/2}\left(J_{m-1+n/2}(\lambda r) + I_{m-1+n/2}(\lambda r)\right), \quad \mathbf{x} \in R^n. \tag{2.41}$$

The high-order RBF general solutions of Berger plate-type operator $\left(\nabla^4 - \lambda^2\nabla^2\right)^m$ are stated as

$$\phi_G^m(\mathbf{x}) = A_m + A_m(\lambda r)^{m+1-n/2} I_{m-1+n/2}(\lambda r), \quad \mathbf{x} \in R^n. \tag{2.42}$$

The high-order RBF general solutions of Winkler plate-type operator $\left(\nabla^4 + \kappa^2\right)^m$ are given by

$$\phi_G^m(\mathbf{x}) = A_m\left(\sqrt{\kappa}r\right)^{m+1-n/2}\left(\mathrm{Bei}_{n/2}\left(\sqrt{\kappa}r\right) + \mathrm{Ber}_{n/2}\left(\sqrt{\kappa}r\right)\right), \quad n = 2, 3, \tag{2.43}$$

where the order m of operator is an odd integer, and

$$\phi_G^m(\mathbf{x}) = A_m\left(\sqrt{\kappa}r\right)^{m+1-n/2}\left(\mathrm{Bei}_{n/2-1}\left(\sqrt{\kappa}r\right) + \mathrm{Ber}_{n/2-1}\left(\sqrt{\kappa}r\right)\right), \quad n = 2, 3, \tag{2.44}$$

where m is an even integer. It should also be mentioned that Eqs. (2.43) and (2.44) do not establish for the Winkler operators of more than 3-dimensions. It remains an open issue to find such high-order general solutions.

2.2.3 Harmonic Functions

As mentioned earlier, the general solution of Laplace equation is a constant rather than a RBF and is not suitable for function interpolation and numerical PDEs. Chen [26] made an attempt to use the nonsingular general solutions of Helmholtz-like equation with a small characteristic parameter to replace the constant general solution of Laplace equation. However, the characteristic parameter such as the wave number should generally be small to get accurate solution. It is somewhat sensitive to the domain geometry of problem of interest. And it is not easy to determine its optimal value as the shape parameter of the MQ.

On the other hand, Hon and Wu [27] applied a translate-invariant 2D harmonic function as the basis function to devise a simple and efficient numerical scheme for solving 2D Laplace problems. Hon and Wu's harmonic function of the two-dimensional Laplace equation $\Delta\left(H_2^0(x_i, y_i)\right) = 0$ is given by

$$H_2^0(x_i, y_i) = \exp(-c(x_{ik}^2 - y_{ik}^2))\cos(2cx_{ik}y_{ik}), \tag{2.45}$$

where c is the shape parameter and is dependent on problem of interest, and $x_{ik} = x_i - x_k$, $y_{ik} = y_i - y_k$.

Compared with the singular fundamental solutions, the harmonic solutions are nonsingular. Thus, it is appealing to choose harmonic functions, which avoid the singularities of Laplace fundamental solution. However, this comes at a price one has to pay that their shape parameter c has to be determined as the MQ shape parameter [28]. The performances such as accuracy and convergence rate of the harmonic functions are largely dependent on the problem-dependent parameter c.

The harmonic functions are guaranteed invertibility if the solution is in the bounded domain or decays to zero at infinite for the unbounded domain. As quoted from Hon and Wu [27], "The result in this paper is given for bounded functions which are harmonic on the upper half plane. This ensures that the functions can be expressed in the form of Poisson integrals so that the solution can be determined by its given values on the boundary. The numerical computations, however, indicate that the result is also valid for unbounded functions (but bounded on the boundary) which are harmonic on the upper half plane."

High-order polyharmonic solutions

Based on Hon and Wu's work [27], the high-order polyharmonic functions in two- and three- dimensional problems are constructed by Chen and Fu [29, 30]. The m-order polyharmonic functions of $\Delta^m \big(H_2^m(x_i, y_i) \big) = 0$ in two-dimension are represented as

$$H_2^m(x_i, y_i) = r^{2m} \exp\big(-c\big(x_{ik}^2 - y_{ik}^2\big)\big) \cos(2cx_{ik}y_{ik}). \tag{2.46}$$

Three-dimensional harmonic solutions

The harmonic function of three-dimensional Laplace equation $\Delta\big(H_3^0(x_i, y_i, z_i)\big) = 0$ can be intuitively obtained as

$$\begin{aligned}
H_3^0(x_i, y_i, z_i) &= \exp\big(-c\big(x_{ik}^2 - y_{ik}^2\big)\big) \cos(2cx_{ik}y_{ik}) + \\
&\quad \exp\big(-c\big(y_{ik}^2 - z_{ik}^2\big)\big) \cos(2cy_{ik}z_{ik}) + \exp\big(-c\big(z_{ik}^2 - x_{ik}^2\big)\big) \cos(2cz_{ik}x_{ik})
\end{aligned} \tag{2.47}$$

Similarly, the m-order polyharmonic functions of $\Delta^m \big(H_3^m(x_i, y_i, z_i) \big) = 0$ in three dimension are represented as

$$\begin{aligned}
H_3^m(x_i, y_i, z_i) &= r^{2m} \big\{ \exp\big(-c\big(x_{ik}^2 - y_{ik}^2\big)\big) \cos(2cx_{ik}y_{ik}) + \\
&\quad \exp\big(-c\big(y_{ik}^2 - z_{ik}^2\big)\big) \cos(2cy_{ik}z_{ik}) + \exp\big(-c\big(z_{ik}^2 - x_{ik}^2\big)\big) \cos(2cz_{ik}x_{ik}) \big\}
\end{aligned} \tag{2.48}$$

2.2.4 Particular Solutions

Another important type of problem-dependent RBFs are particular solutions. A splitting approach [31] is used to split the solution of the nonhomogeneous governing Eq. (2.27) into homogeneous solution and particular solution. The key issue is to construct the particular solutions $\Phi(r)$ to satisfy the following equation

$$\Re\Phi(r) = \phi(r). \tag{2.49}$$

Typically, there are two approaches to construct the particular solutions $\Phi(r)$. The first approach is utilizing the above-mentioned RBFs as the particular solutions $\Phi(r)$, then deriving the basis functions $\phi(r)$ from Eq. (2.49) by differentiation process. This scheme is easy to derive the particular solutions, however, such RBFs $\phi(r)$ may not remain in the positive definite property to guarantee the matrix invertibility, which depends on the governing differential operator $\Re$.

The second approach is utilizing the existing RBFs discussed before as the functions $\phi(r)$, then deriving the particular solutions $\Phi(r)$ from Eq. (2.49) by reverse differentiation process. The deriving process in this strategy is far more challenging than the former one. Nevertheless, the corresponding derived particular solutions $\Phi(r)$ inherit the positive definite property from the existing RBFs. In virtue of this excellent property, various particular solutions have been derived by the second approach. Chen and Rashed [32] were the first to extend the derivation of TPS-based solutions for Helmholtz-type operators. Muleshkov et al. [33] and Cheng [34] further derived the particular solutions by Polyharmonic splines. Recently, Muleshkov and Golberg [35], Chen et al. [36], and Tsai et al. [37] extended the derivation to more composite differential operators. We list some particular solutions $\Phi(r)$ for the traditional RBFs $\phi(r)$ [38] as follows:

(a) The corresponding particular solutions as a prior to satisfy the differential equation $\Delta\Phi(r) = \phi(r)$.

For MQ, $\phi(r) = \sqrt{r^2 + c^2}$, we have the following results

$$\Phi(r) = \frac{4c^2 + r^2}{9}\sqrt{c^2 + r^2} - \frac{c^3}{3}\ln\left(c + \sqrt{c^2 + r^2}\right) \tag{2.50}$$

in R^2, and

$$\Phi(r) = \begin{cases} \frac{5c^2 + 2r^2}{24}\sqrt{c^2 + r^2} + \frac{c^4\ln\left(r + \sqrt{c^2 + r^2}\right)}{8r} - \frac{c^3}{3} - \frac{c^4\ln(c)}{8r}, r \neq 0 \\ 0, r = 0 \end{cases} \tag{2.51}$$

in R^3.

For IMQ, $\phi(r) = 1/\sqrt{r^2 + c^2}$, we obtain

$$\Phi(r) = \sqrt{c^2 + r^2} - c\ln\left(c + \sqrt{c^2 + r^2}\right) \tag{2.52}$$

in R^2, and

$$\Phi(r) = \begin{cases} \frac{\sqrt{c^2 + r^2}}{2} + \frac{c^2}{2r}\ln\left(\frac{r + \sqrt{c^2 + r^2}}{c}\right) - \frac{c}{2}, r \neq 0 \\ 0, r = 0 \end{cases} \tag{2.53}$$

in R^3.

For Polyharmonic splines $\phi(r) = r^k\ln(r), k = 2, 4, 6, \ldots$, in R^2, we derive

$$\Phi(r) = \frac{r^{k+2}\ln(r)}{4(k/2+1)^2} - \frac{r^{k+2}}{4(k/2+1)^3}, \tag{2.54}$$

which can be regarded as high-order fundamental solutions of Laplace operator.

For Polyharmonic splines, $\phi(r) = r^k, k = 1, 3, 5, \ldots$, in R^3, we get

$$\Phi(r) = \frac{r^{k+3}}{(k+3)(k+2)}. \tag{2.55}$$

(b) The corresponding particular solutions as a prior to satisfy the differential equation $(\Delta + \lambda^2)\Phi(r) = \phi(r)$.

For TPS, $\phi(r) = r^2\ln(r)$ in R^2, we have the following results

$$\Phi(r) = \begin{cases} -\frac{r^2\ln(r)}{\lambda^2} + \frac{4\ln(r)+4}{\lambda^4} + \frac{4}{\lambda^4}K_0(\lambda r), r \neq 0 \\ \frac{4}{\lambda^4} - \frac{4\gamma}{\lambda^4} - \frac{4}{\lambda^4}\ln\left(\frac{\lambda}{2}\right), r = 0 \end{cases}. \tag{2.56}$$

For Polyharmonic splines of order two, $\phi(r) = r^4\ln(r)$ in R^2, we derive the following results

$$\Phi(r) = \begin{cases} -\frac{r^4\ln(r)}{\lambda^2} + \frac{8r^2(2\ln(r)+1)}{\lambda^4} + \frac{64\ln(r)+96}{\lambda^6} + \frac{64K_0(\lambda r)}{\lambda^6}, r \neq 0 \\ \frac{96}{\lambda^6} - \frac{64\gamma}{\lambda^6} - \frac{64}{\lambda^6}\ln\left(\frac{\lambda}{2}\right), r = 0 \end{cases}. \tag{2.57}$$

For Polyharmonic splines of higher order, $\phi(r) = r^k\ln(r), k = 4, 6, 8, \cdots$ in R^2, we get

$$\Phi(r) = -\frac{1}{\lambda^2}\sum_{i=0}^{k/2}\left(-\frac{\Delta}{\lambda^2}\right)^i r^k\ln(r) - \frac{(-1)^{k/2}(k)!!^2}{\lambda^{k+2}}K_0(\lambda r). \tag{2.58}$$

For TPS $\phi(r) = r$ in R^3, we find the following particular solution

$$\Phi(r) = \begin{cases} -\frac{r}{\lambda^2} + \frac{2}{\lambda^4 r} - \frac{2e^{-\lambda r}}{\lambda^4 r}, r \neq 0 \\ \frac{2}{\lambda^3}, r = 0 \end{cases}. \tag{2.59}$$

For Polyharmonic splines $\phi(r) = r^k, k = 1, 3, 5, \cdots$ in R^3, we derive the particular solution

$$\Phi(r) = -\sum_{i=0}^{k/2}\frac{(-1)^i(k+1)!r^{k-2i}}{(k+1-2i)!\lambda^{2i+2}} + \frac{2(-1)^i(k+1)!}{\lambda^{2k+4}}\frac{e^{-\lambda r}}{r}. \tag{2.60}$$

(c) The corresponding particular solutions as a prior to satisfy the differential equation $(\Delta - \lambda^2)\Phi(r) = \phi(r)$.

For TPS $\phi(r) = r^2\ln(r)$ in R^2, we obtain

$$\Phi(r) = \begin{cases} -\frac{r^2 \ln(r)}{\lambda^2} - \frac{4\ln(r)+4}{\lambda^4} - \frac{4}{\lambda^4} K_0(\lambda r), r \neq 0 \\ -\frac{4}{\lambda^4} + \frac{4\gamma}{\lambda^4} + \frac{4}{\lambda^4} \ln\left(\frac{\lambda}{2}\right), r = 0 \end{cases}. \tag{2.61}$$

For Polyharmonic splines of order 2, $\phi(r) = r^4 \ln(r)$ in R^2, the corresponding particular solution is

$$\Phi(r) = \begin{cases} -\frac{r^4 \ln(r)}{\lambda^2} - \frac{8r^2(2\ln(r)+1)}{\lambda^4} - \frac{64\ln(r)+96}{\lambda^6} - \frac{64K_0(\lambda r)}{\lambda^6}, r \neq 0 \\ -\frac{96}{\lambda^6} + \frac{64\gamma}{\lambda^6} + \frac{64}{\lambda^6} \ln\left(\frac{\lambda}{2}\right), r = 0 \end{cases}. \tag{2.62}$$

For Polyharmonic splines of higher order $\phi(r) = r^k \ln(r), k = 4, 6, 8, \cdots$ in R^2, we have

$$\Phi(r) = -\frac{1}{\lambda^2} \sum_{i=0}^{k/2} \left(\frac{\Delta}{\lambda^2}\right)^i r^k \ln(r) - \frac{(k)!!^2}{\lambda^{k+2}} K_0(\lambda r). \tag{2.63}$$

For TPS $\phi(r) = r$ in R^3, we get

$$\Phi(r) = \begin{cases} -\frac{r}{\lambda^2} - \frac{2}{\lambda^4 r} + \frac{2e^{-\lambda r}}{\lambda^4 r}, r \neq 0 \\ -\frac{2}{\lambda^3}, r = 0 \end{cases}. \tag{2.64}$$

For Polyharmonic splines $\phi(r) = r^k, k = 1, 3, 5, \cdots$ in R^3, we obtain

$$\Phi(r) = -\sum_{i=0}^{k/2} \frac{(k+1)! r^{k-2i}}{(k+1-2i)! \lambda^{2i+2}} + \frac{2(k+1)!}{\lambda^{k+3}} \frac{e^{-\lambda r}}{r}. \tag{2.65}$$

(d) The corresponding particular solutions as a prior to satisfy the differential equation $\Delta^2 \Phi(r) = \phi(r)$.

For MQ, $\phi(r) = \sqrt{r^2 + c^2}$ in R^2, we derive the particular solution

$$\begin{aligned} \Phi(r) = &\frac{1}{12} r^2 c^3 - \frac{7}{60} c^4 \sqrt{c^2 + r^2} + \frac{2}{45} c^2 \left(c^2 + r^2\right)^{\frac{3}{2}} \\ &+ \frac{1}{225} c^2 \left(c^2 + r^2\right)^{\frac{5}{2}} + \frac{2c^2 - 5r^2}{60} \ln\left(c + \sqrt{c^2 + r^2}\right) \end{aligned} \tag{2.66}$$

For IMQ, $\phi(r) = 1/\sqrt{r^2 + c^2}$ in R^2, the particular solution is stated as

$$\Phi(r) = \begin{cases} -\frac{5c^2 \sqrt{c^2+r^2}}{12} + \frac{(c^2+r^2)^{\frac{3}{2}}}{9} + \frac{cr^2}{2} + \frac{(2c^3 - 3cr^2)\ln(c+\sqrt{c^2+r^2})}{12}, r \neq 0 \\ \frac{c^3}{36}(6\ln(2c) - 11), r = 0 \end{cases}. \tag{2.67}$$

For Polyharmonic splines $\phi(r) = r^k, k = 1, 3, 5, \cdots$ in R^3, we have

$$\Phi(r) = \frac{r^{k+4}}{(k+2)(k+3)(k+4)(k+5)} \tag{2.68}$$

(e) The corresponding particular solutions as a prior to satisfy the differential equation $\left(\nabla^4 - \lambda^4\right)\Phi(r) = \phi(r)$.

For Polyharmonic splines of order 2, $\phi(r) = r^4 \ln(r)$ in R^2, we get

$$\Phi(r) = \begin{cases} -\frac{r^4 \ln(r)}{\lambda^4} - \frac{64 \ln(r) + 96}{\lambda^8} - \frac{16(K_0(\lambda r) - \pi Y_0(\lambda r))}{\lambda^8}, r \neq 0 \\ -\frac{96}{\lambda^8} + \frac{64\gamma}{\lambda^8} + \frac{64}{\lambda^8} \ln\left(\frac{\lambda}{2}\right), r = 0 \end{cases}. \quad (2.69)$$

For Polyharmonic splines $\phi(r) = r^k \ln(r), k = 2, 4, 6, \cdots$ in R^2, we obtain

$$\Phi(r) = -\frac{1}{\lambda^4} \sum_{i=0}^{k/2} \left(\frac{\Delta^2}{\lambda^4}\right)^i r^k \ln(r) - \frac{(k/2)!^2}{\lambda^{k+4}} \left(2K_0(\lambda r) + (-1)^{k/2+1} \pi Y_0(\lambda r)\right). \quad (2.70)$$

For Polyharmonic splines $\phi(r) = r^k, k = 1, 3, 5, \cdots$ in R^3, we have

$$\Phi(r) = -\frac{1}{\lambda^4} \sum_{i=0}^{(k-1)/2} \left(\frac{\Delta^2}{\lambda^4}\right)^i r^{k+2} + \frac{(k+1)!}{2\lambda^{k+5} r} \left(e^{-\lambda r} + (-1)^{(k+1)/2} \cos(\lambda r)\right). \quad (2.71)$$

(f) The corresponding particular solutions as a prior to satisfy the differential equation $(\nabla^4 + \kappa^2)\Phi(r) = \phi(r)$.

For Polyharmonic splines $\phi(r) = r^k \ln(r), k = 2, 4, 6, \cdots$ in R^2, we have the following results

$$\Phi(r) = \frac{\sum_{i=0}^{k/2} \left(-\frac{\Delta^2}{\kappa^2}\right)^i r^k \ln(r)}{\kappa^2} + \frac{(-1)^{k/2}(k/2)!^2 \left(2K_0(\sqrt{\kappa}r) + (-1)^{k/2+1} \pi Y_0(\sqrt{\kappa}r)\right)}{\kappa^{k/2+2}}. \quad (2.72)$$

For Polyharmonic splines $\phi(r) = r^k, k = 1, 3, 5, \cdots$ in R^3, we have

$$\Phi(r) = \frac{\sum_{i=0}^{(k-1)/2} \left(-\frac{\Delta^2}{\kappa^2}\right)^i r^{k+2}}{\kappa^2} + \frac{(-1)^{\frac{k+1}{2}}(k+1)! \left(e^{-\sqrt{\kappa}r} + (-1)^{\frac{k+1}{2}} \cos(\sqrt{\kappa}r)\right)}{2\kappa^{(k+5)/2} r} \quad (2.73)$$

2.2.5 Anisotropic RBFs

Numerical methods based on RBFs appear very efficient for isotropic problems. However, Carlson and Foley [39] found that the isotropic RBFs, such as the MQ and TPS, do not work well for the so-called track or directional data problems. This kind of problems characterizes a preferred direction. For directional data, the anisotropic RBFs can capture the directional property. For instance, consider heat conduction in anisotropic media

$$\sum_{i,j=1}^{d} \frac{\partial}{\partial x_i} \left(K_{ij} \frac{\partial u(\mathbf{x})}{\partial x_j} \right) = 0, \ \mathbf{x} \in \Omega, \tag{2.74}$$

where d denotes the dimensionality of problem. $K = \left[K_{ij} \right]_{1 \le i,j \le d}$ denotes the matrix of anisotropic material parameter, which has the symmetrical and positive-definite properties, for example, $d = 2$, $K_{12} = K_{21}$ and $\Delta_K = \det(K) = K_{11}K_{22} - K_{12}^2 > 0$. Typically, there are two approaches to construct the anisotropic RBFs.

Domain mapping method [40]

The domain mapping method is a transformation technique and can be applied to the anisotropic problem in field theory. The 2D and 3D direct domain mapping formulas are represented by

$$\begin{pmatrix} X_1 - X_{k1} \\ X_2 - X_{k2} \end{pmatrix} = \begin{pmatrix} \sqrt{\Delta_K}/K_{11} & 0 \\ -K_{12}/K_{11} & 1 \end{pmatrix} \begin{pmatrix} x_1 - x_{k1} \\ x_2 - x_{k2} \end{pmatrix}, \tag{2.75}$$

$$\begin{pmatrix} X_1 - X_{k1} \\ X_2 - X_{k2} \\ X_3 - X_{k3} \end{pmatrix} = \begin{pmatrix} \sqrt{\Delta_K}/K_{11} & 0 & 0 \\ -K_{12}/K_{11} & 1 & 0 \\ \beta_1 & \beta_2 & \beta_3 \end{pmatrix} \begin{pmatrix} x_1 - x_{k1} \\ x_2 - x_{k2} \\ x_3 - x_{k3} \end{pmatrix}, \tag{2.76}$$

where

$\beta_1 = (K_{12}K_{13} - K_{23}K_{11})/\sqrt{w}, \ \beta_2 = (K_{12}K_{23} - K_{13}K_{22})/\sqrt{w}, \ \beta_3 = \Delta_K/\sqrt{w}$,
and $w = K_{11}K_{33}\Delta_K - K_{11}K_{22}K_{13}^2 + 2K_{11}K_{12}K_{13}K_{23} - K_{23}^2 K_{11}^2$.

Geodesic distance functions [41]

Another strategy is to construct geodesic distance functions. The standard Euclidean distance $r_k = \|\mathbf{x} - \mathbf{x}_k\|_2$ is replaced by the geodesic distance R_k between points $\mathbf{x} = (x_1, x_2, \cdots, x_d)$ and $\mathbf{x}_k = (x_{k1}, x_{k2}, \cdots, x_{kd})$ defined as below

$$R_k^2 = \sum_{i=1}^{d} \sum_{j=1}^{d} K_{ij}^{-1}(x_i - x_{ki})(x_j - x_{kj}) = (\mathbf{x} - \mathbf{x}_k)^T K^{-1}(\mathbf{x} - \mathbf{x}_k), \tag{2.77}$$

where $K^{-1} = \left[K_{ij}^{-1} \right]$ is the inverse anisotropic coefficient matrix. In case of isotropic media, K is an identity matrix and the geodesic distance is reduced to the Euclidean distance.

It is straightforward to construct the anisotropic RBFs from the corresponding isotropic RBFs described above via the variable transformation Eqs. (2.75), (2.76), and (2.77).

2.2.6 Time–Space RBFs

In terms of generalized time–space field, an interesting and significant extension of the RBF concept is to introduce time–space RBFs for time-dependent problems. One of the proposed methodology defines the interpolation function on

$R^n \times T$ [42], where T is the additional time axis. Hence the time–space RBFs have the representation form $\sqrt{r^2 + c^2|t|^2}$. The parameter c reflects a realistic relationship between space and time. Such a metric considers the time axis being "orthogonal" to all of the space axes but with a different unit.

Yet another type of the time–space RBFs originates from transient fundamental solution and general solution of time-dependent partial differential equations [43–45]. Consider the diffusion equation

$$\frac{\partial u(\mathbf{x}, t)}{\partial t} = k\nabla^2 u(\mathbf{x}, t), \ \mathbf{x} \in \Omega \subset R^n, \tag{2.78}$$

where $\mathbf{x}$ is the general spatial coordinate, t the time, k the diffusion coefficient. By applying the Fourier and the inverse Fourier transforms to Eq. (2.78), the fundamental solutions in R^n and the general solutions in R^3 can be obtained, respectively, and stated as

$$\phi_F^m(\mathbf{x}, t, \mathbf{s}, \tau) = \frac{e^{\frac{-\|\mathbf{x}-\mathbf{s}\|_2^2}{4k(t-\tau)}}}{(4k\pi(t-\tau))^{n/2}} H(t-\tau), \mathbf{x} \in R^n, \tag{2.79}$$

$$\phi_G^m(\mathbf{x}, t, \mathbf{s}, \tau) = e^{-k(t-\tau)} \frac{\sin\|\mathbf{x}-\mathbf{s}\|_2}{\|\mathbf{x}-\mathbf{s}\|_2}, \mathbf{x} \in R^3, \tag{2.80}$$

where n is the spatial dimensionality and $H(t)$ represents the Heaviside step function, $\mathbf{x}$ denotes the location of the field points, and $\mathbf{s}$ means the location of the source points. t and τ are the time of the field and source points, respectively.

2.3 Kernel RBFs

As the motto goes "the laws of universe are written in the language of partial differential equation," the construction of an efficient and stable RBF is not an exception. Building on the firm grounds of integral equation theory (distribution theory), this section presents a recent approach for constructing the novel RBFs in terms of the potential theory.

The Green second identity was found to be a powerful alternative tool to create and analyze efficient RBFs [43, 46, 47]. The kernel solutions of partial differential equations can be used to create the kernel RBFs. By using the Green second theorem, the solution of Eq. (2.27) can be expressed as

$$u(\mathbf{x}) = \int_\Omega f(\mathbf{s})u^*(\mathbf{x}, \mathbf{s})d\Omega(\mathbf{s}) + \int_\Gamma \left\{ u\frac{\partial u^*(\mathbf{x}, \mathbf{s})}{\partial n(\mathbf{s})} - \frac{\partial u}{\partial n(\mathbf{s})}u^*(\mathbf{x}, \mathbf{s}) \right\}d\Gamma(\mathbf{s}), \tag{2.81}$$

where u^* represents the fundamental solutions of governing operator $\Re$, and $\mathbf{s}$ denotes source point. It is noted that the first and second terms of Eq. (2.81) are the

particular and the homogeneous solutions in the PDE splitting approach [31]. Applying a numerical integral scheme to approximate Eq. (2.81), we have

$$u(\mathbf{x}) = \sum_{j=1}^{N} w(\mathbf{x}, \mathbf{x}_j) f(\mathbf{x}_j) u^* + \sum_{j=N_i+1}^{N} w(\mathbf{x}, \mathbf{x}_j) \left[u \frac{\partial u^*}{\partial n} - \frac{\partial u}{\partial n} u^* \right], \qquad (2.82)$$

where N_i is the number of the interior knots in Ω, N the total number of knots in the domain and on the boundary, and $w(\mathbf{x}, \mathbf{x}_j)$ the integration weighting functions. We can further restate the approximate representation (2.82) as

$$u(\mathbf{x}) = \sum_{j=1}^{N} \alpha_j h_j(\mathbf{x}, \mathbf{x}_j) u^* f(\mathbf{x}_j) - \sum_{j=N_i+1}^{N} \beta_j p_j(\mathbf{x}, \mathbf{x}_j) u^* + \sum_{j=N_i+1}^{N} \gamma_j q_j(\mathbf{x}, \mathbf{x}_j), \quad (2.83)$$

where $\{\alpha_j\}, \{\beta_j\}$ and $\{\gamma_j\}$ are unknown expansion coefficients, $\{h_j\}$ and $\{p_j\}$ represents weighting functions to be specified. hu^*f, pu^* are in fact the radial basis functions. Therefore, the first term of Eq. (2.83) suggests that the RBFs can be constructed using interior source points $\{\mathbf{x}_j\}$ [43, 46, 47] by

$$\phi(\mathbf{x}, \mathbf{x}_j) = h_j(\mathbf{x}, \mathbf{x}_j) u^*(\mathbf{x}, \mathbf{x}_j) f(\mathbf{x}_j). \qquad (2.84)$$

When u^* is a singular fundamental solution, h_j is an augmented RBF function to remove the singularities of fundamental solutions and guarantee that the function $\phi(x, x_j)$ has enough differentiability. Power function $h_j = r^m$ is a convenient choose where r denotes the Euclidean distance. For instance, the TPS is a special case of the kernel RBFs for 2D biharmonic operator. Polyharmonic splines RBFs are recommended for higher dimensional problems. On the other hand, u^* in Eq. (2.84) can be replaced by nonsingular general solutions [46, 48].

Regarding the boundary source points, we suggest a RBF as

$$\phi(\mathbf{x}, \mathbf{x}_j) = p_j(\mathbf{x}, \mathbf{x}_j) u^*(\mathbf{x}, \mathbf{x}_j). \qquad (2.85)$$

The weighting function $p_j = r^m$ is also a simple choice. It is of worthy noting that the high-order fundamental solutions, general solutions, and harmonic functions in Sects. 2.2.1–2.2.3 are not singular and appear similar to the fundamental solutions augmented with a power function. Table 2.8 lists some typical kernel RBFs augmented by a power function [43].

Another strategy is to construct shifted kernel RBFs [43] by replacing Euclidean distance r in the fundamental solutions with a shifted distance variable $\sqrt{c^2 + r^2}$ to remedy the singularity, where c is a dilution shape parameter. For instance, the MQ RBF can be used as a correcting function to determine local optimal shape parameter by establishing the reproducing conditions. These shifted kernel RBFs are especially attractive for multiscale problems. Table 2.9 lists some shifted kernel RBFs.

Table 2.8 Kernel RBFs augmented by a power function

Power augmented scheme	$\phi(\mathbf{x})$
Polyharmonic spline	$\begin{cases} r^m, m = 1, 3, 5, \cdots \\ r^m \ln(r), m = 2, 4, 6, \cdots \end{cases}$
Thin plate spline	$r^2 \ln(r)$
Power exponential functions	$r^m e^{-r^2}$
High-order fundamental solutions	See Sect. 2.2.1
High-order RBF general solutions	See Sect. 2.2.2
High-order harmonic functions	See Sect. 2.2.3

With the help of the kernel solutions of time-dependent PDEs, we can also construct the time–space kernel RBFs. For instance, consider the wave propagation equation

$$\frac{\partial^2 u}{\partial x^2} = \frac{1}{c^2} \frac{\partial^2 u}{\partial t^2} + f(x, t). \tag{2.86}$$

Let

$$s = ict, \tag{2.87}$$

where $i = \sqrt{-1}$. We have

$$\frac{\partial^2 u}{\partial x^2} + \frac{\partial^2 u}{\partial s^2} = f(x, t). \tag{2.88}$$

Similar to the definition of Euclidean distance, the generalized time–space distance is defined by

$$r_j = \sqrt{(x - x_j)^2 + (s - s_j)^2} = \sqrt{(x - x_j)^2 - c^2 (t - t_j)^2}. \tag{2.89}$$

However, such a definition can lead to complex value of distance variable. Thus, it is better to use

$$r_j = \sqrt{(x - x_j)^2 + c^2 (t - t_j)^2}. \tag{2.90}$$

Table 2.9 Shifted kernel RBFs

Shape parameter scheme	$\phi(\mathbf{x})$
Multiquadric	$\sqrt{r^2 + c^2}$
Shifted logarithm function	$\ln(\sqrt{r^2 + c^2})$
Shifted Polyharmonic spline	$r^m \ln(\sqrt{r^2 + c^2})$
Shifted exponential function	$e^{-\sqrt{r^2 + c^2}}$
Shifted fundamental solutions	$\phi_F^m(\sqrt{r^2 + c^2})$
Shifted RBF general solutions [49]	$\phi_G^m(\sqrt{r^2 + c^2})$

Here c is the wave velocity. The RBFs with respect to time–space distance (2.90) differ from the standard RBFs in that the time variable is handled equally as the space variables. Time–space RBFs eliminate time dependence directly in the basis functions. The Green second theory suggests that the time–space kernel RBFs can be constructed by [46, 47]

$$\phi(r_j) = h_j(r_j)u^*(r_j)f(\mathbf{x}_j, t), \qquad (2.91)$$

for interior source points, and

$$\phi(r_j) = p_j(r_j)u^*(r_j), \qquad (2.92)$$

for boundary source points.

Another strategy is to construct time-dependent kernel RBFs by augmenting fundamental or general solutions with time power function stated below

$$\phi(r_j) = t^{2m}u^*(r_j)f(\mathbf{x}_j, t), \qquad (2.93)$$

where t^{2m} remedies the singularities of transient fundamental solution $u^*(r_j)$. The time–space RBFs in Sect. 2.2.6 can be modified by utilizing shifted RBF formulas (2.91–2.93). The time–space kernel RBFs have great potential to transient image data processing such as motion pictures.

The other approaches for constructing the appropriate RBFs are also reported in literatures, such as combined RBFs [50], oscillatory RBFs [51], Trefftz RBFs [52], and wavelet-based adaptive RBF method [53]. For more details, the interested readers may look into the respective papers.

References

1. E. Folio, Distance Transform. In: Technical Report no 0806, revision 1748. Laboratoire de Recherche et Dveloppement de l'Epita (Le Kremlin-Bictre cedex-France, 2008)
2. M.D. Buhmann, *Radial Basis Function: Theory and Implementations* (Cambridge University Press, Cambridge, 2003)
3. R. Franke, Scattered data interpolation: tests of some method. Math. Comput. **38**(157), 181–200 (1982)
4. J.G. Wang, G.R. Liu, On the optimal shape parameters of radial basis function used for 2-D meshless methods. Comput. Methods Appl. Mech. Eng. **191**(23–24), 2611–2630 (2002)
5. A.H.D. Cheng, M.A. Golberg, E.J. Kansa, G. Zammito, Exponential convergence and H-c multiquadric collocation method for partial differential equations. Numer. Methods Part. Differ. Eq. **19**(5), 571–594 (2003)
6. C.S. Huang, C.F. Lee, A.H.D. Cheng, Error estimate, optimal shape factor, and high precision computation of multiquadric collocation method. Eng. Anal. Boundary Elem. **31**(7), 614–623 (2007)
7. C.M.C. Roque, A.J.M. Ferreira, Numerical experiments on optimal shape parameters for radial basis function. Numer. Methods Part. Differ. Eq. **26**(3), 675–689 (2010)
8. B. Fornberg, C. Piret, On choosing a radial basis function and a shape parameter when solving a convective PDE on a sphere. J. Comput. Phys. **227**(5), 2758–2780 (2008)

9. J. Duchon, Interpolation des fonctions de deux variables suivant le principe de la flexion des plaques minces. Revue Francaise D Automatique Informatique Recherche Operationnelle **10**(12), 5–12 (1976)

10. W.R. Madych, S.A. Nelson, Multivariate interpolation and conditionally positive definite functions. Approx. Theor. Appl. **4**, 77–89 (1988)

11. W.R. Madych, S.A. Nelson, Multivariate interpolation and conditionally positive definite functions. 2. Math. Comput. **54**(189), 211–230 (1990)

12. W.R. Madych, S.A. Nelson, Bounds on multivariate polynomials and exponential error-estimates for multiquadric interpolation. J. Approx. Theor. **70**(1), 94–114 (1992)

13. Z.M. Wu, R.S. Schaback, Local error-estimates for radial basis function interpolation of scattered data. IMA J. Numer. Anal. **13**(1), 13–27 (1993)

14. A.H.D. Cheng, Multiquadric and its shape parameter-A numerical investigation of error estimate, condition number, and round-off error by arbitrary precision computation. Eng. Anal. Boundary Elem. **36**, 220–239 (2012)

15. H. Wendland, *Scattered Data Approximation* (Cambridge University Press, Cambridge, 2005)

16. W.R. Madych, Miscellaneous error-bounds for multiquadric and related interpolators. Comput. Math. Appl. **24**(12), 121–138 (1992)

17. W.K. Liu, J. Sukky, Multiple-scale reproducing kernel particle methods for large deformation problems. Int. J. Numer. Meth. Eng. **41**(7), 1339–1362 (1998)

18. Z. Wu, Compactly supported positive definite radial functions. Adv. Comput. Math. **4**(1), 283–292 (1995)

19. H. Wendland, Piecewise polynomial, positive definite and compactly supported radial functions of minimal degree. Adv. Comput. Math. **4**(1), 389–396 (1995)

20. M.D. Buhmann, Radial functions on compact support, in *Proceedings of the Edinburgh Mathematical Society (Series 2)* **41**(01), 33–46 (1998)

21. K.K. Prem, *Fundamental Solutions for Differential Operators and Applications*. (Birkhauser Boston Inc., Cambridge, 1996)

22. A.J. Nowak, A.C. Neves, *The Multiple Reciprocity Boundary Element Method.* (Computational Mechanics Publication, Southampton, 1994)

23. M. Itagaki, Higher order three-dimensional fundamental solutions to the Helmholtz and the modified Helmholtz equations. Eng. Anal. Boundary Elem. **15**, 289–293 (1995)

24. W. Chen, Z.J. Shen, L.J. Shen, G.W. Yuan, General solutions and fundamental solutions of varied orders to the vibrational thin, the Berger, and the Winkler plates. Eng. Anal. Boundary Elem. **29**(7), 699–702 (2005)

25. W. Chen, Meshfree boundary particle method applied to Helmholtz problems. Eng. Anal. Boundary Elem. **26**(7), 577–581 (2002)

26. W. Chen, L.J. Shen, Z.J. Shen, G.W. Yuan, Boundary knot method for Poisson equations. Eng. Anal. Boundary Elem. **29**(8), 756–760 (2005)

27. Y.C. Hon, Z. Wu, A numerical computation for inverse boundary determination problem. Eng. Anal. Boundary Elem. **24**(7–8), 599–606 (2000)

28. E.J. Kansa, Multiquadrics–A scattered data approximation scheme with applications to computational fluid-dynamics–II solutions to parabolic, hyperbolic and elliptic partial differential equations. Comput. Math. Appl. **19**(8–9), 147–161 (1990)

29. Z.J. Fu, W. Chen, A truly boundary-only Meshfree method applied to Kirchhoff plate bending problems. Adv. Appl. Math. Mech. **1**(3), 341–352 (2009)

30. W. Chen, Z.J. Fu, B.T. Jin, A truly boundary-only Meshfree method for inhomogeneous problems based on recursive composite multiple reciprocity technique. Eng. Anal. Boundary Elem. **34**(3), 196–205 (2010)

31. K.E. Atkinson, The numerical evaluation of particular solutions for Poisson's equation. IMA J. Numer. Anal. **5**, 319–338 (1985)

32. C.S. Chen, Y.F. Rashed, Evaluation of thin plate spline based particular solutions for helmholtz-type operators for the drm. Mech. Res. Commun. **25**, 195–201 (1998)

33. A.S. Muleshkov, M.A. Golberg, C.S. Chen, Particular solutions of helmholtz-type operators using higher order polyharmonic splines. Comput. Mech. **24**, 411–419 (1999)
34. A.H.D. Cheng, Particular solutions of Laplacian, helmholtz-type, and polyharmonic operators involving higher order radial basis function. Eng. Anal. Boundary Elem. **24**, 531–538 (2000)
35. A.S. Muleshkov, M.A. Golberg, Particular solutions of the multi-helmholtz-type equation. Eng. Anal. Boundary Elem. **31**, 624–630 (2007)
36. C.S. Chen, Y.C. Hon, R.S. Schaback, *Radial basis function with Scientific Computation* (University of Southern Mississippi, Mississippi, 2007)
37. C.C. Tsai, Particular solutions of splines and monomials for polyharmonic and products of Helmholtz operators. Eng. Anal. Boundary Elem. **33**(4), 514–521 (2009)
38. G.M. Yao, Local Radial Basis Function Methods for Solving Partial Differential Equations. Ph.D. Dissertation, University of Southern Mississippi, 2010
39. R.E. Carlson, T.A. Foley, Interpolation of track data with radial basis methods. Comput. Math. Appl. **24**, 27–34 (1992)
40. Y.C. Shiah, C.L. Tan, BEM treatment of three-dimensional anisotropic field problems by direct domain mapping. Eng. Anal. Boundary Elem. **28**(1), 43–52 (2004)
41. B.T. Jin, W. Chen, Boundary knot method based on geodesic distance for anisotropic problems. J. Comput. Phys. **215**(2), 614–629 (2006)
42. D.E. Myers, S. De Iaco, D. Posa, L. De Cesare, Space-time radial basis function. Comput. Math. Appl. **43**(3–5), 539–549 (2002)
43. W. Chen, New RBF collocation schemes and kernel RBF with applications. Lect. Notes Comput. Sci. Eng. **26**, 75–86 (2002)
44. D.L. Young, C.C. Tsai, K. Murugesan, C.M. Fan, C.W. Chen, Time-dependent fundamental solutions for homogeneous diffusion problems. Eng. Anal. Boundary Elem. **28**(12), 1463–1473 (2004)
45. C.C. Tsai, D.L. Young, C.M. Fan, C.W. Chen, MFS with time-dependent fundamental solutions for unsteady Stokes equations. Eng. Anal. Boundary Elem. **30**(10), 897–908 (2006)
46. W. Chen, M. Tanaka, New Insights into Boundary-only and Domain-type RBF Methods. Int. J. Nonlinear Sci. Numer. Simul. **1**(3), 145–151 (2000)
47. W. Chen, M. Tanaka, Relationship between boundary integral equation and radial basis function. Paper presented at the 52th symposium of Japan society for computational methods in engineering (JASCOME) on BEM, Tokyo
48. W. Chen, M. Tanaka, A meshless, integration-free, and boundary-only RBF technique. Comput. Math. Appl. **43**(3–5), 379–391 (2002)
49. J. Lin, W. Chen, K.Y. Sze, A new radial basis function for Helmholtz problems. Eng. Anal. Boundary Elem. **36**(12), 1923–1930 (2012)
50. S.G. Ahmed, A collocation method using new combined radial basis function of thin plate and multiquadraic types. Eng. Anal. Boundary Elem. **30**(8), 697–701 (2006)
51. B. Fornberg, E. Larsson, G. Wright, A new class of oscillatory radial basis function. Comput. Math. Appl. **51**(8), 1209–1222 (2006)
52. V. Kompis, M. Stiavnicky, M. Zmindak, Z. Murcinkova, Trefftz radial basis function (TRBF), in *Proceedings of Lsame.08: Leuven Symposium on Applied Mechanics in Engineering, Pts 1 and 2*, 25–35 (2008)
53. N.A. Libre, A. Emdadi, E.J. Kansa, M. Shekarchi, M. Rahimian, Wavelet based adaptive RBF method for nearly singular poisson-type problems on irregular domains. CMES Comput. Model. Eng. Sci. **50**(2), 161–190 (2009)

Chapter 3
Different Formulations of the Kansa Method: Domain Discretization

Abstract In contrast to the traditional meshed-based methods such as finite difference, finite element, and boundary element methods, the RBF collocation methods are mathematically very simple to implement and are truly free of troublesome mesh generation for high-dimensional problems involving irregular or moving boundary. This chapter introduces the basic procedure of the Kansa method, the very first domain-type RBF collocation method. Following this, several improved formulations of the Kansa method are described, such as the Hermite collocation method, the modified Kansa method, the method of particular solutions, the method of approximate particular solutions, and the localized RBF methods. Numerical demonstrations show the convergence rate and stability of these domain-type RBF collocation methods for several benchmark examples.

Keywords Kansa method · Hermite collocation method · Modified Kansa method · Method of particular solutions · Method of approximate particular solutions · Localized formulations

In the last two decades, much effort has been devoted to developing a variety of meshless schemes for numerical discretization of partial differential equations. The driving force behind the scene is that mesh-based methods such as the standard FEM and BEM often require excessive computational effort to mesh or remesh the computational domain for high-dimensional, moving boundary, or complex-shaped boundary problems. Many of the meshless techniques available today are based on moving least squares (MLS). However, in some cases, shadow elements are still required for the numerical integration. Therefore, these methods are not entirely meshless. In contrast, the RBF collocation methods are exceedingly simple for numerical implementation and are truly meshless and integration-free because of their independency of dimensionality and complexity of problem geometry. Nardini and Brebbia in 1982 have actually applied the RBF concept to develop the popular dual reciprocity BEM without a notion of "RBF." Only after Kansa's pioneer work in 1990 [1, 2], the research on the RBF method for PDEs has

become very active. In general, RBF collocation methods can be classified into domain- and boundary-type categories. This chapter focuses primarily on the domain-type RBF collocation methods.

The Kansa method [1, 2] is the very first domain-type RBF collocation scheme with easy-to-use merit, but the method lacks symmetric interpolation matrix due to the boundary collocation of mixed boundary conditions. The Hermite collocation method (HCM) [3] alleviates the unsymmetrical drawback. Similar to the Kansa method, however, the HCM suffers relatively lower accuracy in boundary-adjacent region. Namely, the numerical accuracy in the vicinity of boundary deteriorates by one to two orders compared with those in the central region. By using the Green second identity, Chen presented the symmetric domain-type modified Kansa method (MKM) [4] to significantly improve the numerical accuracy in the region near the boundary.

Inspired by the boundary collocation RBF techniques, the method of particular solutions (MPS) [5, 6] and the method of approximate particular solutions (MAPS) [5, 7] are developed to use the particular solution RBFs for the solution of PDEs.

The ill-conditioning and fully-populated interpolation matrix is the main challenge for the application of the traditional Kansa method and its variants mentioned above to large-scale problems. In addition, it remains an opening issue to determine the optimal shape parameter using the MQ-RBF in a global interpolation. To remedy these two perplexing problems, a number of the localized RBF methods [8–18] have been proposed in recent years and have attracted great attention in the science and engineering communities.

Let Ω be a bounded and connected domain, and $\partial\Omega = \Gamma_1 \cup \Gamma_2$, $\Gamma_1 \cap \Gamma_2 = \emptyset$. Without loss of generality, we make a straightforward illustration of these methods through the following elliptical partial differential equation:

$$\begin{aligned}
\Re\{u(\mathbf{x})\} &= f(\mathbf{x}), \ \mathbf{x} \in \Omega \subset R^n, \\
B_1 u(\mathbf{x}) &= R(\mathbf{x}), \ \mathbf{x} \in \Gamma_1, \\
B_2 u(\mathbf{x}) &= N(\mathbf{x}), \ \mathbf{x} \in \Gamma_2,
\end{aligned} \tag{3.1}$$

where $\Re$ is governing differential operator, B_1, B_2 boundary differential operators, and $f(\mathbf{x}), R(\mathbf{x}), N(\mathbf{x})$ are given functions.

3.1 The Kansa Method

First, we introduce the well-known Kansa method [1, 2]. The method employs both the RBFs and the polynomial basis to approximate the PDE solutions. However, Wertz et al. [19] recently found that it is unnecessary to augment polynomial term with the RBF approximate representation in solving PDEs. Thus, this book only introduces the Kansa method without augmented polynomial basis functions.

Let $\{\mathbf{x}_j\}_{j=1}^{N_i}$ be the interior points in the domain Ω, $\{\mathbf{x}_j\}_{j=N_i+1}^{N_i+N_1} \in \Gamma_1$, and $\{\mathbf{x}_j\}_{j=N_i+N_1+1}^{N} \in \Gamma_2$, where $N = N_i + N_1 + N_2$. The Kansa method assumes the solution $u(\mathbf{x})$ in Eq. (3.1) can be approximated by a linear combination of the RBFs at discrete nodes

$$u(\mathbf{x}) \simeq \tilde{u}(\mathbf{x}) = \sum_{j=1}^{N} \alpha_j \phi\big(\|\mathbf{x} - \mathbf{x}_j\|_2\big), \tag{3.2}$$

where $\{\alpha_j\}$ are unknown coefficients, N the total number of the collocation knots, and $\phi(\mathbf{x})$ denotes the RBFs, such as MQ, IMQ, TPS, and Gaussian, etc. Substituting Eq. (3.2) into Eq. (3.1), the linear equations can be expressed in the following matrix form:

$$\mathbf{A}\alpha = \mathbf{b}, \tag{3.3}$$

where $\boldsymbol{\alpha} = (\alpha_1, \alpha_2, \ldots, \alpha_N)^T$ is the unknown vector to be determined, and

$$\mathbf{b} = (f(\mathbf{x}_1), \cdots, f(\mathbf{x}_{N_i}), R(\mathbf{x}_{N_i+1}), \cdots, R(\mathbf{x}_{N_i+N_1}), N(\mathbf{x}_{N_i+N_1+1}), \cdots, N(\mathbf{x}_N))^T.$$

The RBF interpolation matrix can be of the form

$$\mathbf{A} = \begin{bmatrix} \Re\{\Phi\} \\ B_1\{\Phi\} \\ B_2\{\Phi\} \end{bmatrix}, \tag{3.4}$$

where $\Phi = (\Phi_{ij}) = (\phi(\|\mathbf{x}_i - \mathbf{x}_j\|_2))$. The Kansa method has been successfully applied to various physical and engineering problems, such as fractional diffusion problems [20], radiative transport problems [21], combustion problems [22], electromagnetic problems [23], electrostatic problems [24], heat conduction analysis [25], moving boundary problems [26], plate and shell analysis [27–32], fluid flow problems [33], Stefan problems [34, 35], microelectromechanical system analysis [36], groundwater contaminant transport [37], convection–diffusion problems [38–40]. However, the Kansa method produces unsymmetric interpolation matrix, and the rigorous mathematical proof of its solvability is still not available [41]. In addition, the method suffers relatively lower accuracy in boundary-adjacent region.

3.2 The Hermite Collocation Method

To make a symmetric RBF interpolation matrix, Fasshauer [3] applies the operator $\Re^*$ and B_1^*, B_2^* on both sides of the governing equation and the boundary conditions in Eq. (3.1), respectively, where $\Re^*$ and B_1^*, B_2^* are the self-adjoint operators of $\Re$ and B_1, B_2. We call this modified version of the Kansa method as the Hermite

collocation method (HCM). The HCM interpolation representation for Eq. (3.1) is given by

$$\tilde{u}(\mathbf{x}) = \sum_{j=1}^{N_i} \alpha_j \Re^* \phi\big(||\mathbf{x} - \mathbf{x}_j||_2\big) + \sum_{j=N_i+1}^{N_i+N_1} \alpha_j B_1^* \phi\big(||\mathbf{x} - \mathbf{x}_j||_2\big)$$
$$+ \sum_{j=N_i+N_1+1}^{N} \alpha_j B_2^* \phi\big(||\mathbf{x} - \mathbf{x}_j||_2\big). \tag{3.5}$$

Its interpolation matrix is expressed as

$$\mathbf{A} = \begin{bmatrix} \Re\Re^*\{\Phi\} & \Re B_1^*\{\Phi\} & {}_2^*\{\Phi\} \\ B_1\Re^*\{\Phi\} & B_1 B_1^*\Phi & B_1 B_2^*\{\Phi\} \\ B_2\Re^*\{\Phi\} & B_2 B_1^*\{\Phi\} & B_2 B_2^*\{\Phi\} \end{bmatrix}. \tag{3.6}$$

It is worth noting that the matrix $\mathbf{A}$ is symmetric. Hence the numerical discretization equations are always solvable. The HCM is applied to 2D elastostatic [42], time-dependent [43–46], and nonlinear plate problems [47].

3.3 The Modified Kansa Method

In order to reduce the loss of accuracy near the boundary-adjacent region, Fedoseye et al. [4] propose the PDE collocation on the boundary (PDECB), which requires an additional set of nodes inside or outside of the physical domain yet adjacent to the boundary. It is not a trivial task to optimally place these fictitious boundary nodes for the best numerical accuracy and stability. Larsson [48] investigated and compared the numerical accuracy of the Kansa method, the HCM, and the PDECB in the context of the RBF shape parameter and the distribution of nodes.

Zhang et al. [49] also proposed a Hermite-type method to improve the numerical accuracy of 2D elasticity problems, which collocates both governing equations and boundary conditions on the same boundary nodes. However, the method is unsymmetric for mixed boundary problems and lacks the theoretical support.

Based on the Green second identity, Chen [50] developed a symmetric Hermite formulation, called the modified Kansa method (MKM). As mentioned in Sect. 2.3, the Green second identity leads to the following solution of a PDE problem

$$\tilde{u}(\mathbf{x}) = \int_\Omega f(\mathbf{s}) u^*(\mathbf{x}, \mathbf{s}) d\Omega(\mathbf{s}) + \int_\Gamma \left\{ u \frac{\partial u^*(\mathbf{x}, \mathbf{s})}{\partial n(\mathbf{s})} - \frac{\partial u}{\partial n(\mathbf{s})} u^*(\mathbf{x}, \mathbf{s}) \right\} d\Gamma(\mathbf{s}), \tag{3.7}$$

where u^* represents the fundamental solutions of differential operator $\Re$. If a numerical integral scheme is employed to discretize Eq. (3.7), we have

$$\tilde{u}(\mathbf{x}) = \sum_{j=1}^{N} w(\mathbf{x}, \mathbf{x}_j) f(\mathbf{x}_j) u^* + \sum_{j=N_i+1}^{N} Q(\mathbf{x}, \mathbf{x}_j) \left[u \frac{\partial u^*}{\partial n} - \frac{\partial u}{\partial n} u^* \right], \tag{3.8}$$

where $w(\mathbf{x}, \mathbf{x}_j)$ and $Q(\mathbf{x}, \mathbf{x}_j)$ denote the weighting functions dependent on the integral schemes. Perceiving the RBF as an approximate Green function, we can restate the representation (3.8) to construct the following interpolation formula:

$$\tilde{u}(\mathbf{x}) = \sum_{j=1}^{N} \alpha_j \Re^* \phi\big(||\mathbf{x} - \mathbf{x}_j||_2\big) + \sum_{j=N_i+1}^{N_i+N_1} \alpha_{j+N_1+N_2} B_1^* \phi\big(||\mathbf{x} - \mathbf{x}_j||_2\big),$$
$$+ \sum_{j=N_i+N_1+1}^{N} \alpha_{j+N_1+N_2} B_2^* \phi\big(||\mathbf{x} - \mathbf{x}_j||_2\big) \tag{3.9}$$

where N_1, N_2 and N are defined as in Sect. 3.1. Note that the boundary nodes here are used twice to satisfy both the governing equation and boundary conditions. On the other hand, the MKM interpolation matrix inherits the symmetrical property of the HCM. It is noted that the MKM differs from the PDECB in that it no longer requires auxiliary boundary nodes and is derived naturally from the Green second identity. Consequently, theoretical and operational ambiguities in the PDECB are eliminated. At the end of this chapter, some numerical experiments will be presented to compare the MKM with the Kansa method and the HCM.

3.4 The Method of Particular Solutions

This section introduces the method of particular solutions (MPS). The PDE splitting approach [51] considers the solution u of Eq. (3.1) a sum of homogeneous solution u_h and particular solutions u_p

$$u = u_h + u_p. \tag{3.10}$$

Note that the particular solution u_p satisfies

$$\Re\{u_p\} = f(\mathbf{x}), \mathbf{x} \in \Omega, \tag{3.11}$$

but does not necessarily satisfy boundary conditions. In contrast, the homogeneous solution has to satisfy not only the corresponding homogeneous equation

$$\Re\{u_h\} = 0, \mathbf{x} \in \Omega, \tag{3.12}$$

but also the updated boundary conditions

$$u_h(\mathbf{x}) = R(\mathbf{x}) - u_p(\mathbf{x}), \mathbf{x} \in \Gamma_1, \tag{3.13}$$

$$\frac{\partial u_h(\mathbf{x})}{\partial n} = N(\mathbf{x}) - \frac{\partial u_p(\mathbf{x})}{\partial n}, \mathbf{x} \in \Gamma_2. \tag{3.14}$$

From Eqs. (3.10–3.14), it can be found that the nonhomogeneous problem is reduced to a homogeneous problem after the particular solution u_p is separately

obtained from Eq. (3.11). One can use the RBFs or some other basis functions [52] to evaluate the particular solution. In this study, we only consider the RBF methods.

Let $\{\mathbf{x}_j\}_{j=1}^{N_k} \in \Omega$. We first approximate $f(\mathbf{x})$ by a finite expansion series

$$f(\mathbf{x}) \approx \hat{f}(\mathbf{x}) = \sum_{j=1}^{N_k} \alpha_j \phi(r_j), \tag{3.15}$$

where $\{\alpha_j\}$ are the unknown coefficients to be determined, and $r_j = \|\mathbf{x} - \mathbf{x}_j\|$ denotes the Euclidean distance between each pair of points $\mathbf{x}$ and $\mathbf{x}_j$. Then,

$$f(\mathbf{x}_i) = \hat{f}(\mathbf{x}_i) = \sum_{j=1}^{N_k} \alpha_j \phi(r_{ij}), \ 1 \leq i \leq N_k. \tag{3.16}$$

Assuming $\{\alpha_j\}$ can uniquely be solved, the approximate particular solution $\hat{u}_p$ of Eq. (3.11) is given by

$$\hat{u}_p = \sum_{j=1}^{N_k} \alpha_j \Phi(r_j), \tag{3.17}$$

where

$$\phi(r_j) = \Re\{\Phi(r_j)\}. \tag{3.18}$$

The above evaluation procedure for the particular solution is called reverse differentiation process, which is introduced in Chap. 2, since the basis functions $\Phi(r)$ in Eq. (3.17) are derived from Eq. (3.18) indirectly [5, 53, 54]. Some particular solutions $\Phi(r)$ are presented in Sect. 2.2.4.

Another technique is called the direct differentiation approach and utilizes a traditional RBF $\Phi(r)$ in Eq. (3.17) as the basis function. Then $\phi(r)$ in Eq. (3.15) can be easily derived from Eq. (3.18) by a differentiation process. This scheme is easy to implement, however, $\phi(r)$ may not be positive definite or conditionally positive definite RBFs to guarantee the invertibility of the resultant matrix in Eq. (3.16).

By implementing one of the above two approaches, evaluating particular solution u_p is reduced to a function interpolation problem. Giving N_k nonhomogeneous function values $\{f(\mathbf{x}_j)\}$ at all the collocation knots $\{\mathbf{x}_j\}_{j=1}^{N_k}$, the unknown coefficients $\{\alpha_j\}$ can be determined by using formula (3.16) and then the particular solution u_p is obtained via the expression (3.17). After the particular solution is obtained, the homogeneous solution u_h can be approximated by

$$u_h \approx \hat{u}_h = \sum_{i=1}^{N_1+N_2} \beta_i \phi_h(r_i) \tag{3.19}$$

where $\{\beta_i\}$ are the unknown coefficients, N_1, N_2 are, respectively, the number of the collocation knots on Γ_1 and Γ_2, $\phi_h(r_j)$ represents the fundamental solution, RBF general solution, or harmonic function of the homogeneous governing equation in Eq. (3.12). For more details of these functions satisfying homogeneous equation, please see Sect. 2.2.1–2.2.3. Then, substituting Eq. (3.19) into boundary condition in Eqs. (3.13) and (3.14), the unknown coefficients $\{\beta_i\}$ can be determined and the approximate homogeneous solution $\hat{u}_h$ can be calculated via Eq. (3.19). Finally, the solution of the original PDE can be obtained by using Eq. (3.10). The above solution procedure is commonly called the two-stage MPS.

More recently, Chen et al. [5, 6] presented one-stage MPS to combine the particular and homogeneous solutions together in a one-step process for solving PDEs. This one-stage MPS interpolation formula is given by

$$\tilde{u}(\mathbf{x}) = \sum_{j=1}^{N_k} \alpha_j \Phi(r_j) + \sum_{i=1}^{N_1+N_2} \beta_i \phi_h(r_i) \qquad (3.20)$$

It should be mentioned that the MPS solution procedure is equivalent to the boundary-type RBF collocation methods in conjunction with dual reciprocity method (DRM). However, the MPS conducts the whole domain discretization to evaluate the particular solutions and is considered a special kind of domain-type RBF collocation method.

3.5 The Method of Approximate Particular Solutions

Recently, Chen et al. [5, 7] proposed the method of approximate particular solutions (MAPS) to improve the MPS by omitting the homogeneous solution part. The MAPS approximate solution $\hat{u}$ of Eq. (3.1) is represented by

$$\hat{u}(\mathbf{x}) = \sum_{j=1}^{N_k} \alpha_j \Phi(r_j). \qquad (3.21)$$

It is worth noting that the MAPS representation (3.21) appears similar to Eq. (3.2) in the Kansa method. The major distinction between the MAPS and the Kansa method is that the MAPS uses the corresponding derived particular solution RBF by reverse differentiation process. Thus, the MAPS may have more sound mathematical foundation. Some numerical experiments demonstrate that the MAPS outperforms the Kansa method in both stability and accuracy, particularly in the evaluation of partial derivatives.

However, if the governing differential operator $\Re$ is complicated, it is difficult to find the integral-derived particular solutions $\Phi(r)$ of Eq. (3.18). To implement the MAPS, we rewrite Eq. (3.1) as

$$\Re'\{u\} = f(\mathbf{x}) + (\Re' - \Re)\{u\}, \mathbf{x} \in \Omega, \qquad (3.22)$$

where $\Re'$ is a simpler differential operator, and the corresponding formula

$$\Re'\Phi(r) = \phi(r), \tag{3.23}$$

has the known particular solution $\Phi(r)$ for the RBF $\phi(r)$. This approach allows the MAPS to solve a broad types of linear and nonlinear PDEs [55].

3.6 Localized RBF Methods

In the previous sections, the RBF numerical solution of a PDE of interest is interpolated by all the collocation points in the whole physical domain and boundary. Such methods are called global approximation. As a result, the resultant matrices are fully populated and thus ill-conditioned. This leads to unstable computation. In addition, the dense matrix equation is also computationally very expensive to solve. These RBF collocation methods are not applicable for large-scale problems.

In recent decades, several techniques have been developed to overcome the above-mentioned difficulties. The singular value decomposition (SVD) [56] performs well to regularize the ill-conditioning of the moderate-size RBF dense interpolation matrix [57–59]. Alternatively, one could also utilize the multi-grid approach [60], the greedy algorithm [61, 62], the extended precision arithmetic [63]. If a large number of interpolation points are required, the fast matrix computational algorithms have been introduced in the RBF collocation methods to significantly reduce computing costs and ill-conditioning, such as preconditioning methods [64, 65], Fast Multipole Methods (FMM) [66, 67], H-matrix [68], Domain Decomposition Method (DDM) [69–74], pre-corrected Fast Fourier Transform (pFFT) [75], and Adaptive Cross Approximation (ACA) [76].

Different from the above-mentioned methodologies and inspired by the idea of CS-RBFs, a number of localized RBF methods [8–18] have been proposed to alleviate the ill-conditioning of the resultant matrix, costly dense matrix of the RBF interpolation, and the uncertainty of the selection of the optimal shape parameter.

Consider the elliptical PDE (3.1) again and let $\{\mathbf{x}_s\}_{s=1}^N \in \Omega$, the solution $u(\mathbf{x})$ can be approximated by a localized formulation as follows:

$$\tilde{u}(\mathbf{x}_s) = \sum_{j=1}^n \alpha_j^s \phi\left(||\mathbf{x}_s - \mathbf{x}_j^s||_2\right), \tag{3.24}$$

where n is the number of nearest neighboring points $\left\{\mathbf{x}_j^s\right\}_{j=1}^n$ surrounding collocation point x_s, including the collocation point itself. $\left\{\alpha_j^s\right\}$ are the unknown coefficients to be determined, $\phi(\mathbf{x})$ is an RBF. If all the collocation points are

distinct, it can be proved that the RBF interpolation matrix $\Phi = \left(\phi \left(||\mathbf{x}_i^s - \mathbf{x}_j^s||_2 \right) \right)$ is nonsingular if $\phi(\mathbf{x})$ is a positive definite RBF. Hence, the unknown coefficients in Eq. (3.24) have the following matrix form:

$$\boldsymbol{\alpha}^s = \Phi^{-1}\mathbf{u}^s, \tag{3.25}$$

where $\boldsymbol{\alpha}^s = \left(\alpha_1^s, \ldots, \alpha_n^s \right)^T$, $\mathbf{u}^s = \left(u(\mathbf{x}_1^s), \cdots, u(\mathbf{x}_n^s) \right)^T$. Then the approximate solution $\tilde{u}(\mathbf{x}_s)$ can be rewritten in terms of the given nodal values $u\left(\mathbf{x}_j^s \right)$ at its n-nearest neighboring points

$$\tilde{\mathbf{u}}^s = \Phi^s \boldsymbol{\alpha}^s = \Phi^s \Phi^{-1}\mathbf{u}^s = \Psi^s \mathbf{u}^s, \tag{3.26}$$

where $\Phi^s = \left(\phi \left(||\mathbf{x}_s - \mathbf{x}_j^s||_2 \right) \right)$ and $\Psi^s = \Phi^s \Phi^{-1} = \left\{ \psi_j^s \right\}$.

It stresses to point out that the number of selected nearest neighboring points for a specified collocation point is far smaller than the total number of collocation points, namely, $n \ll N$. If we rewrite Eq. (3.26) in terms of the approximate solution $\tilde{u}(\mathbf{x}_j)$ at all of the collocation points, it has

$$\tilde{\mathbf{u}}^s = \Psi \mathbf{u}, \tag{3.27}$$

where Ψ is a $N \times N$ sparse matrix only having $N \times n$ nonzero elements. Substituting Eq. (3.27) into Eq. (3.1) yields

$$\begin{bmatrix} \Re\Psi \\ B_1\Psi \\ B_2\Psi \end{bmatrix} \tilde{\mathbf{u}} = [\mathbf{b}]. \tag{3.28}$$

Then, solving the above linear sparse system of equations, we get the approximate solutions $\tilde{u}$ at all of the collocation points. Comparing with the aforementioned global RBF collocation schemes, a wide variety of efficient sparse matrix solvers can be utilized to solve the localized RBF formulation of very large scale in a far more efficient manner.

Concerning the localized RBF methods, an important issue is an efficient algorithm to search the nearest neighboring source points surrounding a given collocation point from a large number of collocation points in a high-dimensional space. Lee et al. [15] defined an influence domain for each collocation point as the cut-off function, and then the nearest n neighbors of a given collocation point are located inside this influence domain. Chen and Yao [16, 17] employed the kd-tree algorithm [77, 78] for the method of approximate particular solutions (MAPS) to solve large-scale problems, for example, calcium dynamics in ventricular myocytes [79]. In computer science, there exist several other search algorithms to deal with this issue such as the quad-tree algorithm, the locality sensitive hashing algorithm [80], and the R-tree algorithm [81].

For reasons of limitations of space, we will only mention a few more RBF domain methods for numerical PDEs, such as the radial basis function network method [82, 83], global and local integrated radial basis function collocation

method [84, 85], the MQ quasi-interpolation method [86], the local MQ-DQ method [87–89], the RBF-FD method [90–93], the RBF pseudo-spectral method [94], and the radial point interpolation method [95, 96], the Hermite-type radial point interpolation method [97], and the subdomain RBF collocation method [98].

3.7 Numerical Experiments

In this section, we first investigate the accuracy, stability, and convergence rate of the Kansa method, the Hermite collocation method (HCM), and the modified Kansa method (MKM) for some benchmark examples. In the following, Aerr represents the L_2 absolute error, Lerr represents the L_2 relative error, which are defined as follows:

$$\text{Aerr} = \sqrt{\frac{1}{NT} \sum_{i=1}^{NT} \left(u(\mathbf{x}_i) - \tilde{u}(\mathbf{x}_i)\right)^2}, \tag{3.29}$$

$$\text{Lerr} = \sqrt{\frac{1}{NT} \sum_{i=1}^{NT} \left(\frac{u(\mathbf{x}_i) - \tilde{u}(\mathbf{x}_i)}{u(\mathbf{x}_i)}\right)^2}, \tag{3.30}$$

where NT is the total number of test points in the domain and on the boundary. In the following tests, the MQ-RBF $\phi(r) = \sqrt{r^2 + c^2}$ is chosen as the basis function.

First, we compare the convergence rate and stability of the three schemes in the unit square domain. Figure 3.1 shows the mixed-type boundary conditions covered by uniform and random collocation points, respectively. In this case, the MQ shape parameter $c = 16/\sqrt{N}$ is selected and the test point is 51×51 uniform mesh grid, namely, $NT = 2,601$.

Example 3.1: Consider the 2D Poisson equation in the unit square domain shown in Fig. 3.1

$$\Delta u = \left(3 + 4x^2\right)e^{x^2+y}, \mathbf{x} = (x, y) \in \Omega, \tag{3.31}$$

whose boundary conditions are assigned in terms of the analytical solution $u = e^{x^2+y}$. Γ_1 and Γ_2 shown in Fig. 3.1 denote Dirichlet and Neumann boundary conditions, respectively.

Figure 3.2 depicts the accuracy variation of these three methods with respect to the number of uniform and random collocation points. In all three methods, the numerical accuracy improved with the increasing number of collocation points N. We observe that the HCM numerical result is as accurate as the Kansa method. The MKM performs much better than both the Kansa method and the HCM using the same number of collocation points. Figure 3.3 shows the condition number Cond of the interpolation matrix $\mathbf{A} = \left[\mathbf{A}_{ij}\right]$ of the three methods verses the number
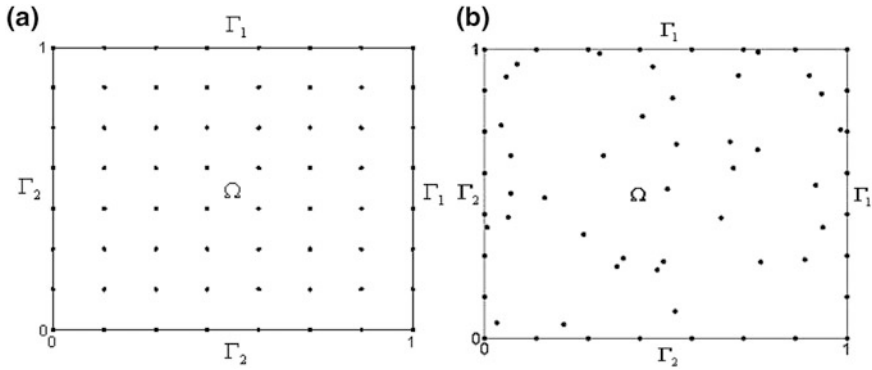
Fig. 3.1 Mixed-type boundary problem in square domain with (**a**) uniform and (**b**) random collocation points
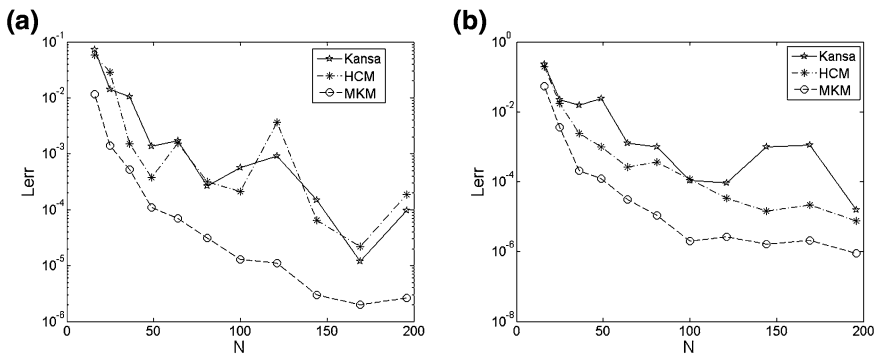

Fig. 3.2 Convergence rates with (**a**) uniform and (**b**) random collocation points in Example 3.1
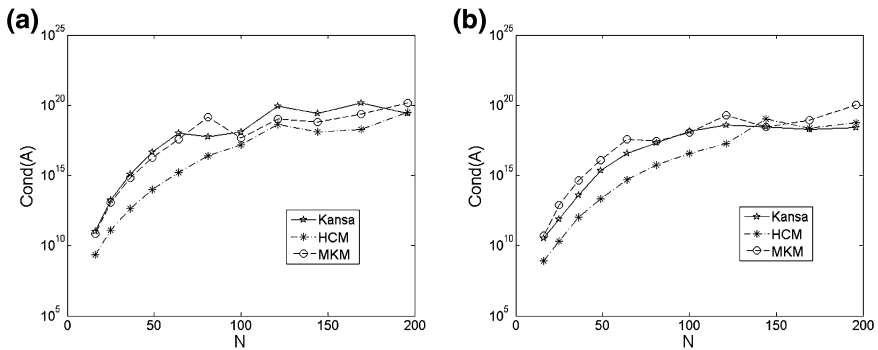

Fig. 3.3 Condition numbers with (**a**) uniform and (**b**) random collocation points in Example 3.1

of collocation points N. We can see that all the condition numbers of these three methods increase rapidly when N becomes large.

Example 3.2: Consider the following 2D modified Helmholtz equation in multi-connected domain shown in Fig. 3.4

$$(\Delta - 2)u = (2 - 4x)e^{-(x+y)}, \ \mathbf{x} = (x, y) \in \Omega. \tag{3.32}$$

The mixed-type boundary conditions can be easily derived from the analytical solution $u = x^2 e^{-(x+y)}$, where Γ_1 and Γ_2 shown in Fig. 3.4 denote Dirichlet and Neumann boundary conditions, respectively. In the numerical implementation, we choose MQ shape parameter $c = 12/\sqrt{N}$ and $NT = 1,510$.
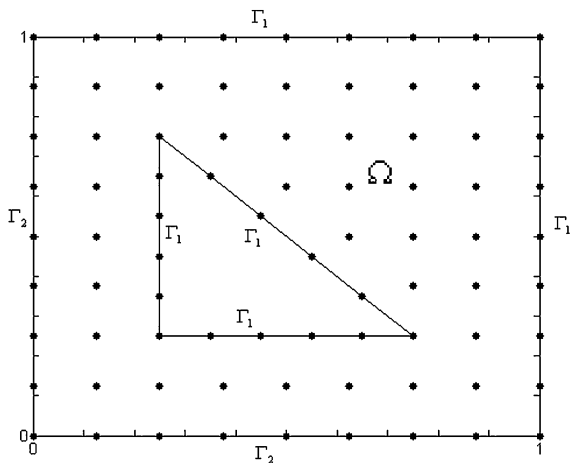
Figure 3.5 displays the convergence rates and condition number curves by these three schemes. Both the Kansa method and the HCM produce similar results. Although having the largest condition number, the MKM performs the most accurate solutions among these three schemes. The numerical accuracy of the MKM is almost one order of magnitude better than the other two schemes. Figure 3.6 shows the profile of the analytical solution and relative errors by these three RBF schemes. Figure 3.6b–d illustrates that the errors are smaller on the boundary and the maximum error appears in the boundary-adjacent region. Compared with the other two methods, it can be observed from Fig. 3.6 that the MKM obtains better accuracy at close-to-boundary nodes by almost one order of magnitude.

Example 3.3: Plate bending of the simply-supported unit square plate

The governing equation of a simply-supported thin plate under uniform loading is

$$\nabla^4 w = \frac{q_0}{D}, \tag{3.33}$$

Fig. 3.4 The profile of the multi-connected domain
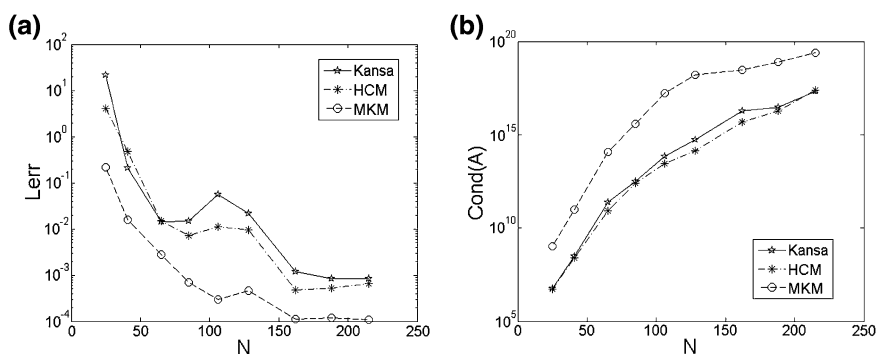
Fig. 3.5 (**a**) Accuracy and (**b**) condition numbers versus collocation points N in Example 3.2
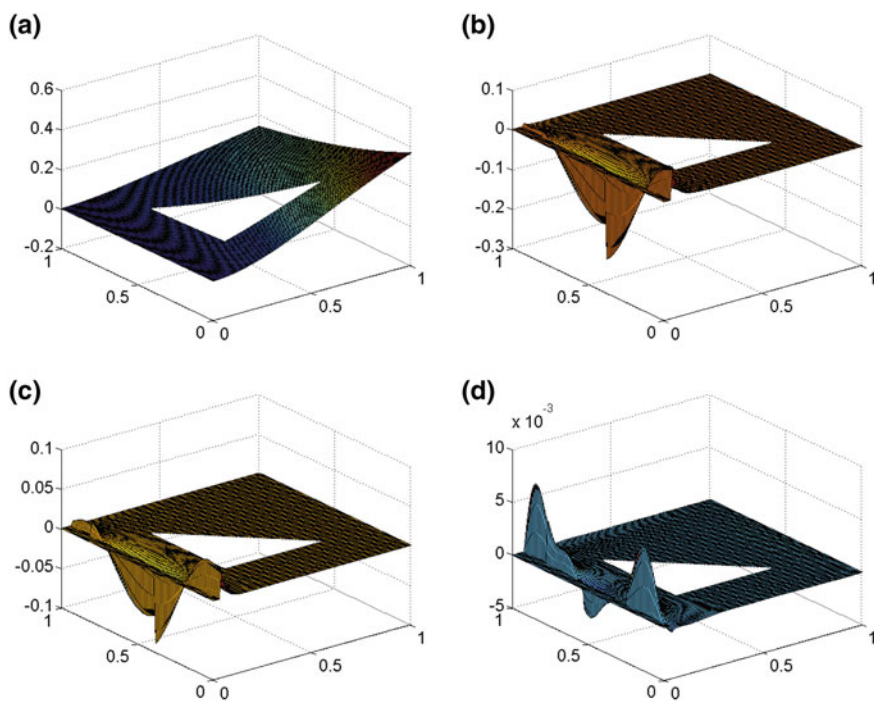

Fig. 3.6 (**a**) The profile of analytical solution. (**b–d**) The relative numerical errors of Kansa, HCM, and MKM, respectively

with boundary conditions

$$w = 0, \tag{3.34}$$

$$M_n = -D\left\{v\nabla^2 w + (1-v)\left(\cos^2\theta\frac{\partial^2 w}{\partial x^2} + \sin^2\theta\frac{\partial^2 w}{\partial y^2} + \sin 2\theta\frac{\partial^2 w}{\partial x\partial y}\right)\right\} = 0,$$
$$\tag{3.35}$$

where w represents the deflection of the middle surface of the plate, ∇^4 denotes the biharmonic operator, and $D = Eh^3/[12(1-v^2)]$ is the flexural rigidity of the plate, $n = [\cos\theta, \sin\theta]$ the unit outward normal vector. The parameter values are $E = 2.1 \times 10^{11}$, $h = 0.01$, $v = 0.3$, $q_0 = 10^6$. We choose MQ-RBF with shape parameter $c = 40/N_i$. This case study will also investigate convergence rate and stability.

Numerical accuracy variation of these three methods with respect to the number of unknown coefficients is shown in Fig. 3.7a. The numerical accuracy improves with the increasing number of points. We observe from Fig. 3.7a that the HCM achieves similar accuracy as the Kansa method, but eliminates the error oscillation with the increasing number of points. It is noted that the MKM obtains the most accurate results among these three methods. On the other hand, the condition numbers of interpolation matrixes increase rapidly with the increasing number of points. This ill-conditioning problem may affect the numerical stability of these RBF collocation methods. It is necessary to introduce the additional techniques to mitigate the effect of ill-conditioning as mentioned in Sect. 3.5.
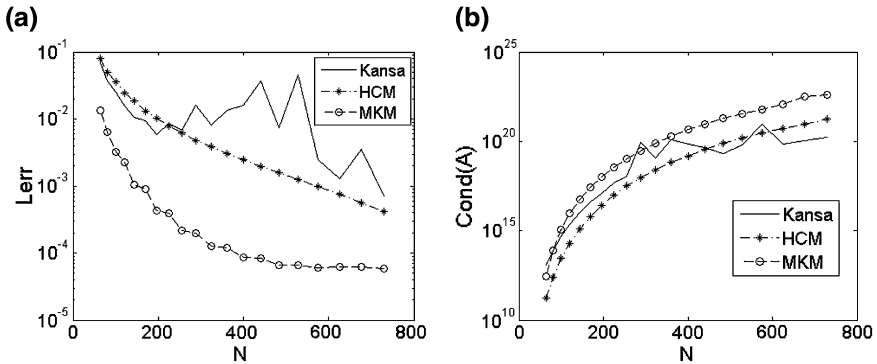

Fig. 3.7 (**a**) Numerical accuracy variations and (**b**) condition numbers versus the number of unknown coefficients in Example 3.3

Example 3.4: This example compares the method of approximate particular solutions (MAPS) with the Kansa method of a 2D convection–diffusion problem

$$\Delta u + \left(x^2 + y^2\right)u + y \, \cos(y)\frac{\partial u}{\partial x} + \sin h(x)\frac{\partial u}{\partial x} = f(x, y), \ (x, y) \in \Omega, \qquad (3.36)$$

$$u = R(x, y), \ (x, y) \in \Gamma, \qquad (3.37)$$

where the physical domain Ω is a star-shaped region as shown in Fig. 3.8 and its boundary is defined by the following parametric equation:

$$\Gamma = \{(x, y)|x = \rho \, \cos\theta, y = \rho \, \sin\theta, 0 \le \theta < 2\pi\}, \qquad (3.38)$$

in which $\rho = 1 + (\cos(4\theta))^2$. The given functions $f(x, y), R(x, y)$ are easily derived from the following analytical solution

$$u(x, y) = \sin(\pi x)\cosh(y) - \cos(\pi x)\sinh(y). \qquad (3.39)$$

Tsai et al. [99] employed a golden search method to find the good shape parameter c in the MQ RBF. Table 3.1 shows the comparison of the absolute errors Aerr by the MAPS and the Kansa method. The MAPS achieves the similar accuracy as the Kansa method using the same placement of the collocation points.

Example 3.5: Let us consider the localized RBF formulations in the solution of the following Poisson problem:

$$\begin{aligned}
\Delta u &= f(x, y), \ (x, y) \in \Omega \\
u &= R(x, y), \ (x, y) \in \partial\Omega
\end{aligned}, \qquad (3.40)$$

Fig. 3.8 Profiles of computational domain of Example 3.4 (Reprinted from Ref. [99], Copyright 2012, with permission from Elsevier)
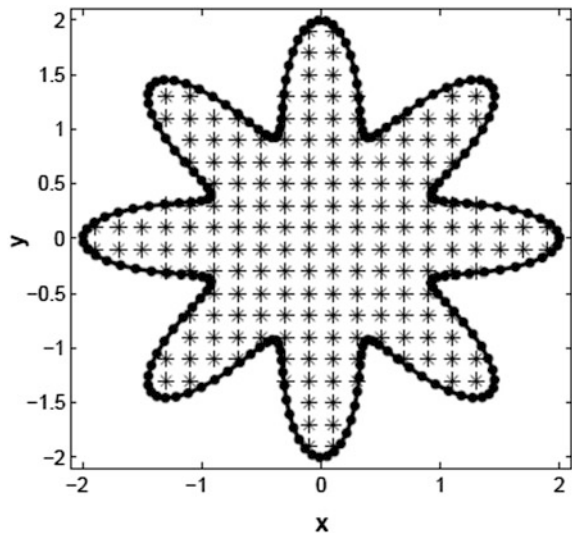
Table 3.1 Comparison of Aerr by the MAPS and the Kansa method for Example 3.4

N	N_i	MAPS		Kansa	
		Aerr	Optimal c	Aerr	Optimal c
213	113	1.68e−4	2.45	1.08e−4	2.94
313	193	4.74e−5	1.48	2.47e−5	2.17
401	261	2.48e−5	1.34	1.35e−5	1.89

where the physical domain Ω is a rectangular $[0, 1] \times [0, H]$. The given functions $f(x, y), R(x, y)$ are given based on the following analytical solution:

$$u(x, y) = \frac{1.25 + \cos(5.4y + 2.7)}{6\left(1 + (3x + 0.5)^2\right)} \tag{3.41}$$

In the numerical implementation, all the interior and boundary points are distributed uniformly. The number of internal nodes is $N = S_n^2(H - 1) + (S_n - 1)H$, and the number of boundary nodes is $N_i = 2(S_n - 1)(H + 1)$. n is the number of nearest neighbor points, and S_n denotes the number of partition in [0,1]. Table 3.2 lists numerical results obtained by the Localized Kansa method (LKM) and the Localized MAPS (LMAPS) using various number of nearest neighbor points and $H = 20, S_n = 25$. We observe that the LKM and the LMAPS have similar accuracy with the optimal shape parameter in Table 3.2. As n increases, the accuracy of the localized RBF formulations improves while the computational efficiency decreases. Therefore, $n = 9$ is fixed to apply the localized formulations to the large-scale problems with millions of points. Table 3.3 shows numerical errors of the LKM and the LMAPS with various values H for $n = 9, S_n = 30$. It should be mentioned that 30×30 uniform nodes are distributed inside $[0, 1] \times [i - 1, i], i = 1, \cdots, H$. Since the same collocation nodes in each square $[0, 1] \times [i - 1, i]$ are used, the optimal shape parameter c is stable and independent on H. From Table 3.3, it can be found that the localized methods can solve the problem with 900,000 interpolation points and obtain good accuracy. In Fig. 3.9 we present the errors Aerr with respect to the shape parameter c by the global MAPS (GMAPS) and the LMAPS with $n = 9, S_n = 10, H = 1$. In Fig. 3.9 the shape parameter c in the LMAPS is more stable than the GMAPS. Hence the

Table 3.2 Numerical results obtained by Localized Kansa and Localized MAPS with various number of nearest neighbor points using $S_n = 25, H = 20$ for Example 3.5

n	Localized MAPS		Localized Kansa (MQ)	
	Aerr	Optimal c	Aerr	Optimal c
7	9.46e−5	9.3	5.87e−5	0.8
9	5.88e−5	5.3	8.34e−5	0.5
11	1.10e−4	2.4	8.29e−5	0.4

Table 3.3 Numerical results obtained by Localized Kansa and Localized MAPS with various H values using $n = 9, S_n = 30$ for Example 3.5

N	H	Localized MAPS		Localized Kansa (MQ)	
		Aerr	*Optimal c*	Aerr	*Optimal c*
99,232	100	1.10e−4	1.6	5.96e−5	0.5
198,432	200	1.08e−4	1.6	5.97e−5	0.5
376,992	380	1.11e−4	1.6	5.99e−5	0.5
496,032	500	1.11e−4	1.6	5.98e−5	0.5
595,232	600	1.11e−4	1.6	5.99e−5	0.5
694,432	700	1.10e−4	1.6	5.98e−5	0.5
803,552	810	1.09e−4	1.6	5.97e−5	0.5
922,592	930	1.11e−4	1.6	5.98e−5	0.5

Fig. 3.9 The errors Aerr with respect to the shape parameter c by MAPS and Localized MAPS with $n = 9, S_n = 10, H = 1$ for Example 3.5 (Reprinted from Ref. [17], Copyright 2012, with permission from Elsevier)

LMAPS alleviates the difficulty of choosing the shape parameter c in the traditional RBF approaches. In this example it also reveals that the localized RBF formulation can provide highly accurate results for large-scale problems.

References

1. E.J. Kansa, Multiquadrics–A scattered data approximation scheme with applications to computational fluid-dynamics–II solutions to parabolic, hyperbolic and elliptic partial differential equations. Comput. Math. Appl. **19**(8–9), 147–161 (1990)
2. E.J. Kansa, Multiquadrics–A scattered data approximation scheme with applications to computational fluid-dynamics–I surface approximations and partial derivative estimates. Comput. Math. Appl. **19**(8–9), 127–145 (1990)
3. G.E. Fasshauer, Solving partial differential equations by collocation with radial basis functions. In: *Surface Fitting and Multiresolution Methods,* ed. by A. Mehaute, C. Rabut, L.L. Schumaker (Vanderbilt University Press, Nashville, 1997), pp. 131–138

4. A.L. Fedoseyev, M.J. Friedman, E.J. Kansa, Improved multiquadric method for elliptic partial differential equations via PDE collocation on the boundary. Comput. Math. Appl. **43**(3–5), 439–455 (2002)

5. C.S. Chen, Y.C. Hon, R.S. Schaback, Radial basis functions with scientific computation. Department of Mathematics, University of Southern Mississippi, Mississippi (2007)

6. C.S. Chen, A. Karageorghis, Y.S. Smyrlis, *The Method of Fundamental Solutions – A Meshless Method* (Dynamic Publishers, 2008)

7. C.S. Chen, C.M. Fan, P.H. Wen The method of particular solutions for solving certain partial differential equations. *Numerical Methods for Partial Differential Equations*, 28, 506–522 (2012)

8. S. Chantasiriwan, Investigation of the use of radial basis functions in local collocation method for solving diffusion problems. Int. Commun. Heat Mass Transfer **31**(8), 1095–1104 (2004)

9. B. Sarler, R. Vertnik, Meshfree explicit local radial basis function collocation method for diffusion problems. Comput. Math. Appl. **51**(8), 1269–1282 (2006)

10. R. Vertnik, B. Sarler, Meshless local radial basis function collocation method for convective-diffusive solid-liquid phase change problems. Int. J. Numer. Meth. Heat Fluid Flow **16**(5), 617–640 (2006)

11. E. Divo, A.J. Kassab, An efficient localized radial basis function Meshless method for fluid flow and conjugate heat transfer. J. Heat Transf. Trans. ASME **129**(2), 124–136 (2007)

12. B. Sarler, From global to local radial basis function collocation method for transport phenomena. Adv. Meshfree Techniq. **5**, 257–282 (2007)

13. G. Kosec, B. Sarler, Local RBF collocation method for Darcy flow. CMES Comput. Model. Eng. Sci. **25**(3), 197–207 (2008)

14. Y. Sanyasiraju, G. Chandhini, Local radial basis function based gridfree scheme for unsteady incompressible viscous flows. J. Comput. Phys. **227**(20), 8922–8948 (2008)

15. C.K. Lee, X. Liu, S.C. Fan, Local multiquadric approximation for solving boundary value problems. Comput. Mech. **30**, 396–409 (2003)

16. G.M. Yao, Local radial basis function methods for solving partial differential equations. Ph.D. Dissertation, University of Southern Mississippi (2010)

17. G.M. Yao, J. Kolibal, C.S. Chen, A localized approach for the method of approximate particular solutions. Comput. Math. Appl. **61**, 2376–2387 (2011)

18. G.R. Liu, Y.T. Gu, A local radial point interpolation method (LRPIM) for free vibration analyses of 2-D solids. J. Sound Vib. **246**(1), 29–46 (2001)

19. J. Wertz, E.J. Kansa, L. Ling, The role of the multiquadric shape parameters in solving elliptic partial differential equations. Comput. Math. Appl. **51**(8), 1335–1348 (2006)

20. W. Chen, L.J. Ye, H.G. Sun, Fractional diffusion equations by the Kansa method. Comput. Math. Appl. **59**(5), 1614–1620 (2010)

21. M. Kindelan, F. Bernal, P. Gonzalez-Rodriguez, M. Moscoso, Application of the RBF Meshless method to the solution of the radiative transport equation. J. Comput. Phys. **229**(5), 1897–1908 (2010)

22. E.J. Kansa, R.C. Aldredge, L. Ling, Numerical simulation of two-dimensional combustion using mesh-free methods. Eng. Anal. Boundary Elem. **33**(7), 940–950 (2009)

23. Y. Zhang, K.R. Shao, Y.G. Guo, J.G. Zhu, D.X. Xie, J.D. Lavers, An improved multiquadric collocation method for 3-D electromagnetic problems. IEEE Trans. Magn. **43**(4), 1509–1512 (2007)

24. Y. Duan, P.F. Tang, T.Z. Huang, S.J. Lai, Coupling projection domain decomposition method and Kansa's method in electrostatic problems. Comput. Phys. Commun. **180**(2), 209–214 (2009)

25. S. Chantasiriwan, Multiquadric collocation method for time-dependent heat conduction problems with temperature-dependent thermal properties. J. Heat Transf. Trans. ASME **129**(2), 109–113 (2007)

26. X. Zhou, Y.C. Hon, K.F. Cheung, A grid-free, nonlinear shallow-water model with moving boundary. Eng. Anal. Boundary Elem. **28**(8), 967–973 (2004)

27. A.J.M. Ferreira, C.M.C. Roque, P. Martins, Radial basis functions and higher-order shear deformation theories in the analysis of laminated composite beams and plates. Compos. Struct. **66**(1–4), 287–293 (2004)
28. A.J.M. Ferreira, C.M.C. Roque, R.M.N. Jorge, Static and free vibration analysis of composite shells by radial basis functions. Eng. Anal. Boundary Elem. **30**(9), 719–733 (2006)
29. C.M.C. Roque, A.J.M. Ferreira, R.M.N. Jorge, A radial basis function approach for the free vibration analysis of functionally graded plates using a refined theory. J. Sound Vib. **300**(3–5), 1048–1070 (2007)
30. P.H. Wen, Y.C. Hon, Geometrically nonlinear analysis of Reissner-Mindlin plate by Meshless computation. CMES Comput. Model. Eng. Sci. **21**, 177–191 (2007)
31. H.J. Al-Gahtani, M. Naffa'a, RBF meshless method for large deflection of thin plates with immovable edges. Eng. Anal. Boundary Elem. **33**(2), 176–183 (2009)
32. S. Xiang, K.M. Wang, Free vibration analysis of symmetric laminated composite plates by trigonometric shear deformation theory and inverse multiquadric RBF. Thin Walled Struct. **47**(3), 304–310 (2009)
33. S. Chantasiriwan, Performance of multiquadric collocation method in solving lid-driven cavity flow problem with low Reynolds number. CMES Comput. Model. Eng. Sci. **15**(3), 137–146 (2006)
34. I. Kovacevic, A. Poredos, B. Sarler, Solving the Stefan problem with the radial basis function collocation mehod. Nume. Heat Transf. Part B Fundament. **44**(6), 575–599 (2003)
35. L. Vrankar, E.J. Kansa, L. Ling, F. Runovc, G. Turk, Moving-boundary problems solved by adaptive radial basis functions. Comput. Fluids **39**(9), 1480–1490 (2010)
36. Y. Liu, K.M. Liew, Y.C. Hon, X. Zhang, Numerical simulation and analysis of an electroactuated beam using a radial basis function. Smart Mater. Struct. **14**(6), 1163–1171 (2005)
37. J. Li, Y. Chen, D. Pepper, Radial basis function method for 1-D and 2-D groundwater contaminant transport modeling. Comput. Mech. **32**(1–2), 10–15 (2003)
38. J.C. Li, C.S. Chen, Some observations on unsymmetric radial basis function collocation methods for convection-diffusion problems. Int. J. Numer. Meth. Eng. **57**(8), 1085–1094 (2003)
39. B. Sarler, J. Perko, C.S. Chen, Radial basis function collocation method solution of natural convection in porous media. Int. J. Numer. Meth. Heat Fluid Flow **14**(2), 187–212 (2004)
40. P.P. Chinchapatnam, K. Djidjeli, P.B. Nair, Unsymmetric and symmetric meshless schemes for the unsteady convection-diffusion equation. Comput. Methods Appl. Mech. Eng. **195**(19–22), 2432–2453 (2006)
41. Y.C. Hon, R. Schaback, On unsymmetric collocation by radial basis functions. Appl. Math. Comput. **119**(2–3), 177–186 (2001)
42. V.M.A. Leitao, RBF-based meshless methods for 2D elastostatic problems. Eng. Anal. Boundary Elem. **28**(10), 1271–1281 (2004)
43. A. LaRocca, A.H. Rosales, H. Power, Symmetric radial basis function meshless approach for time dependent PDEs. Boundary Elements **Xxvi**(19), 81–90 (2004)
44. A. La Rocca, H. Power, V. La Rocca, M. Morale, A meshless approach based upon radial basis function hermite collocation method for predicting the cooling and the freezing times of foods. CMC Comput. Mater. Continua **2**(4), 239–250 (2005)
45. A. La Rocca, A.H. Rosales, H. Power, Radial basis function Hermite collocation approach for the solution of time dependent convection-diffusion problems. Eng. Anal. Boundary Elem. **29**(4), 359–370 (2005)
46. A.H. Rosales, A. La Rocca, H. Power, Radial basis function Hermite collocation approach for the numerical simulation of the effect of precipitation inhibitor on the crystallization process of an over-saturated solution. Numer. Methods Partial Differ. Eq. **22**(2), 361–380 (2006)
47. M. Naffa, H.J. Al-Gahtani, RBF-based meshless method for large deflection of thin plates. Eng. Anal. Boundary Elem. **31**(4), 311–317 (2007)
48. E. Larsson, B. Fornberg, A numerical study of some radial basis function based solution methods for elliptic PDEs. Comput. Math. Appl. **46**(5–6), 891–902 (2003)

49. X. Zhang, K.Z. Song, M.W. Lu, X. Liu, Meshless methods based on collocation with radial basis functions. Comput. Mech. **26**, 333–343 (2000)
50. W. Chen, New RBF collocation schemes and kernel RBFs with applications. Lect. Notes Comput. Sci. Eng. **26**, 75–86 (2002)
51. K.E. Atkinson, The numerical evaluation of particular solutions for Poisson's equation. IMA J. Numer. Anal. **5**, 319–338 (1985)
52. M.A. Golberg, A.S. Muleshkov, C.S. Chen, A.H.D. Cheng, Polynomial particular solutions for certain partial differential operators. Numer. Methods Partial Differ. Eq. **19**(1), 112–133 (2003)
53. C.S. Chen, M.A. Golberg, The method of fundamental solutions for potential, Helmholtz and diffusion problems, in *Boundary Integral Method-Numerical and Mathematical Aspects*, ed. by M.A. Golberg (Computational Mechanics Publications, Southampton, 1998), pp. 103–176
54. G. Yao, C.H. Tsai, W. Chen, The comparison of three meshless methods using radial basis functions for solving fourth-order partial differential equations. Eng. Anal. Boundary Elem. **34**(7), 625–631 (2010)
55. M. Li, W. Chen, C.H. Tsai, A regularization method for the approximate particular solution of nonhomogeneous Cauchy problems of elliptic partial differential equations with variable coefficients. Eng. Anal. Boundary Elem. **36**(3), 274–280 (2012)
56. P. Hansen, Regularization tools: a matlab package for analysis and solution of discrete ill-posed problems. Numer. Algor. **6**(1), 1–35 (1994)
57. P.A. Ramachandran, Method of fundamental solutions: singular value decomposition analysis. Commun. Numer. Methods Eng. **18**(11), 789–801 (2002)
58. T. Wei, Y.C. Hon, L.V. Ling, Method of fundamental solutions with regularization techniques for Cauchy problems of elliptic operators. Eng. Anal. Boundary Elem. **31**(4), 373–385 (2007)
59. A. Emdadi, E.J. Kansa, N.A. Libre, M. Rahimian, M. Shekarchi, Stable PDE solution methods for large multiquadric shape parameters. CMES Comput. Model. Eng. Sci. **25**(1), 23–41 (2008)
60. G.E. Fasshauer, Solving differential equations with radial basis functions: multilevel methods and smoothing. Adv. Comput. Math. **11**, 139–159 (1999)
61. Y.C. Hon, R.S. Schaback, X. Zhou, An adaptive greedy algorithm for solving large RBF collocation problems. Numer. Algor. **32**(1), 13–25 (2003)
62. R.S. Schaback, L. Ling, Stable and convergent unsymmetric meshless collocation methods. SIAM J. Numer. Anal. **46**, 1097–1115 (2008)
63. C.S. Huang, C.F. Lee, A.H.D. Cheng, Error estimate, optimal shape factor, and high precision computation of multiquadric collocation method. Eng. Anal. Boundary Elem. **31**(7), 614–623 (2007)
64. D. Brown, L. Ling, E. Kansa, J. Levesley, On approximate cardinal preconditioning methods for solving PDEs with radial basis functions. Eng. Anal. Boundary Elem. **29**(4), 343–353 (2005)
65. L.V. Ling, E.J. Kansa, A least-squares preconditioner for radial basis functions collocation methods. Adv. Comput. Math. **23**(1–2), 31–54 (2005)
66. Y.J. Liu, N. Nishimura, Z.H. Yao, A fast multipole accelerated method of fundamental solutions for potential problems. Eng. Anal. Boundary Elem. **29**(11), 1016–1024 (2005)
67. J.C. Carr, R.K. Beatson, J.B. Cherrie, T.J. Mitchell, W.R. Fright, B.C. McCallum, T.R. Evans, Reconstruction and representation of 3D objects with radial basis functions. SIGGRAPH '01 Proceedings of 28th annual conference on computer graphics and interactive techniques, ACM New York, 67–76 (2001)
68. M. Bebendorf, *Hierarchical Matrices: A Means to Efficiently Solve Elliptic Boundary Value Problems* (Springer, Berlin, 2008)
69. J.C. Li, Y.C. Hon, Domain decomposition for radial basis meshless methods. Numer. Methods Partial Differ. Eq. **20**(3), 450–462 (2004)

70. E. Divo, A. Kassab, Iterative domain decomposition meshless method modeling of incompressible viscous flows and conjugate heat transfer. Eng. Anal. Boundary Elem. **30**(6), 465–478 (2006)

71. H. Adibi, J. Es'haghi, Numerical solution for biharmonic equation using multilevel radial basis functions and domain decomposition methods. Appl. Math. Comput. **186**(1), 246–255 (2007)

72. P.P. Chinchapatnam, K. Djidjeli, P.B. Nair, Domain decomposition for time-dependent problems using radial based meshless methods. Numer. Methods Partial Differ. Eq. **23**(1), 38–59 (2007)

73. G. Gutierrez, W. Florez, Comparison between global, classical domain decomposition and local, single and double collocation methods based on RBF interpolation for solving convection-diffusion equation. Int. J. Mod. Phys. C **19**(11), 1737–1751 (2008)

74. P. Gonzalez-Casanova, J.A. Munoz-Gomez, G. Rodriguez-Gomez, Node adaptive domain decomposition method by radial basis functions. Numer. Methods Partial Differ. Eq. **25**(6), 1482–1501 (2009)

75. J.R. Phillips, J. White, A precorrected-FFT method for electrostatic analysis of complicated 3-D structures. IEEE Trans. Comput. Aided Des. Integr. Circuits Syst. **16**(10), 1059–1072 (1997)

76. M. Bebendorf, S. Rjasanow, Adaptive low-rank approximation of collocation matrices. Computing **70**(1), 1–24 (2003)

77. J.L. Bentley, Multidimensional divide and conquer. Commun. ACM **23**, 214–229 (1980)

78. S.M. Omohundro, Efficient algorithms with neural network behaviour. J. Complex Syst. **1**, 273–347 (1987)

79. G.M. Yao, Z.Y. Yu, A localized meshless approach for modeling spatial-temporal calcium dynamics in ventricular myocytes. Int. J. Numer. Meth. Biomed. Eng. **28**(2), 187–204 (2011)

80. P. Indyk, R. Motwani, Approximate nearest neighbors: towards removing the curse of dimensionality. In: the 30th Annual ACM Symposium on Theory of Computing, 1998, pp. 604–613

81. A. Guttman, R-trees: a dynamic index structure for spatial searching. In: The International Conference of Management of Data (ACM SIGMOD) (ACM Press, 1984), pp. 47–57

82. L. Mai-Cao, T. Tran-Cong, A meshless IRBFN-based method for transient problems. CMES Comput. Model. Eng. Sci. **7**(2), 149–171 (2005)

83. N. Mai-Duy, A. Khennane, T. Tran-Cong, Computation of laminated composite plates using integrated radial basis function networks. CMC Comput. Mater. Continua **5**(1), 63–77 (2007)

84. N. Mai-Duy, T. Tran-Cong, A multidomain integrated radial basis function collocation method for elliptic problems. Numer. Methods Partial Differ. Eq. **24**, 1301–1320 (2008)

85. N. Mai-Duy, T. Tran-Cong, Compact local integrated-RBF approximations for second-order elliptic differential problems. J. Comput. Phys. **230**(12), 4772–4794 (2011)

86. R.H. Chen, Z.M. Wu, Solving hyperbolic conservation laws using multiquadric quasi-interpolation. Numer. Methods Partial Differ. Eq. **22**(4), 776–796 (2006)

87. C. Shu, H. Ding, K.S. Yeo, Local radial basis function-based differential quadrature method and its application to solve two-dimensional incompressible Navier-Stokes equations. Comput. Methods Appl. Mech. Eng. **192**, 941–954 (2003)

88. S. Quan, Local RBF-based differential quadrature collocation method for the boundary layer problems. Eng. Anal. Boundary Elem. **34**(3), 213–228 (2010)

89. C. Shu, H. Ding, H.Q. Chen, T.G. Wang, An upwind local RBF-DQ method for simulation of inviscid compressible flows. Comput. Methods Appl. Mech. Eng. **194**(18–20), 2001–2017 (2005)

90. G.B. Wright, B. Fornberg, Scattered node compact finite difference-type formulas generated from radial basis functions. J. Comput. Phys. **212**(1), 99–123 (2006)

91. V. Bayona, M. Moscoso, M. Kindelan, Optimal constant shape parameter for multiquadric based RBF-FD method. J. Comput. Phys. **230**(19), 7384–7399 (2011)

92. V. Bayona, M. Moscoso, M. Carretero, M. Kindelan, RBF-FD formulas and convergence properties. J. Comput. Phys. **229**(22), 8281–8295 (2010)
93. N. Flyer, B. Fornberg, Radial basis functions: developments and applications to planetary scale flows. Comput. Fluids **46**(1), 23–32 (2011)
94. G.B. Wright, N. Flyer, D.A. Yuen, A hybrid radial basis function–pseudospectral method for thermal convection in a 3-D spherical shell. Geochem. Geophys. Geosyst. **11**(7), n/a-n/a (2010)
95. G.R. Liu, L. Yan, J.G. Wang, Y.T. Gu, Point interpolation method based on local residual formulation using radial basis functions. Struct. Eng. Mech. **14**(6), 713–732 (2002)
96. J.G. Wang, G.R. Liu, A point interpolation meshless method based on radial basis functions. Int. J. Numer. Meth. Eng. **54**(11), 1623–1648 (2002)
97. Y. Liu, Y.C. Hon, K.M. Liew, A meshfree Hermite-type radial point interpolation method for Kirchhoff plate problems. Int. J. Numer. Meth. Eng. **66**(7), 1153–1178 (2006)
98. J.-S. Chen, L. Wang, H.-Y. Hu, S.-W. Chi, Subdomain radial basis collocation method for heterogeneous media. Int. J. Numer. Meth. Eng. **80**(2), 163–190 (2009)
99. C.H. Tsai, J. Kolibal, M. Li, The golden section search algorithm for finding a good shape parameter for meshless collocation methods. Eng. Anal. Boundary Elem. **34**, 738–746 (2010)

Chapter 4
Boundary-Type RBF Collocation Methods

Abstract The mesh generation in the standard BEM is still not trivial as one may imagine, especially for high-dimensional moving boundary problems. To overcome this difficulty, the boundary-type RBF collocation methods have been proposed and endured a fast development in the recent decade thanks to being integration-free, spectral convergence, easy-to-use, and inherently truly meshless. First, this chapter introduces the basic concepts of the method of fundamental solutions (MFS). Then a few recent boundary-type RBF collocation schemes are presented to tackle the issue of the fictitious boundary in the MFS, such as boundary knot method (BKM), regularized meshless method, and singular boundary method. Following this, an improved multiple reciprocity method (MRM), the recursive composite MRM (RC-MRM), is introduced to establish a boundary-only discretization of nonhomogeneous problems. Finally, numerical demonstrations show the convergence rate and stability of these boundary-type RBF collocation methods for several benchmark examples.

During the past two decades we have witnessed a research boom on the boundary-type meshless techniques since the construction of a mesh in the standard BEM is not trivial. Among the typical techniques are the boundary node method, the local boundary integral equation method, the boundary cloud method, the boundary point method, the boundary point interpolation method (BPIM), and the method of fundamental solutions (MFS). The essence of all these techniques, excluding the MFS and BPIM, is basically a combination of the moving least square (MLS) technique with various boundary element schemes, whereas the MFS is a boundary-type RBF collocation scheme.

Such MLS-based methods involve singular integration and are mathematically complicated, and their low-order approximations also depress computational efficiency. The numerical integration requires a background mesh, and thus the

methods of this type are not truly meshless. In addition, accurate numerical integration of kernel transcendental functions is computationally very expensive.

In contrast, the boundary-type RBF collocation methods are integration-free, spectral convergence, easy-to-use, and inherently truly meshless. This chapter is aimed at a survey of the latest advances regarding these numerical schemes. The MFS [1] is a popular boundary-type RBF collocation method in the past two decades, which distributes the source nodes on fictitious boundary outside the physical domain to avoid the singularities of fundamental solutions. However, such a fictitious boundary is often arbitrary and hinders its practical applicability. In the case of complex-shaped boundary and multiple connected domain problems, a tricky placement of source knots in terms of boundary conditions and geometry is required and often leads to severe ill-conditioning of the resulting interpolation matrix and even failure of numerical solution.

The boundary knot method (BKM) [2] was proposed as an alternative boundary-type RBF collocation method to overcome the artificial boundary issue in the MFS, in which the nonsingular RBF general solutions are employed to replace the singular fundamental solutions. However, the BKM encounters severely ill-conditioned interpolation matrix as the MFS and cannot apply to the problems whose general solutions do not exist. Young et al. [3–5] proposed an alternative meshless method, namely the regularized meshless method (RMM), to remedy this drawback of the MFS. By employing the desingularization of subtracting and adding-back technique, the RMM can place the source points on the real physical boundary. In addition, the ill-conditioned interpolation matrix of the MFS is also circumvented in the RMM. However, the original RMM requires the uniform distribution of nodes and severely reduces its applicability to complex-shaped boundary problems. Similar to the RMM, Sarler [6] proposes the modified method of fundamental solutions (MMFS) to solve potential flow problems. However, the MMFS demands a complicate calculation of the diagonal elements of interpolation matrix. Recently, Chen and his research group [7, 8] introduced an inverse interpolation technique (IIT) to regularize the singularities of the fundamental solutions upon the coincidence of the source and collocation points, which named as origin intensity factors or source intensity factors, and then proposed a novel improved RBF formulation, the singular boundary method (SBM). This method has better accuracy than the RMM and the MMFS. Recently, some analytical formulas were also derived to accurately calculate the origin intensity factors of the SBM.

For nonhomogeneous problems, the boundary-type RBF collocation methods should be combined with an additional technique to evaluate the particular solution. The dual reciprocity method (DRM) [9] and multiple reciprocity method (MRM) [10] have emerged as two promising particular solution techniques. The DRM has become de facto the method of choice in conjunction with boundary-type RBF collocation methods to evaluate the particular solutions. However, it requires the inner nodes to guarantee the convergence and stability in the calculation of the particular solution. The MRM has the advantage over the DRM in that it does not demand using inner nodes at all. However, comparing to the DRM, the

MRM has more restrictions in that the standard MRM is computationally much more expensive in the construction of the different interpolation matrices by using high-order fundamental or general solutions [11, 12] and has limited applicability for general nonhomogeneous problems due to its conventional use of high-order Laplacian operators in the annihilation process. To remedy this problem, an improved MRM, the recursive composite multiple reciprocity method (RC-MRM) [13], has been proposed to handle various nonhomogeneous terms in the governing equation.

To clearly illustrate these approaches, without loss of generality, we consider the following problem

$$\Re\{u\} = f(\mathbf{x}), \qquad \mathbf{x} \in \Omega \subset R^n, \tag{4.1}$$

$$u(\mathbf{x}) = R(\mathbf{x}), \qquad \mathbf{x} \in \Gamma_1, \tag{4.2}$$

$$\frac{\partial u(\mathbf{x})}{\partial n} = N(\mathbf{x}), \quad \mathbf{x} \in \Gamma_2 \tag{4.3}$$

where $\Re$ is a differential operator, Ω is a bounded and connected domain, $\Gamma_1 \cup \Gamma_2 = \partial\Omega$, $\Gamma_1 \cap \Gamma_2 = \varnothing$. $f(\mathbf{x}), R(\mathbf{x})$, and $N(\mathbf{x})$ are known functions.

4.1 Homogeneous Problems

First we consider the homogeneous PDE, namely, $\Delta u = 0$ in (4.1). The governing equation (4.1) becomes

$$\Re\{u\} = 0, \quad \mathbf{x} \in \Omega. \tag{4.4}$$

For homogeneous problem (4.4), (4.2), and (4.3), the following section will introduce several efficient and accurate boundary-type RBF collocation schemes which attract growing attention and appear promising in some areas.

4.1.1 The Method of Fundamental Solutions

The MFS was first proposed by Kupradze and Aleksidze [1] which is also known as the regular BEM, the superposition method [14], desingularized method [15], and the charge simulation method [16], to name just a few.

Since the MFS utilizes the fundamental solutions $\phi_F(\mathbf{x})$ which satisfy the governing differential equation of interest, the approximate solution $\tilde{u}(\mathbf{x})$ can be expressed only in terms of boundary knots

$$u(\mathbf{x}) \approx \tilde{u}(\mathbf{x}) = \sum_{j=1}^{N} a_j \phi_F \left(\left\| \mathbf{x} - \mathbf{s}_j \right\|_2 \right), \quad \mathbf{x} \in \Omega, \tag{4.5}$$

where $\tilde{u}(\mathbf{x})$ is the approximate solution, $\left\{ \mathbf{s}_j \right\}_{j=1}^{N}$ are the source points located on the fictitious boundary outside the domain to avoid the singularities of the fundamental solutions, $\{a_j\}$ the unknown coefficients to be determined. Let $\left\{ \mathbf{x}_j \right\}_{j=1}^{N_1} \in \Gamma_1$, $\left\{ \mathbf{x}_j \right\}_{j=N_1+1}^{N_1+N_2+1} \in \Gamma_2$ be the collocation knots on the physical boundary $\partial\Omega$. A list of commonly used fundamental solutions is shown in Sect. 2.3.1. By the collocation method, we have

$$
\begin{aligned}
R(\mathbf{x}_i) &= \sum_{j=1}^{N} a_j \phi_F(\left\| \mathbf{x}_i - \mathbf{s}_j \right\|_2), i = 1, 2, \cdots, N_1, \\
N(\mathbf{x}_i) &= \sum_{j=1}^{N} a_j \frac{\partial}{\partial n} \phi_F(\left\| \mathbf{x}_i - \mathbf{s}_j \right\|_2), i = N_1 + 1, N_1 + 2, \cdots, N.
\end{aligned}
\tag{4.6}
$$

The MFS interpolation matrix can be of the following form

$$\mathbf{A} = \begin{bmatrix} \Phi_F \\ \frac{\partial}{\partial n} \Phi_F \end{bmatrix}, \tag{4.7}$$

where $\Phi_F = \left(\phi_F \left(\left\| \mathbf{x}_i - \mathbf{s}_j \right\|_2 \right) \right)_{1 \leq i,j \leq N}$.

The MFS is a simple and efficient scheme and has been widely applied to various engineering and science problems, such as heat conduction [17–19], acoustics [20, 21], diffusion–reaction [22, 23], axisymmetric elasticity [24], stokes problem [25–28], and free vibration [29–31], just to mention a few. Furthermore, Smyrlis and Karageorghis [32–36], Drombosky [37], Marin [38], and Lin et al. [39] presented some fundamental theoretical analysis about the MFS. More details about the MFS can be found from an excellent review report by Fairweather and Karageorghis [40, 41], and editorial book by Liu [42] and Chen et al. [6].

4.1.2 The Boundary Knot Method

Despite the great effort of past several decades, the placement of the fictitious boundary outside the physical domain in the MFS remains a perplexing issue when one deals with complex-shaped boundary or multiconnected domain problems. It is noted that the location of the fictitious boundary is vital to the accuracy of the MFS solution. Therefore, great attention is paid to the placement of fictitious boundary or simple eliminations.

The BKM, proposed by Chen [2], surpasses the MFS in that it employs the nonsingular RBF general solutions instead of the singular fundamental solutions and thus no longer requires the troublesome fictitious boundary. Namely, the BKM

places both source and collocation knots on the physical boundary. The BKM interpolation formula can be written as follows

$$\tilde{u}(\mathbf{x}) = \sum_{j=1}^{N} a_j \phi_G\big(\|\mathbf{x} - \mathbf{x}_j\|_2\big), \quad \mathbf{x} \in \Omega, \tag{4.8}$$

where $\phi_G(\mathbf{x})$ is RBF general solutions satisfying the governing equation. Let $\{\mathbf{x}_j\}$ be the N collocation knots on the physical boundary $\Gamma = \partial\Omega$. The BKM differs from the MFS in that nonsingular RBF general solutions are employed to replace singular fundamental solutions as the interpolation basis functions and thus avoids the fictitious boundary at all. The BKM keeps all the features of the MFS which are meshless, integration-free, and easy-to-use. Chen [43] also proposed a symmetrical BKM as follows

$$\tilde{u}(\mathbf{x}) = \sum_{j=1}^{N_1} a_j \phi_G\big(\|\mathbf{x} - \mathbf{x}_j\|_2\big) - \sum_{j=N_1+1}^{N} a_j \frac{\partial \phi_G\big(\|\mathbf{x} - \mathbf{x}_j\|_2\big)}{\partial n}. \tag{4.9}$$

The above formulation will result in a symmetric BKM interpolation matrix for self-adjoint equation problems with mixed boundary conditions. The BKM has been applied to various problems such as Helmholtz [44], convection–diffusion [45, 46], membrane vibration [47], plate vibration [48]. The key issue in the BKM is to construct the nonsingular RBF general solutions satisfying the governing equation, which has been discussed in Sect. 2.3.2. It should be mentioned that the nonsingular RBF general solutions are not available in some cases. For instance, the Laplace equation has no suitable nonsingular RBF general solution. As a result, some remedies have been proposed, such as the translate-invariant 2D harmonic functions by Hon and Wu [49] and the nonsingular general solutions of Helmholtz-like equations by Chen et al. [3].

4.1.3 The Regularized Meshless Method

It is a difficult task to find efficient RBF nonsingular general solutions for certain PDEs. Another strategy is to remain using the singular fundamental solution without the fictitious boundary. Young et al. [3–5] proposed an alternative RBF collocation meshless method, called RMM. The method uses the outward normal derivative of fundamental solutions $\partial\phi_F/\partial n_s$ at source points $\{\mathbf{s}_j\}$ as the interpolation basis functions, also called double-layer potentials in the MFS literatures [3–5]. Similar to the MFS and BKM, the corresponding approximate formulations can be expressed by

$$\tilde{u}(\mathbf{x}) = \sum_{j=1}^{N} a_j \frac{\partial \phi_F \left(\left\| \mathbf{x} - \mathbf{s}_j \right\|_2 \right)}{\partial n_s}, \ \mathbf{x} \in \Omega, \tag{4.10}$$

$$\tilde{q}(\mathbf{x}) = \frac{\partial \tilde{u}(\mathbf{x})}{\partial n} = \sum_{j=1}^{N} a_j \frac{\partial}{\partial n} \left(\frac{\partial \phi_F \left(\left\| \mathbf{x} - \mathbf{s}_j \right\|_2 \right)}{\partial n_s} \right), \ \mathbf{x} \in \Omega, \tag{4.11}$$

where n_s denotes the unit outward normal at source point $\{\mathbf{s}_j\}$ on the boundary.

As an example, we consider the potential problem. The differential operator in Eq. (4.4) is the Laplace operator Δ, and its 2D fundamental solution is $\ln(r_{ij})$. Then the corresponding kernel functions in Eqs. (4.10) and (4.11) can be represented as follows

$$M \left(\left\| \mathbf{x}_i - \mathbf{s}_j \right\|_2 \right) = \frac{\partial \phi_F \left(\left\| \mathbf{x}_i - \mathbf{s}_j \right\|_2 \right)}{\partial n_s} = - \frac{\left\langle (\mathbf{x}_i - \mathbf{s}_j), (\mathbf{n}_s)_j \right\rangle}{r_{ij}^2}, \tag{4.12}$$

$$T \left(\left\| \mathbf{x}_i - \mathbf{s}_j \right\|_2 \right) = \frac{\partial}{\partial n} \left(\frac{\partial \phi_F \left(\left\| \mathbf{x}_i - \mathbf{s}_j \right\|_2 \right)}{\partial n_s} \right)$$
$$= \frac{2 \left\langle (\mathbf{x}_i - \mathbf{s}_j), (\mathbf{n}_s)_j \right\rangle \left\langle (\mathbf{x}_i - \mathbf{s}_j), (\mathbf{n})_i \right\rangle}{r_{ij}^4} - \frac{(\mathbf{n}_s)_j (\mathbf{n})_i^T}{r_{ij}^2}, \tag{4.13}$$

where the notation $\langle \cdot, \cdot \rangle$ denotes the inner product of vectors. Apparently, when the collocation point $\mathbf{x}_i$ approaches the source point $\mathbf{s}_j$, Eqs. (4.12) and (4.13) tend to be singular and even hyper-singular. By subtracting and adding-back regularization technique, the following null-field integral equations can be employed to remove the singularities in Eqs. (4.12) and (4.13)

$$\int_{\Gamma} M^{(E)} \left(\mathbf{x}_i^{(E)}, \mathbf{s} \right) d\Gamma(\mathbf{s}) = 0, \quad \mathbf{x}_i^{(E)} \in D^{(E)}, \tag{4.14}$$

$$\int_{\Gamma} T^{(E)} \left(\mathbf{x}_i^{(E)}, \mathbf{s} \right) d\Gamma(\mathbf{s}) = 0, \quad \mathbf{x}_i^{(E)} \in D^{(E)}, \tag{4.15}$$

where the superscript (E) denotes the exterior domain. When the point $\mathbf{x}_i^{(E)}$ approaches the collocation point $\mathbf{x}_i$, Eqs. (4.14) and (4.15) can be discretized as follows

$$\sum_{j=1}^{N} M^{(E)} \left(\mathbf{x}_i, \mathbf{s}_j \right) |l_j| = 0, \quad \mathbf{x}_i \in \partial D, \tag{4.16}$$

$$\sum_{j=1}^{N} T^{(E)}(\mathbf{x}_i, \mathbf{s}_j) \, |l_j| = 0, \qquad \mathbf{x}_i \in \partial D, \tag{4.17}$$

where $|l_j|$ is the distance between points $\mathbf{s}_{j-1/2}$ and $\mathbf{s}_{j+1/2}$ defined in Ref. [11]. $\mathbf{s}_{j-1/2}$ denotes the midpoint of $\mathbf{s}_{j-1}$ and $\mathbf{s}_j$ on boundary Γ, while $\mathbf{s}_{j+1/2}$ represents the midpoint in between $\mathbf{s}_j$ and $\mathbf{s}_{j+1}$ on boundary Γ.

In terms of the dependency of the normal vectors on inner and outer boundaries [3], the relationships of the double-layer kernel functions in interior and exterior problems can be given by

$$\begin{cases} M^{(I)}(\mathbf{x}_i, \mathbf{s}_j) = -M^{(E)}(\mathbf{x}_i, \mathbf{s}_j), & i \neq j \\ M^{(I)}(\mathbf{x}_i, \mathbf{s}_j) = M^{(E)}(\mathbf{x}_i, \mathbf{s}_j), & i = j, \end{cases} \tag{4.18}$$

$$T^{(I)}(\mathbf{x}_i, \mathbf{s}_j) = T^{(E)}(\mathbf{x}_i, \mathbf{s}_j), \text{ for any } i, j, \tag{4.19}$$

where the superscript (I) denotes the interior domain. When the distribution of source nodes is uniformly distributed, we can obtain the diagonal elements of the interpolation matrix, which are originally singular or hyper-singular, via Eqs. (4.16)–(4.19) by the desingularization of subtracting and adding-back technique [3]

$$M^{(I)}(\mathbf{x}_i, \mathbf{s}_i) = \sum_{j=1, j\neq i}^{N} M^{(I)}(\mathbf{x}_i, \mathbf{s}_j), \tag{4.20}$$

$$T^{(I)}(\mathbf{x}_i, \mathbf{s}_i) = -\sum_{j=1, j\neq i}^{N} T^{(I)}(\mathbf{x}_i, \mathbf{s}_j), \tag{4.21}$$

for interior problems and

$$M^{(E)}(\mathbf{x}_i, \mathbf{s}_i) = -\sum_{j=1, j\neq i}^{N} M^{(E)}(\mathbf{x}_i, \mathbf{s}_j), \tag{4.22}$$

$$T^{(E)}(\mathbf{x}_i, \mathbf{s}_i) = -\sum_{j=1, j\neq i}^{N} T^{(E)}(\mathbf{x}_i, \mathbf{s}_j), \tag{4.23}$$

for exterior problems.

However, it is not an easy task to generate uniformly distributed boundary knots in 3D problems, especially with complex-shaped surface. To tackle this issue, the weighted RMM [50] is proposed and the diagonal elements of interpolation matrix for interior problems are given by

$$M^{(I)}(\mathbf{x}_i, \mathbf{s}_i) = \frac{1}{|l_i|} \sum_{j=1, j\neq i}^{N} M^{(I)}(\mathbf{x}_i, \ \mathbf{s}_j) |l_j|, \tag{4.24}$$

$$T^{(I)}(\mathbf{x}_i, \mathbf{s}_i) = -\frac{1}{|l_i|} \sum_{j=1, j\neq i}^{N} T^{(I)}(\mathbf{x}_i, \mathbf{s}_j)|l_j|. \tag{4.25}$$

Similarly, we can obtain the following diagonal elements for exterior problems [51]

$$M^{(E)}(\mathbf{x}_i, \mathbf{s}_i) = -\frac{1}{|l_i|} \sum_{j=1, j\neq i}^{N} M^{(E)}(\mathbf{x}_i, \mathbf{s}_j)|l_j|, \tag{4.26}$$

$$T^{(E)}(\mathbf{x}_i, \mathbf{s}_i) = -\frac{1}{|l_i|} \sum_{j=1, j\neq i}^{N} T^{(E)}(\mathbf{x}_i, \mathbf{s}_j)|l_j|. \tag{4.27}$$

It is worth noting that $|l_j|$ can be easily determined via the numerical integration. Upon regular domain problems with a uniform distribution of boundary nodes, the weighted RMM is reduced to the traditional RMM. Thanks to the desingularization of subtracting and adding-back technique, the RMM places the source points on the real physical boundary to circumvent the fictitious boundary of the MFS. In addition, the RMM also cures the ill-conditioned interpolation matrix of the MFS and the BKM. The RMM has so far been applied to acoustic eigenproblem [52], exterior acoustics [53], antiplane shear problem [54], and antiplane piezoelectricity problem [55]. Similar to the RMM, Sarler [6] proposes the MMFS to solve potential flow problems.

4.1.4 The Singular Boundary Method

Inspired by great success of the RMM, Chen and his collaborators [7, 8] introduced a novel RBF boundary discretization formulation, called the singular boundary method (SBM). Unlike the RMM, the SBM directly applies the fundamental solutions instead of double-layer potentials while it remedies the artificial boundary problem in the MFS. The main idea in the SBM is to introduce the concept of origin intensity factors to remove the singularities of fundamental solutions upon the coincidence of the source and collocation points on physical boundary. By now the two techniques have been developed to evaluate the origin intensity factors. The first one is called the inverse interpolation technique (IIT) [7, 8, 56–58], which numerically evaluates the origin intensity factors. The second approach is to derive the analytical formula for calculating the origin intensity factors [59–65].

The SBM allows placing all nodes on the physical boundary. The source points $\{\mathbf{s}_j\}$ and the collocation points $\{\mathbf{x}_i\}$ are usually the same set of boundary nodes. The SBM formulation is given by

$$u(\mathbf{x}_i) = \sum_{j=1}^{N} a_j \phi_S(\mathbf{x}_i, \mathbf{s}_j), \tag{4.28}$$

in which

$$\phi_S(\mathbf{x}_i, \mathbf{s}_j) = \begin{cases} \phi_{ii}, \ \mathbf{x}_i = \mathbf{s}_j, \ \mathbf{x}_i \in \Gamma_1 \cup \Omega \\ \phi_F(\mathbf{x}_i, \mathbf{s}_j), \ \mathbf{x}_i \neq \mathbf{s}_j, \ \mathbf{x}_i \in \Gamma_1 \cup \Omega \end{cases}, \tag{4.29}$$

$$\frac{\partial \phi_S(\mathbf{x}_i, \mathbf{s}_j)}{\partial n} = \begin{cases} \bar{\phi}_{ii}, \ \mathbf{x}_i = \mathbf{s}_j, \ \mathbf{x}_i \in \Gamma_2 \\ \frac{\partial \phi_F(\mathbf{x}_i, \mathbf{s}_j)}{\partial n}, \ \mathbf{x}_i \neq \mathbf{s}_j, \ \mathbf{x}_i \in \Gamma_2 \end{cases}, \tag{4.30}$$

where ϕ_{ii} and $\bar{\phi}_{ii}$ are defined as the origin intensity factors, namely, the diagonal elements of the SBM interpolation matrix. This method employs a simple numerical technique, called the IIT, to determine the origin intensity factors. Taking the Laplace equation as an illustrative case, the first step of the IIT requires a known sample solution u_I of the Laplace problem and locates some sample points $\{\mathbf{y}_k\}$ inside the physical domain. It is noted that the sample points $\{\mathbf{y}_k\}$ do not coincide with the source points $\{\mathbf{s}_j\}$, and the sample point number NK should not be less than the physical boundary source node number N. By using the interpolation Eq. (4.28), we can then determine the influence coefficients $\{\beta_j\}$ by the following linear system of equations

$$[\Phi_F(\mathbf{y}_k, \mathbf{s}_j)][\beta_j] = [u_I(\mathbf{y}_k)], \quad 1 \leq k \leq NK, \ 1 \leq j \leq N. \tag{4.31}$$

Replacing the sample points $\{\mathbf{y}_k\}$ with the boundary collocation points $\{\mathbf{x}_i\}$, the SBM interpolation matrix of the potential problem (homogeneous problem (4.4), (4.2), and (4.3) with $\Re = \Delta$) can be written as

$$\begin{bmatrix} \Phi_S(\mathbf{x}_i, \mathbf{s}_j) \\ \frac{\partial}{\partial n} \Phi_S(\mathbf{x}_i, \mathbf{s}_j) \end{bmatrix} [\beta_j] = \begin{bmatrix} u_I(\mathbf{x}_i) \\ \frac{\partial}{\partial n} u_I(\mathbf{x}_i) \end{bmatrix}. \tag{4.32}$$

The origin intensity factors can be calculated by the following formulations

$$\phi_{ii} = \left(u_I(\mathbf{x}_i) - \sum_{j=1, \mathbf{s}_j \neq \mathbf{x}_i}^{N} \beta_j \phi_F(\mathbf{x}_i, \mathbf{s}_j) \right) \Big/ \beta_j, \ \mathbf{x}_i = \mathbf{s}_j \in \Gamma_1, \tag{4.33}$$

$$\bar{\phi}_{ii} = \left(\frac{\partial u_I(\mathbf{x}_i)}{\partial n} - \sum_{j=1, \mathbf{s}_j \neq \mathbf{x}_i}^{N} \beta_j \frac{\partial \phi_F(\mathbf{x}_i, \mathbf{s}_j)}{\partial n} \right) \Big/ \beta_j, \ \mathbf{x}_i = \mathbf{s}_j \in \Gamma_2. \tag{4.34}$$

Note that the origin intensity factors depend only on the distribution of the source points, the fundamental solutions of the governing equation, and the

boundary conditions. Theoretically, the origin intensity factors calculated by the IIT remain unchanged with different sample solutions. The origin intensity factors circumvent the singularities of the fundamental solutions upon the coincidence of the source and collocation points.

It is worth noting that the SBM performs well for diverse potential problems. The SBM formulation (4.28) cannot, however, get the correct solution in some cases whose solution includes a constant potential. For instance, the SBM formulation (4.28) yields the incorrect solution for a Dirichlet problem in a circular domain with analytical solution $u(x, y) = e^y(\sin(x) + \cos(x))$ [7]. As a result, a constant term is proposed to add to the SBM approximate Eq. (4.28) to guarantee the uniqueness of the SBM interpolation matrix in the solution of potential problems. The modified SBM formulation with a constant term is given by

$$\tilde{u}(\mathbf{x}) = \sum_{j=1}^{N} a_j \phi_S(\mathbf{x}, \mathbf{s}_j) + a_{N+1}, \tag{4.35}$$

with the constraint

$$\sum_{j=1}^{N} a_j = 0. \tag{4.36}$$

This technique is also called as moment condition in the RBF approximation [66]. The above SBM formulation (4.35) has successfully been applied to interior and exterior Laplace [7, 8, 56], Helmholtz [67], and elastostatic [57] problems.

Numerical experiments of 3D cases indicate that the SBM accuracy may be sensitive to the placement of inner sample nodes in the IIT. To tackle this issue, Chen and Gu [59, 60, 64] recently used subtracting and adding-back desingularization technique to accurately evaluate origin intensity factors for interior and exterior potential problems. This is an analytical–numerical technique and does not require inner sample nodes and employs the null-field and full-field integral equations to evaluate analytically the origin intensity factors on Neumann boundary condition for interior and exterior problems, and then uses the IIT to determine the origin intensity factors on Dirichlet boundary.

When the collocation point $\mathbf{x}_i$ approaches the source point $\mathbf{s}_j$, Eqs. (4.29) and (4.30) tend to be singular. By adopting the subtracting and adding-back technique, Eq. (4.30) can be regularized as follows

$$
\begin{aligned}
q(x_i) &= \sum_{j=1}^{N} a_j \frac{\partial \phi_s(\mathbf{x}_i, \mathbf{s}_j)}{\partial n_x} \\
&= \sum_{j=1}^{N} (a_j - a_i) \frac{\partial \phi_s(\mathbf{x}_i, \mathbf{s}_j)}{\partial n_x} + a_i \sum_{j=1}^{N} \left(\frac{\partial \phi_s(\mathbf{x}_i, \mathbf{s}_j)}{\partial n_x} + \frac{\partial \phi_s^C(\mathbf{x}_i, \mathbf{s}_j)}{\partial n_s} \right),
\end{aligned}
\tag{4.37}
$$

in which

$$\sum_{j=1}^{N} \frac{\partial \phi_s^C(\mathbf{x}_i, \mathbf{s}_j)}{\partial n_s} = 0, \tag{4.38}$$

where n_x and n_s represent respectively the outward normal unit vector on the collocation points $\mathbf{x}_i$ and source points $\mathbf{s}_j$, and $\phi_s^C(\mathbf{x}_i, \mathbf{s}_j)$ denotes the fundamental solution of the exterior problems. The derivation of Eq. (4.38) is based on the discretization of the reduced null-fields equations given in Ref. [3].

According to the dependency of the outward normal vectors on the two kernel functions of interior and exterior problems, we can obtain the following relationships

$$\begin{cases} \frac{\partial \phi_s(\mathbf{x}_i, \mathbf{s}_j)}{\partial n_s} = -\frac{\partial \phi_s^C(\mathbf{x}_i, \mathbf{s}_j)}{\partial n_s}, & i \neq j, \\ \frac{\partial \phi_s(\mathbf{x}_i, \mathbf{s}_j)}{\partial n_s} = \frac{\partial \phi_s^C(\mathbf{x}_i, \mathbf{s}_j)}{\partial n_s}, & i = j, \end{cases} \tag{4.39}$$

$$\lim_{\mathbf{s}_j \to \mathbf{x}_i} \left(\frac{\partial \phi_s(\mathbf{x}_i, \mathbf{s}_j)}{\partial n_x} + \frac{\partial \phi_s(\mathbf{x}_i, \mathbf{s}_j)}{\partial n_s} \right) = 0, \quad i = j, \tag{4.40}$$

when the boundary shape is of a straight line, Eq. (4.40) is explicitly equal to zero since $n_x(\mathbf{x}_i) = n_s(\mathbf{s}_j)$ at all boundary knots. For a smooth boundary of arbitrary shape, we assume that the source point $\mathbf{s}_j$ approaches inchmeal to the collocation point $\mathbf{x}_i$ along a line segment, then Eq. (4.40) is tenable.

From Eqs. (4.39) and (4.40), Eq. (4.37) can be rewritten as

$$\begin{aligned} q(\mathbf{x}_i) &= \sum_{j=1}^{N} a_j \frac{\partial \phi_s(\mathbf{x}_i, \mathbf{s}_j)}{\partial n_x} \\ &= \sum_{j=1, i \neq j}^{N} (a_j - a_i) \frac{\partial \phi_s(\mathbf{x}_i, \mathbf{s}_j)}{\partial n_x} + a_i \sum_{j=1, i \neq j}^{N} \left(\frac{\partial \phi_s(\mathbf{x}_i, \mathbf{s}_j)}{\partial n_x} - \frac{\partial \phi_s(\mathbf{x}_i, \mathbf{s}_j)}{\partial n_s} \right). \\ &= \sum_{j=1, i \neq j}^{N} a_j \frac{\partial \phi_s(\mathbf{x}_i, \mathbf{s}_j)}{\partial n_x} - a_i \sum_{j=1, i \neq j}^{N} \frac{\partial \phi_s(\mathbf{x}_i, \mathbf{s}_j)}{\partial n_s} \end{aligned} \tag{4.41}$$

Comparing Eqs. (4.41) and (4.30) at $\mathbf{x}_i = \mathbf{s}_j$, we easily obtain

$$\bar{\phi}_{ii} = -\sum_{j=1, i \neq j}^{N} \frac{\partial \phi_s(\mathbf{x}_i, \mathbf{s}_j)}{\partial n_s}, \tag{4.42}$$

which is the origin intensity factors $\bar{\phi}_{ii}$ for Neumann boundary conditions in Eq. (4.30). Then the origin intensity factors ϕ_{ii} for Dirichlet boundary conditions in Eq. (4.29) can be calculated by the IIT. In this strategy, we first choose a simple particular solution as the sample solution, e.g., $u_I(\mathbf{x}) = x + y$ in Laplace equation

case. Then, from Eq. (4.41) we can evaluate the corresponding densities $\{\beta_j\}$ for all the boundary points. Finally, from Eq. (4.29) we have the following algebraic equations

$$\{\Phi_{ij}\}\{\beta_j\} = \{x_i + y_i + c\}, \tag{4.43}$$

where c is a constant and can be solved by using an arbitrary field point inside the domain. It is noted that only the origin intensity factors ϕ_{ii} are unknown in the above Eq. (4.43). And we get the following expression for the diagonal terms using the known density values $\{\beta_j\}$

$$\phi_{ii} = \left(x_i + y_i + c - \sum_{j=1,i\neq j}^{N} \beta_j \phi_s(\mathbf{x}_i, \mathbf{s}_j) \right) \Big/ a_i, \quad i = 1, 2, \dots, N. \tag{4.44}$$

Then, the following standard linear system of equations is formed after applying either Eqs. (4.29) or (4.30) at all the collocation points $\{\mathbf{x}_i\}_{i=1}^{N}$

$$\begin{bmatrix} A_{11} & A_{12} & \dots & A_{1N} \\ A_{21} & A_{22} & \dots & A_{2N} \\ \vdots & \vdots & \ddots & \vdots \\ A_{N1} & A_{N2} & \dots & A_{NN} \end{bmatrix} \begin{Bmatrix} a_1 \\ a_2 \\ \vdots \\ a_N \end{Bmatrix} = \begin{Bmatrix} b_1 \\ b_2 \\ \vdots \\ b_N \end{Bmatrix} \text{ or } \mathbf{A}\mathbf{a} = \mathbf{b}, \tag{4.45}$$

where $\mathbf{A}$ is the interpolation matrix, $\mathbf{a}$ the unknown coefficient vector, and $\mathbf{b}$ the right-hand side vector. Once all $\{a_j\}$ in Eq. (4.45) are determined, then the potentials and their derivatives at any point inside the domain and on the boundary can be evaluated via Eqs. (4.29) and (4.30).

Note that this improved SBM formulation avoids the inner sampling points in the traditional SBM by using the desingularization of subtracting and adding-back technique. The improved SBM formulation has been successfully applied to heat condition [65, 68] and exterior time-harmonic wave problems [61, 62, 69].

4.2 Nonhomogeneous Problems

By implementing PDE splitting approach [70], the approximate solution of non-homogeneous Eqs. (4.1)–(4.3) can be expressed as

$$u = u_h + u_p, \tag{4.46}$$

where u_h and u_p are the homogeneous and the particular solution, respectively. The particular solution u_p satisfies

$$\Re\{u_p\} = f(\mathbf{x}), \tag{4.47}$$

but does not necessarily satisfy boundary conditions. In contrast, the homogeneous solution has to satisfy not only the corresponding homogeneous equation

$$\Re\{u_h\} = 0, \tag{4.48}$$

but also the updated boundary conditions

$$u_h(\mathbf{x}) = R(\mathbf{x}) - u_p(\mathbf{x}), \, x \in \Gamma_1, \tag{4.49}$$

$$\frac{\partial}{\partial n} u_h(\mathbf{x}) = N(\mathbf{x}) - \frac{\partial}{\partial n} u_p(\mathbf{x}), \, x \in \Gamma_2. \tag{4.50}$$

Equations (4.48)–(4.50) can be solved by a boundary-type RBF collocation method introduced in Sect. 4.1. And then the key issue is to calculate the particular solution u_p from Eq. (4.47). During the past two decades, the DRM [9] and MRM [10] have emerged as two promising techniques to approximate the particular solution u_p.

The DRM has become de facto the method of choice in conjunction with the MFS [71–78], the BKM [2, 12, 43, 45, 79], the RMM [80], and the SBM [58] to evaluate the particular solution. Since the DRM is actually equivalent to the MPS, one can find the DRM solution procedure in Sect. 3.4. However, it requires the additional inner nodes to guarantee the convergence and stability. It is also noted that the appropriate choice of the RBFs in the DRM is not a trivial task. This is because it is not easy-to-tailor a RBF to reflecting the properties of both differential operator and nonhomogeneous function.

Another popular approach is the MRM, which has the advantage over the DRM in that it does not require using inner nodes at all for evaluating the particular solution. To take full advantage of its truly boundary-only merit for a more broad range of problems, Chen [81] developed the MRM-based meshless boundary particle method (BPM). However, the MRM does also have some disadvantages compared with the DRM in that the standard MRM is computationally much more expensive in the construction of the different interpolation matrices by using high-order fundamental or general solutions [11, 12] and has limited feasibility for general nonhomogeneous problems due to its conventional use of high-order Laplacian operators in the annihilation process.

4.2.1 Recursive Composite Multiple Reciprocity Method: The Boundary Particle Method

Recently, Chen et al. [13] proposed an improved MRM, called RC-MRM technique, to efficiently handle various inhomogeneous terms in the governing equation. The RC-MRM has since been successfully applied to inverse Cauchy problem [82, 83], plate analysis [84, 85]. The technique uses the recursive process to significantly reduce the computational costs and employs the composite

differential operator instead of conventional high-order Laplace operators to eliminate various nonhomogeneous function terms. The RC-MRM differs from the DRM in that the former evaluates the particular solution u_p in Eq. (4.46) by a sum of higher order homogeneous solutions, namely,

$$u_p = \sum_{m=1}^{\infty} u_h^m, \tag{4.51}$$

where u_h^m represents the m-order composite homogeneous solutions, i.e.,

$$L_m \cdots L_2 L_1 \Re\{u_h^m\} = 0, \quad \mathbf{x} \in \Omega, \tag{4.52}$$

where $L_1, L_2, \cdots, L_m$ are differential operators of the same or different kinds. When $L_m = \cdots L_2 = L_1 = \Re$, this RC-MRM degenerates into the original MRM. Let the zero-order homogeneous solution u_h^0 represent the homogeneous solution u_h in Eq. (4.46), then the solution of problem of interest is represented by a sum of varied-order homogeneous solutions

$$u = u_h + u_p = \sum_{m=0}^{\infty} u_h^m. \tag{4.53}$$

The basic assumption in the composite MRM is

$$\lim_{m \to \infty} L_m \ldots L_2 L_1 \{f(x)\} \to 0. \tag{4.54}$$

In the practical implementation, the sum of an infinite series Eq. (4.53) has to be truncated at certain order M. Namely,

$$u \approx \sum_{m=0}^{M} u_h^m. \tag{4.55}$$

To evaluate the homogeneous solutions of various orders, we need to update the corresponding boundary conditions. First, we have the zero-order boundary condition equation

$$\begin{cases} u_h^0(\mathbf{x}) = R(\mathbf{x}) - u_p^0(\mathbf{x}), & \mathbf{x} \in \Gamma_1 \\ \frac{\partial}{\partial n} u_h^0(\mathbf{x}) = N(\mathbf{x}) - \frac{\partial}{\partial n} u_p^0(\mathbf{x}), & \mathbf{x} \in \Gamma_2 \end{cases}. \tag{4.56}$$

Equation (4.56) is in fact the DRM formula without any inner nodes. For the m-order homogeneous solutions, we have the successively higher boundary condition equations

$$\begin{cases} \Re\{u_h^1(\mathbf{x})\} = f(\mathbf{x}) - \Re\{u_p^1(\mathbf{x})\}, & \mathbf{x} \in \Gamma_1, \\ \frac{\partial}{\partial n} \Re\{u_h^1(\mathbf{x})\} = \frac{\partial}{\partial n}\left(f(\mathbf{x}) - \Re\{u_p^1(\mathbf{x})\}\right), & \mathbf{x} \in \Gamma_2, \end{cases} \tag{4.57}$$

$$\begin{cases} L_{m-1}\cdots L_2 L_1 \Re\{u_h^m(\mathbf{x})\} = L_{m-1}\cdots L_2 L_1\{f(\mathbf{x})\} \\ \qquad\qquad\qquad -L_{m-1}\cdots L_2 L_1 \Re\{u_p^m(\mathbf{x})\}, \quad \mathbf{x}\in\Gamma_1, \\ \frac{\partial}{\partial n}L_{m-1}\cdots L_2 L_1 \Re\{u_h^m(\mathbf{x})\} = \frac{\partial}{\partial n}\left(L_{m-1}\cdots L_2 L_1\{f(\mathbf{x})\}\right) \\ \qquad\qquad\qquad -\frac{\partial}{\partial n}\left(L_{m-1}\cdots L_2 L_1 \Re\{u_p^m(\mathbf{x})\}\right), \mathbf{x}\in\Gamma_2, \end{cases}$$
(4.58)

for $m = 2,3,\ldots M$. The nonhomogeneous term $f(\mathbf{x})$ was repeatedly differentiated as the Dirichlet and Neumann boundary conditions of the higher order homogeneous solutions. u_p^m denotes the m-order particular solutions which are approximated by

$$u_p^m = \sum_{k=m+1}^{M} u_h^k.$$
(4.59)

To numerically solve the homogeneous problems (4.56)–(4.58), the m-order homogeneous solutions are approximately represented by

$$u_h^m(\mathbf{x}) = \sum_{k=1}^{L} \beta_k^m \phi_F^m(\mathbf{x},\mathbf{x}_k),$$
(4.60)

where L is the number of boundary collocation nodes, β_k^m the corresponding unknown coefficients for m-order homogeneous problems, and ϕ_F^m the m-order composite fundamental solutions of the operator $L_m\ldots L_2 L_1 \Re$.

Collocating Eqs. (4.56)–(4.58) at all boundary nodes in terms of Eq. (4.60), we have the boundary discretization equations

$$\begin{cases} \sum_{k=1}^{L} \beta_k^0 \phi_F^0(\mathbf{x},\mathbf{x}_k) = R(\mathbf{x}) - u_p^0(\mathbf{x}), \quad \mathbf{x}\in\Gamma_1, \\ \sum_{k=1}^{L} \beta_k^0 \frac{\partial}{\partial n}\phi_F^0(\mathbf{x},\mathbf{x}_k) = N(\mathbf{x}) - \frac{\partial}{\partial n}u_p^0(\mathbf{x}), \mathbf{x}\in\Gamma_2, \end{cases}$$
(4.61)

$$\begin{cases} \sum_{k=1}^{L} \beta_k^1 \Re\{\phi_F^1(\mathbf{x},\mathbf{x}_k)\} = f(\mathbf{x}) - \Re\{u_p^1(\mathbf{x})\}, \quad \mathbf{x}\in\Gamma_1, \\ \sum_{k=1}^{L} \beta_k^1 \frac{\partial}{\partial n}\Re\{\phi_F^1(\mathbf{x},\mathbf{x}_k)\} = \frac{\partial}{\partial n}\left(f(\mathbf{x}) - \Re\{u_p^1(\mathbf{x})\}\right), \mathbf{x}\in\Gamma_2, \end{cases}$$
(4.62)

$$
\begin{cases}
\sum_{k=1}^{L} \beta_k^m L_{m-1} \ldots L_2 L_1 \Re\big\{\phi_F^m(\mathbf{x}, \mathbf{x}_k)\big\} = L_{m-1} \ldots L_2 L_1 \{f(\mathbf{x})\} \\
\qquad\qquad\qquad\qquad\qquad\qquad\qquad - L_{m-1} \ldots L_2 L_1 \Re\big\{u_p^m(\mathbf{x})\big\}, \qquad \mathbf{x} \in \Gamma_1, \\
\sum_{k=1}^{L} \beta_k^m \frac{\partial}{\partial n} L_{m-1} \ldots L_2 L_1 \Re\big\{\phi_F^m(\mathbf{x}, \mathbf{x}_k)\big\} = \frac{\partial}{\partial n}(L_{m-1} \ldots L_2 L_1 \{f(\mathbf{x})\}) \\
\qquad\qquad\qquad\qquad\qquad\qquad - \frac{\partial}{\partial n}\left(L_{m-1} \ldots L_2 L_1 \Re\big\{u_p^m(\mathbf{x})\big\}\right), \mathbf{x} \in \Gamma_2,
\end{cases}
\tag{4.63}
$$

for $m = 2,3,\ldots M$ and $r_k = \|\mathbf{x} - \mathbf{x}_k\|$. The above recursive iteration is truncated at order M, i.e.,

$$
L_M \ldots L_2 L_1 \Re\big\{u_p^M\big\} = 0. \tag{4.64}
$$

The solution procedure of Eqs. (4.61)–(4.63) is a reversible process

$$
\beta^M \rightarrow \beta^{M-1} \rightarrow \cdots \rightarrow \beta^0. \tag{4.65}
$$

Finally, the numerical solution at any inner and boundary node can be obtained by

$$
u(\mathbf{x}) = \sum_{m=0}^{M} \sum_{k=1}^{L} \beta_k^m \phi_F^m(\mathbf{x}, \mathbf{x}_k). \tag{4.66}
$$

Note that throughout the solution procedure, the present RC-MRM does not use any inner nodes. Therefore, the scheme is a truly boundary-only collocation method for solving nonhomogeneous problems. In particular, the algorithm uses the composite high-order differential operators to annihilate the nonhomogeneous term without increasing computing efforts. The major differences between the RC-MRM and the traditional MRM can be summarized by the twofold aspects: (1) differential operators different from the governing differential operator may be used to annihilate the nonhomogeneous terms; (2) the recursive algorithm is used to dramatically reduce computing costs.

More investigations on boundary-type RBF collocation methods for solving PDEs can be found in the extended method of fundamental solutions [86] and time-marching MFS [87] for time-dependent problems, the MFS and BKM in conjunction with Kirchhoff transform [88–90] for heterogeneous medium problem, the MFS coupled with analog equation method (AEM) [91] for nonlinear PDEs [92], and the BPM coupled with Laplace transform for anomalous diffusion problems [93].

4.3 Numerical Experiments

In this section, we first investigate the accuracy, stability, and convergence of several boundary-type RBF collocation approaches in the solution of homogeneous PDEs. Rerr represents the average relative error, Merr the maximum absolute error, and Aerr the average absolute error, which are defined as follows

$$\text{Rerr}(w) = \sqrt{\frac{1}{NT} \sum_{i=1}^{NT} \left| \frac{w(\mathbf{x}_i) - w_e(\mathbf{x}_i)}{w_e(\mathbf{x}_i)} \right|^2}, \tag{4.67}$$

$$\text{Merr}(w) = \max_{1 \le i \le NT} |w(\mathbf{x}_i) - w_e(\mathbf{x}_i)|, \tag{4.68}$$

$$\text{Aerr}(w) = \sqrt{\frac{1}{NT} \sum_{i=1}^{NT} |w(\mathbf{x}_i) - w_e(\mathbf{x}_i)|^2}, \tag{4.69}$$

where NT is the total number of test points in the domain and on the boundary. These nodes are selected to measure the numerical accuracy. Unless otherwise specified, $NT = 2601$ for square problems.

Example 4.1 The Dirichlet problem with a unit square domain
Consider a potential problem $\Delta u = 0$ in a unit square domain with Dirichlet discontinuous boundary conditions as follows:

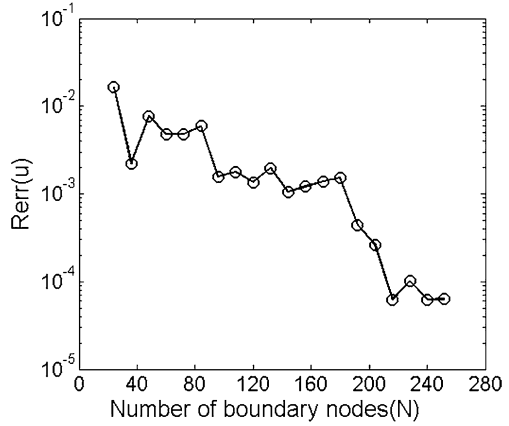$$u(x,0) = x + 3, \ u(x,1) = u(0,y) = u(1,y) = 3. \tag{4.70}$$

The analytical solution of this problem is given by

$$u(x, y) = 3 + \sum_{n=1}^{\infty} \frac{2(-1)^n}{n\pi\sinh(n\pi)} \sinh(n\pi(1 - y))\sin(n\pi x). \tag{4.71}$$

Figure 4.1 displays the SBM accuracy verses the number of boundary nodes. It can be found that the solution accuracy is improved with the increasing boundary node number N. The contour plots of the analytical and the SBM solutions are plotted in Fig. 4.2. Figure 4.3 shows the numerical solutions of the RMM and the MFS ($d = 1.5$, distance of fictitious boundary from physical boundary) with 240 boundary nodes, respectively. It is observed that the SBM results are in good agreement with the analytical solution. The RMM results deteriorate significantly at the boundary-adjacent region. It is noted that the MFS ($d = 1.5$) does not yield reliable and consistent solution.

Table 4.1 shows the results by the SBM and the RMM. The numerical accuracy by the SBM with 28 boundary nodes is comparable with that of the RMM with 120 boundary nodes. Table 4.2 shows the MFS results with different fictitious boundary parameters d. Much oscillation is visible with the increasing boundary

Fig. 4.1 The average
relative errors Rerr(u) with
respect to the boundary node
number N in Example 4.1

node number N by the MFS. The main reason of this instability is due to the severe
ill-conditioning of the MFS interpolation matrix.

Example 4.2 The Dirichlet problem with L-shaped domain

We investigate the SBM for solving potential problem $\Delta u = 0$ in the L-shaped
domain. The exact solution is

$$u(x, y) = \sinh(x)\cos(y) + 4. \tag{4.72}$$

Figure 4.4 displays the contour plots of the exact and the SBM solutions with
240 boundary nodes. It can be found from Fig. 4.4 that the SBM results agree with
the exact solutions very well. Table 4.3 shows that the numerical accuracy is
improved with increasing boundary nodes by the present SBM. This example
verifies that the SBM works equally well in a case having boundary singularities.
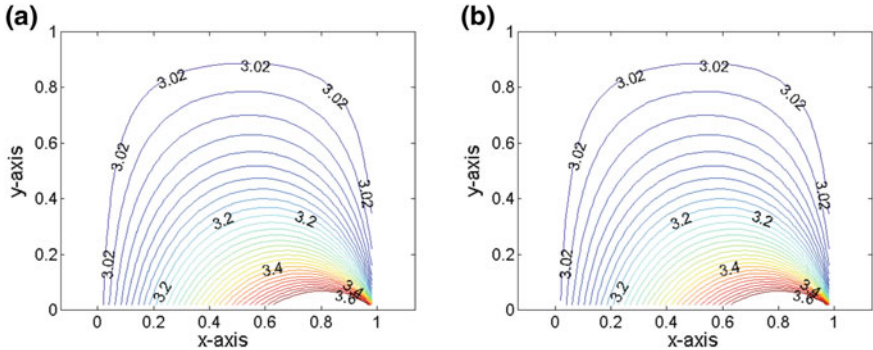

Fig. 4.2 (a) The analytical solution and **(b)** the SBM solution for Example 4.1
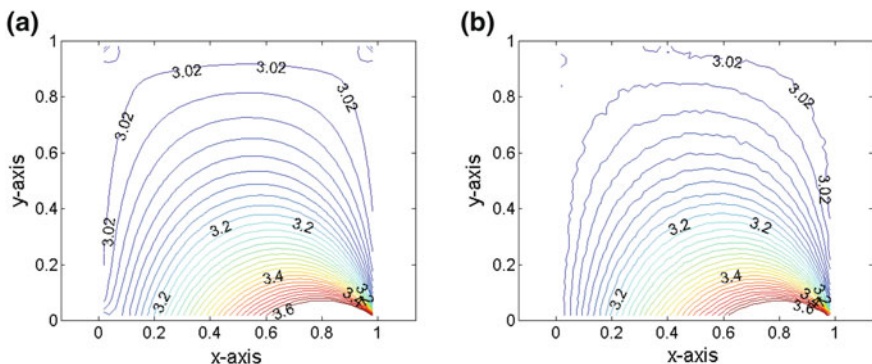
Fig. 4.3 The field solution for Example 4.1 by using (**a**) RMM and (**b**) MFS ($d = 1.5$)

Example 4.3 Exterior heat conduction problem of a circle

This example considers a heat conduction problem $\Delta u = 0$ outside a circle with discontinuous heat source on the boundary

$$u(1, \theta) = \begin{cases} 1 & 0 < \theta < \pi, \\ -1 & \pi < \theta < 2\pi. \end{cases} \tag{4.73}$$

The analytical solution is given as follows

$$u(r, \theta) = \frac{2}{\pi} \arctan\left(\frac{2r\sin\theta}{r^2 - 1}\right). \tag{4.74}$$

Table 4.1 Numerical results by SBM and RMM for Example 4.1 with various numbers of nodes

N	SBM			RMM		
	Rerr(u)	Merr(u)	Cond(**A**)	Rerr(u)	Merr(u)	Cond(**A**)
28	6.22E − 03	3.37E − 01	2.84E + 01	1.21E − 01	1.84E + 00	1.17E + 01
40	1.72E − 03	1.44E − 01	5.82E + 01	6.91E − 02	1.21E + 00	8.69E + 00
120	9.42E − 04	3.43E − 02	2.13E + 06	9.26E − 03	8.51E − 02	4.67E + 00
200	1.24E − 03	6.97E − 02	5.62E + 02	3.73E − 04	1.62E − 02	4.39E + 00
240	4.47E − 05	3.88E − 03	1.72E + 02	2.55E − 03	3.74E − 02	4.34E + 00

Table 4.2 Numerical results (MFS) for Example 4.1 using various numbers of nodes

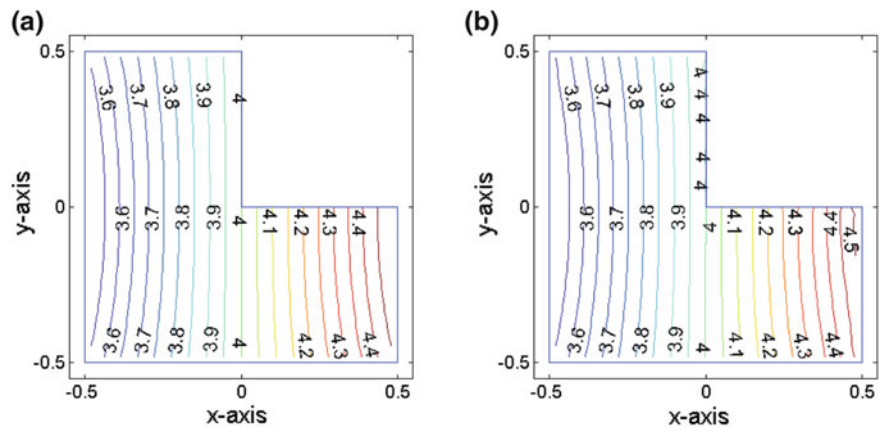| N	MFS ($d = 3$)			MFS ($d = 1.5$)		
	Rerr(u)	Merr(u)	Cond(**A**)	Rerr(u)	Merr(u)	Cond(**A**)
28	9.94E − 03	2.39E − 01	1.83E + 11	9.97E − 03	2.39E − 01	4.13E + 06
40	5.52E − 03	1.65E − 01	7.66E + 17	5.53E − 03	1.65E − 01	1.12E + 17
120	1.61E − 03	4.08E − 02	6.21E + 19	3.74E − 03	4.05E − 02	1.51E + 19
200	4.01E − 03	1.13E − 01	9.66E + 18	4.40E − 03	3.42E − 02	3.49E + 19
240	1.76E − 02	1.50E − 01	1.14E + 20	3.93E − 03	3.67E − 02	6.12E + 19

Fig. 4.4 (**a**) The analytical solution and (**b**) the SBM solution with 240 boundary nodes for Example 4.2

Table 4.3 Numerical results of SBM for Example 4.2 with various numbers of boundary nodes

N	SBM		
	Rerr(u)	Merr(u)	Cond(**A**)
24	3.20E − 03	8.16E − 02	5.10E + 01
40	1.02E − 03	3.49E − 02	6.03E + 01
160	7.04E − 04	2.30E − 02	2.46E + 04
240	3.82E − 04	2.19E − 02	8.46E + 04
320	2.84E − 04	1.70E − 02	2.96E + 05

Here the tested points ($NT = 280$) are uniformly distributed on the upper half plane outside the physical boundary but inside the circle of radius 3. Table 4.4 shows the numerical results by the SBM, BEM, and MFS, in which the MFS uses different fictitious boundary parameters d. We observe from Table 4.4 that the BEM has the lowest accuracy and the largest condition number. It is noted that the accuracy can be improved by using the adaptive BEM. However, this may increase the computational costs. The MFS with the fictitious boundary parameter $d = 0.2$ cannot get the correct solution when the number of boundary source nodes is more than 200. The reason is that the condition number of the MFS interpolation matrix increases exponentially with the increasing boundary node number N. This indicates that the placement of the fictitious boundary could have numerical stability issue. The appropriate fictitious boundary is a tricky issue in the MFS.

It is observed from Table 4.4 that the SBM and the MFS with the fictitious boundary parameter $d = 0.01$ produce the similar accuracy, and their interpolation matrices also have the similar level of condition numbers. Note that the optimal fictitious boundary parameter d is obtained in this case by a trial and error approach. The determination of such a parameter d is not trivial in applications and

Table 4.4 Numerical results for Example 4.3 with various numbers of nodes. Reprinted from Ref. [56] with kind permission from Springer Science+Business Media

Method	SBM		MFS ($d = 0.2$)		MFS ($d = 0.01$)		BEM	
N	Rerr(u)	Cond(**A**)	Rerr(u)	Cond(**A**)	Rerr(u)	Cond(**A**)	Rerr(u)	Cond(**A**)
60	3.00E − 02	3.51E + 01	3.00E − 02	1.57E + 07	4.01E − 02	3.85E + 01	1.21E − 01	1.11E + 03
100	1.80E − 02	4.53E + 01	1.80E − 02	1.96E + 11	2.03E − 02	1.10E + 02	7.35E − 02	3.06E + 03
200	9.00E − 03	7.21E + 01	–	–	9.10E − 03	6.89E + 02	3.70E − 02	1.22E + 04
300	6.00E − 03	1.08E + 02	–	–	6.00E − 03	2.95E + 03	2.47E − 02	2.74E + 04

particularly difficult for problems with complex-shaped or multiply connected domain. It can be concluded from this case study that the SBM is mathematically simple, easy-to-program, accurate, meshless, integration-free, and avoids the controversy of the fictitious boundary in the MFS.

The next case is the boundary-type RBF collocation approaches for solving nonhomogeneous PDEs.

Example 4.4 First consider the Poisson's equation with a polynomial forcing term

$$\begin{cases} \Delta u = -x_1^2, & (x_1, x_2) \in \Omega \\ u = 0, & (x_1, x_2) \in \partial\Omega \end{cases}, \tag{4.75}$$

where Ω is an ellipse with a semi-major axis of length 2 and semi-minor axis of length 1. The exact solution [9] is given by

$$u(\mathbf{x}) = -\left(50x_1^2 - 8x_2^2 + 33.6\right)\left(x_1^2/4 + x_2^2 - 1\right)/246. \tag{4.76}$$

For this example, we consider the following homogeneous problem

$$\begin{cases} \Delta^3 u = 0, & (x_1, x_2) \in \Omega \\ u = 0, & (x_1, x_2) \in \partial\Omega \\ \Delta u = -x_1^2, & (x_1, x_2) \in \partial\Omega \\ \Delta^2 u = -2, & (x_1, x_2) \in \partial\Omega \end{cases}. \tag{4.77}$$

The BPM first utilizes the corresponding high-order singular fundamental solutions, namely, singular formulation as discussed in Sect. 2.3.1, where the source points are located on an ellipse with a semi-major axis length of 10 and semi-minor axis length of 5 centered at the origin. The accuracy variation of the BPM results with respect to the number of collocation points, i.e., L, is shown in Fig. 4.5a. In general, the numerical accuracy will be initially enhanced with the increasing L. And then a further increasing L would not gain much improvement in accuracy. It is observed that a small number of collocation points, say 24, is sufficient to obtain high accuracy. However, much oscillation is noticeable. The main cause of this instability is due to the ill-conditioning of the interpolation matrix. The condition number *Cond* of the interpolation matrix $\mathbf{A}_{00}$ and $\mathbf{A} = (\mathbf{A}_{ij})$ is shown in Fig. 4.5b. To mitigate the effect of ill-conditioning, a regularization method, known as the truncated singular value decomposition (TSVD), is implemented to obtain accurate results, in which the truncation level is determined by the distinct gap in the singular value spectrum of the interpolation matrix $\mathbf{A}$.

Example 4.4 is a benchmark problem in the BEM and has previously been solved using the DR-BEM [9] and MR-BEM [10]. A comparison with the numerical results presented in these studies [9, 10] shows that the proposed method gives a much accurate numerical solution with less computational efforts.

In practical situations, the given data can always be approximated by piecewise polynomials, which can be annihilated by repeatedly applying the Laplace operators. Therefore, the BPM with the RC-MRM is expected to work for a wide range of real-world application problems.
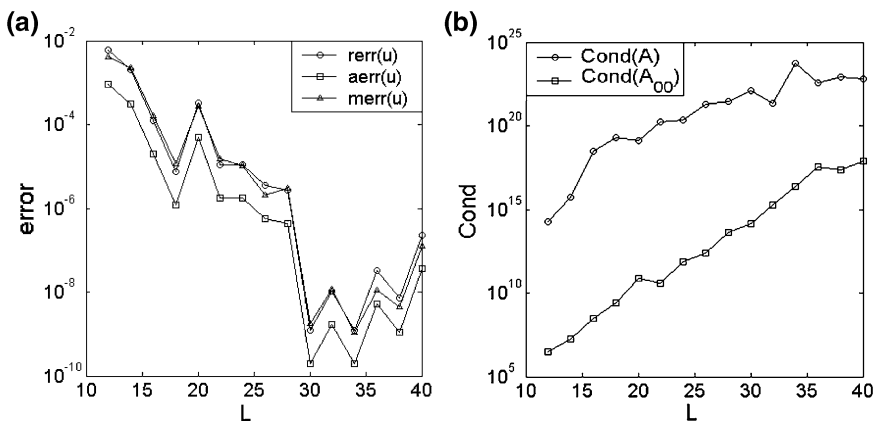
Fig. 4.5 (**a**) Numerical accuracy variation and (**b**) the condition number of the interpolation matrices with respect to boundary node number L. Reprinted from Ref. [13], Copyright 2012, with permission from Elsevier

Then we test the BPM using the corresponding high-order nonsingular general solutions or harmonic functions (nonsingular formulation) as discussed in Sects. 2.3.2 and Sects. 2.3.3. The numerical results of Example 4.4 using various numbers of collocation points are shown in Fig. 4.6a. The shape parameter c in harmonic functions has a significant impact on the numerical accuracy, as in the case of Multiquadric and Gaussian RBFs. c is taken to be 0.1 in this example. The numerical accuracy improves as the node number L increases. However, for $L > 28$, the accuracy starts to deteriorate. The condition numbers of the interpolation matrices $\mathbf{A}$ and $\mathbf{A}_{00}$ are displayed in Fig. 4.6b. One can conclude from this
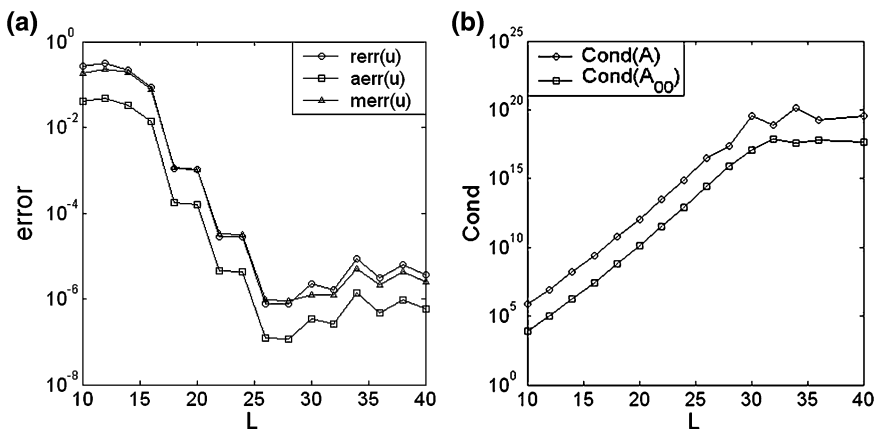

Fig. 4.6 (**a**) Numerical accuracy variation and (**b**) the condition number of the interpolation matrices with respect to boundary node number L. Reprinted from Ref. [13], Copyright 2012, with permission from Elsevier

investigation that the nonsingular formulation also suffers from ill-conditioned interpolation matrix.

Example 4.5 3D Heat conduction problem with intraheat source

Next consider the BPM solution of a three-dimensional heat conduction problem with intra heat source [9].

$$\begin{cases} \Delta u(\mathbf{x}) = -2, & \mathbf{x} = (x_1, x_2, x_3) \in \Omega, \\ u(\mathbf{x}) = -\left(x_1^2 + x_2^2 + x_3^2\right)/3, & \mathbf{x} = (x_1, x_2, x_3) \in \partial\Omega \end{cases}, \qquad (4.78)$$

where $\Omega = [-1, 1]^3$. The source points are distributed evenly on a sphere centered at the origin and with a radius 5, and the shape parameter $c = 0.1$. The analytical solution is given by

$$u(\mathbf{x}) = -\frac{1}{3}\left(x_1^2 + x_2^2 + x_3^2\right). \qquad (4.79)$$

The numerical results for Example 4.5 with various numbers of collocation points are shown in Table 4.5. Numerical accuracy improves at the beginning with increasing boundary node number and reaches a plateau and then oscillates with a further increase of boundary nodes in the nonsingular formulation. In contrast, the singular formulation appears more stably and the numerical accuracy improves consistently with increasing number of boundary nodes.

It is noted that the accuracy of the numerical results using 54 nodes is comparable with the DR-BEM solution, which requires using 48 BEM nodes and 27 internal nodes to obtain the results with the error Rerr(u) less than 10^{-3} [9]. This indicates that the BPM with singular and nonsingular formulations may be a competitive alternative to simulate high-dimensional problems.

Example 4.6 Thin square plate on a Winkler-type elastic foundation

This example investigates the numerical accuracy of the BPM with singular formulation for high-order nonhomogeneous PDE in comparison with the Hermite collocation method (HCM). The MQ RBF with shape parameter $c = 1$ is chosen as

Table 4.5 Numerical results of Example 4.5 with various numbers of boundary collocation knots

Method	Singular formula			Nonsingular formula		
L	Rerr(u)	Aerr(u)	Merr(u)	Rerr(u)	Aerr(u)	Merr(u)
24	$4.23e-3$	$9.28e-3$	$1.00e-2$	$3.25e-4$	$1.69e-4$	$1.21e-3$
54	$6.69e-4$	$1.47e-3$	$2.13e-3$	$6.69e-4$	$1.47e-3$	$2.13e-3$
96	$3.44e-6$	$7.56e-6$	$1.74e-5$	$3.25e-4$	$1.69e-4$	$1.21e-3$
150	$2.46e-7$	$5.39e-7$	$1.87e-6$	$8.35e-6$	$4.55e-6$	$4.60e-5$
216	$1.85e-8$	$4.07e-8$	$1.26e-7$	$1.14e-5$	$1.98e-6$	$1.91e-5$
294	$1.23e-8$	$2.70e-8$	$1.70e-7$	$1.17e-4$	$9.59e-6$	$5.18e-5$
384	$9.32e-10$	$2.05e-9$	$8.79e-9$	$1.55e-4$	$1.06e-5$	$4.85e-5$

the approximate basis function in the HCM. In the BPM, a square fictitious boundary is chosen with length $L = 2$, which is placed outside the unit square physical domain.

Case 4.6.1: A simply supported thin square plate on a Winkler-type elastic foundation under uniform loading

$$\begin{cases} (\nabla^4 + \kappa^2)w = q_0/D, & \mathbf{x} = (x, y) \in \Omega, \\ w = 0, & \mathbf{x} = (x, y) \in \partial\Omega, \\ M_n = 0, & \mathbf{x} = (x, y) \in \partial\Omega, \end{cases} \quad (4.80)$$

where w represents the deflection of the middle surface of the plate, $n = [\cos\alpha, \sin\alpha]$ is the unit outward normal vector, κ denotes the foundation stiffness, $D = Eh^3/[12(1 - v^2)]$ is the flexural rigidity of the plate, and

$$M_n = -D\left\{ v\nabla^2 w + (1 - v)\left(\cos^2\alpha \frac{\partial^2 w}{\partial x^2} + \sin^2\alpha \frac{\partial^2 w}{\partial y^2} + \sin 2\alpha \frac{\partial^2 w}{\partial x \partial y} \right) \right\}. \quad (4.81)$$

The following mechanical parameters are specified: Young's Modulus $E = 2.1 \times 10^{11}$, the thickness of the plate $h = 0.01$, Poisson's ratio of elasticity $v = 0.3$, foundation stiffness $\kappa = \pi^2$, uniform loading $q_0 = 10^6$. The exact solution is given by [94]

$$w_e = \frac{16q_0}{\pi^6 D} \sum_{m=1}^{\infty} \sum_{n=1}^{\infty} \frac{\sin(m\pi x/a)\sin(n\pi y/b)}{mn\left[(m^2/a^2 + n^2/b^2)^2 + k/(\pi^4 D) \right]}, \quad \begin{matrix} m = 1, 3, 5, \cdots, \\ n = 1, 3, 5, \cdots. \end{matrix} \quad (4.82)$$

Case 4.6.2: A clamped Winkler-type square plate under complex loading

$$\begin{cases} (\nabla^4 + \kappa^2)w = q_1(x, y)/D, & \mathbf{x} = (x, y) \in \Omega, \\ w = 0, & \mathbf{x} = (x, y) \in \partial\Omega, \\ \theta_n = 0, & \mathbf{x} = (x, y) \in \partial\Omega, \end{cases} \quad (4.83)$$

where the loading function is

$$\begin{aligned} q_1(x, y) =\ & 0.01q_0\left((64\pi^4 + \kappa^2)(\cos(2\pi x) - 1)(\cos(2\pi y) - 1) \right), \\ & + 0.01q_0\left(48\pi^4(\cos(2\pi x) + \cos(2\pi y)) - 64\pi^4 \right) \end{aligned} \quad (4.84)$$

and

$$\theta_n = \frac{\partial w}{\partial n} = \frac{\partial w}{\partial x}\frac{dx}{dn} + \frac{\partial w}{\partial y}\frac{dy}{dn} = \frac{\partial w}{\partial x}\cos\alpha + \frac{\partial w}{\partial y}\sin\alpha. \quad (4.85)$$

The exact solution is given as follows

$$w_e = \frac{q_0(\cos(2\pi x) - 1)(\cos(2\pi y) - 1)}{100D}. \quad (4.86)$$

Figure 4.7 shows the average and maximum absolute errors (Aerr and Merr) by using the BPM (side length $L = 2$) and the HCM (MQ RBF with $c = 1$) in cases 4.6.1 and 4.6.2. It is observed from Fig. 4.7 that the BPM clearly outperforms the HCM in the numerical accuracy. The BPM solution with 16 boundary nodes is even better than 36 nodes HCM solution. Note that the BPM only requires the boundary discretization and has a particular edge over the domain discretization HCM for some real-world applications such as inverse problems, where only boundary data are accessible in most cases.

Example 4.7 Thin plate on a Winkler-type elastic foundation with trigonometric Loading

We compare the BPM with singular formulation to the MFS-DRM [78] in this case. Consider the deflection of a 2×2 clamped Winkler-type square plate [78]

$$\begin{cases} (\nabla^4 + \kappa^2)w = q_2(x, y)/D, & \mathbf{x} = (x, y) \in \Omega, \\ \qquad\qquad w = 0, & \mathbf{x} = (x, y) \in \partial\Omega, \\ \qquad\qquad \theta_n = 0, & \mathbf{x} = (x, y) \in \partial\Omega. \end{cases} \tag{4.87}$$

The exact solution is given by

$$w_e = \sin(\pi x/2)\sin(\pi y/2). \tag{4.88}$$

The parameters of the plate are $D = 1$, $v = 0.33$, $\kappa = \pi^2$. The trigonometric loading $q_2(x, y)$ is given based on the analytical solution in Eq. (4.88).

In contrast, Fig. 4.8 illustrates the BPM and MFS-DRM convergence curves with the fictitious boundary $d = 8$. We can observe from Fig. 4.8 that the numerical accuracy of 60 nodes BPM solution is comparable with that of 80 nodes MFS-DRM solution. Thus, the BPM uses fewer nodes than the MFS-DRM to achieve the numerical solutions of similar accuracy. It is noted that the BPM
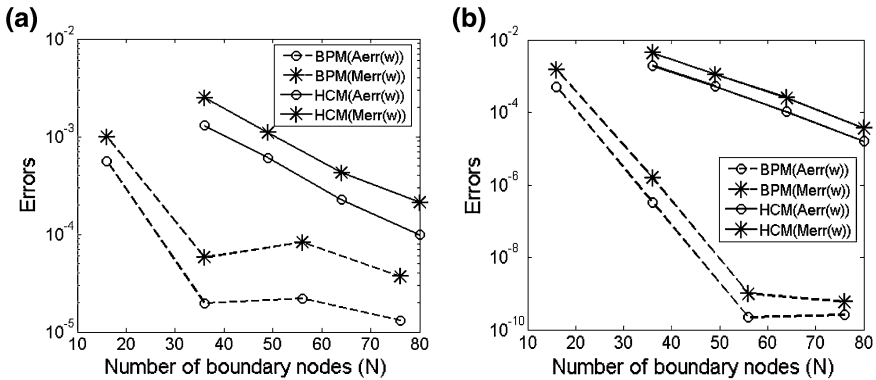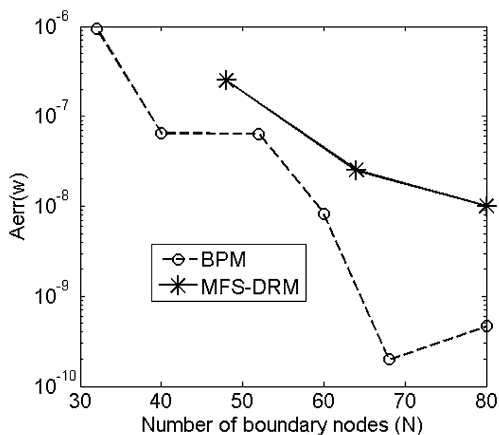

Fig. 4.7 The maximum and average absolute error curves of (**a**) case 4.6.1 and (**b**) case 4.6.2 by using the boundary particle method and the Hermite collocation method. Reprinted from Ref. [85], with kind permission from Springer Science+Business Media

Fig. 4.8 The average absolute error curves of the BPM and the MFS-DRM. Reprinted from Ref. [85], with kind permission from Springer Science+Business Media

solutions do not invariably improve when the nodes increase up to a certain number largely due to the round-off error effect of its ill-conditioned interpolation matrix. This is a common issue in all global collocation methods.

Unlike the MFS-DRM, the BPM does not require any additional interior points to evaluate the particular solution. Thus, the BPM is far more attractive than the MFS in the solution of nonhomogeneous problems.

Example 4.8 Inverse Cauchy problem associated with Poisson equation

The mathematical formulation of the Cauchy problem can be presented as

$$\Delta u(\mathbf{x}) = f(\mathbf{x}), \quad \mathbf{x} \in \Omega, \tag{4.89}$$

subjects to the two types of boundary conditions prescribed on the accessible boundary

$$u(\mathbf{x}) = \bar{u}(\mathbf{x}), \quad \mathbf{x} \in \Gamma_1, \tag{4.90}$$

$$q(\mathbf{x}) = \frac{\partial u(\mathbf{x})}{\partial n} = \bar{q}(\mathbf{x}), \quad \mathbf{x} \in \Gamma_1, \tag{4.91}$$

where Δ denotes the Laplace operator, $f(\mathbf{x})$ is a known potential function, u and q are the prescribed potential and flux, Γ_1 denotes the non-zero measurable boundary part, and n represents the unit outward normal vector. A necessary condition for the above inverse Cauchy problem [95, 96] to be identifiable is that the accessible boundary part Γ_1 is non-zero. However, in the discretization of the above-mentioned Cauchy problem, the corresponding identifiability condition reduces to that the accessible boundary part Γ_1 is longer than the under-specified boundary Γ_2. In this case, we focus on determining the potential u and the flux q on the inaccessible boundary Γ_2. Although this inverse problem may have a unique solution, it is well-known that this solution is unstable for small perturbations on the accessible boundary Γ_1, see Hadamard [97]. Therefore, Cauchy

problems are ill-posed inverse problems. The TSVD with the generalized cross-validation (GCV) function choice criterion is employed to help the BPM to remedy this ill-posed problem. All the computational codes are programmed in MATLAB, partially including the MATLAB TSVD code with the generalized cross-validation (GCV) function choice criterion developed by Hansen [98] for the discrete ill-posed problem.

The measurement data in practical problems always goes with errors, also often referred to noise. The artificial noisy data is generated by

$$u_{noise}(\mathbf{x}) = \bar{u}(\mathbf{x}) + \max|\bar{u}(\mathbf{x})|randn(i)e, \tag{4.92}$$

$$q_{noise}(\mathbf{x}) = \bar{q}(\mathbf{x}) + \max|\bar{q}(\mathbf{x})|randn(i)e, \tag{4.93}$$

where $\bar{u}$ and $\bar{q}$ denote the prescribed functions with the exact data given in Eqs. (4.90) and (4.91). The random number $randn(i)$ is chosen with a standard normal distribution, which is fixed at each example, and e denotes the noise level. It should be mentioned that both the accessible potential and flux are contaminated by artificial measurement noise in the following numerical examples. $NT = 40$ is the number of test nodes distributed uniformly on the under-specified boundary Γ_2. The shape parameter $c = 0.01$ in the harmonic functions of Laplace equation.

First we investigate the effects of some parameters on the BPM computation. Consider Poisson equation on the following circular domain

$$\Omega_1 = \left\{(x_1, x_2)|x_1^2 + x_2^2 \leq 4\right\}, \tag{4.94}$$

with the measured boundary part $\Gamma_1 = \{(r, \theta)|r = 2, 0 \leq \theta \leq 2\pi BL\}$, and the unmeasured boundary part $\Gamma_2 = \{(r, \theta)|r = 2, 2\pi BL < \theta \leq 2\pi\}$, where (r, θ) is the plane polar coordinate, the source points $\{\mathbf{y}_j\}$ are uniformly distributed on the physical boundary, and the ratio parameter of accessible boundary length $BL = \dfrac{\text{boundary length of measured part}}{\text{boundary length of whole boundary}}$.

Case 4.8.1: Poisson equation with the polynomial forcing term $f(\mathbf{x}) = 1$.

The exact solution $u(\mathbf{x}) = 5x_1^2/6 - x_1x_2/2 - x_2^2/3$, and the annihilating operator of this case in Eq. (4.52) is Laplace operator Δ.

Case 4.8.2: Poisson equation with the trigonometric forcing term

$$f(\mathbf{x}) = -8\pi^2 \sin(2\pi x_1) \sin(2\pi x_2).$$

The exact solution is $u(\mathbf{x}) = 2\pi x_2 + \sin(2\pi x_1) \sin(2\pi x_2)$, and the annihilating operator of this case in Eq. (4.52) is Helmholtz operator $(\Delta + 8\pi^2)$.

In these two cases, we set the ratio parameter $BL = 3/4$, and compare the BPM with the BKM-DRM in the solution of Poisson equations. In the BKM-DRM, 100 interior points are uniformly distributed in the square domain $\left[-\sqrt{2}, \sqrt{2}\right]^2$, and Multiquadric (MQ) is employed with the shape parameter $c = 4$. General function (GF) is applied for the evaluation of the particular solution in which GF is the nonsingular RBF general solutions of the annihilating operator in Eq. (4.52).

Figure 4.9a shows the numerical accuracy variation verses the number of boundary points with 1 % noisy data in Case 4.8.1. In general, all of the numerical accuracy of estimated solutions improves with an increasing number of boundary nodes, and all of them have the similar accuracy with the same boundary nodes. In contrast, the BKM-DRM has to choose the appropriate number of the inner additional nodes, determine their placement, and select the suitable interpolation function to evaluate the particular solution. These factors have more or less effect on the numerical accuracy, which require the user to be more experienced in the employment of the BKM-DRM. Note that the present BPM does not require using interior nodes, which saves the computational costs and simplify the implementation.

Figure 4.9b depicts the numerical accuracy variation with respect to boundary measurement data having various levels of noise in the Case 4.8.1. It is observed that all the curves of the relative root mean square error decay with the decreasing noisy data, and the numerical solutions achieve best accuracy with noise-free
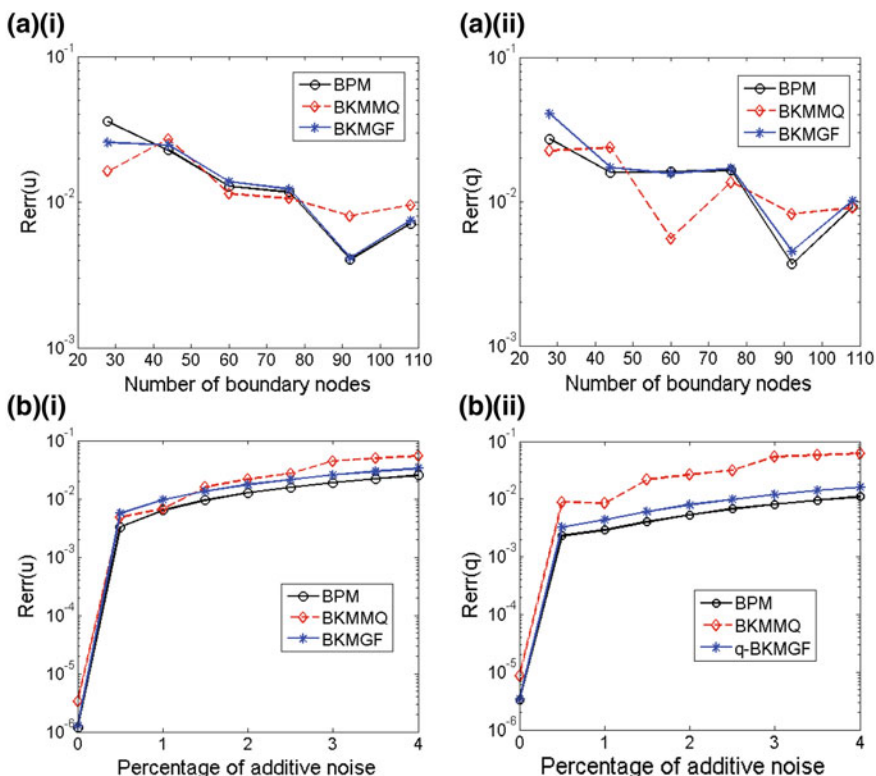

Fig. 4.9   Numerical accuracy variation of (i) the potential u and (ii) the flux q in case 4.8.1 against (**a**) the number of boundary points with 1 % noise level, and (**b**) the noise level percentage using 75 measurement points (100 boundary knots) by the BPM, BKMMQ, and BKMGF

measurement data. It can be seen from Fig. 4.9b that, among these three schemes, the present BPM obtains the best results and the BKMMQ performs the worst.

Figure 4.10a shows the convergent rates of the BPM and BKMGF with 1 % noisy data in Case 4.8.2. It is worth noting that the BKMMQ could not obtain the correct results with the present setting, which indicates that it is a crucial issue on choosing the suitable interpolation function and the appropriate number and placement of interior nodes in the BKM-DRM. It can be observed from Fig. 4.10a that the BPM and the BKMGF have the similar accuracy except that the boundary node number is less than 60. The BKMGF achieves more accurate result than the BPM with 28 boundary nodes, but the former requires 100 interior nodes. Figure 4.10b depicts the numerical accuracy variation with respect to measurement data having various levels of noise in Case 4.8.2. It can be seen that the BPM and BKMGF have the similar accuracy except for noise-free measurement data. The BPM achieves the better results than the BKMGF with noise-free measurement data.
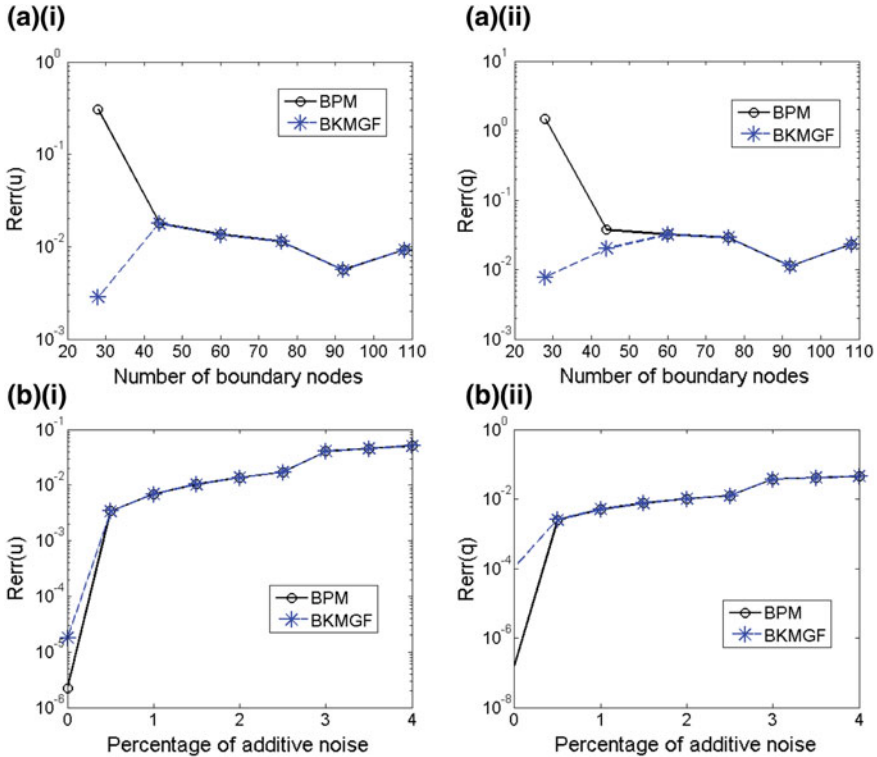

Fig. 4.10 Numerical accuracy variation of (i) the potential u and (ii) the flux q in case 4.8.2 against (**a**) the number of boundary points with 1 % noise level, and (**b**) the noise level percentage using 75 measurement points (100 boundary knots) by the BPM and BKMGF
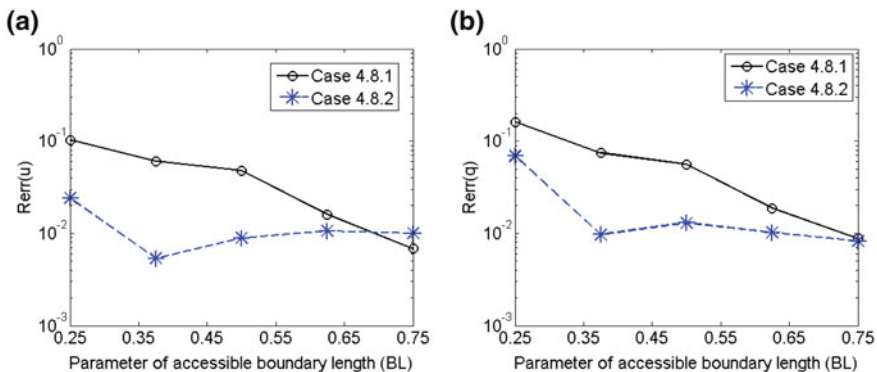
Fig. 4.11 Numerical accuracy variation of (**a**) the potential u and (**b**) the flux q verses BL with 2 % noise level by the BPM using 90 measurement points

Then we perform a sensitivity analysis with respect to the length of the measured boundary. For convenience, 40 test points are uniformly distributed on the part of unmeasured boundary $\{(r, \theta)|r = 2, 3\pi/2 \leq \theta \leq 2\pi\}$. Figure 4.11 presents numerical accuracy variation with respect to the ratio parameter BL with 2 % noisy data by using 90 measurement points in Cases 4.8.1 and 4.8.2, respectively. In general, the accuracy of the BPM improves with an increasing ratio parameter BL in both examples. This implies that the more boundary measurement data is available, the more accurate result we can achieve. Furthermore, it observes that the present BPM can obtain the acceptable results with the ratio parameter $BL = 0.25$ or $BL = 0.375$ in Cases 4.8.1 and 4.8.2, although when $BL < 0.5$ the identifiability condition is not satisfied. Consequently, the BPM results with $BL = 0.25$ or $BL = 0.375$ are not reliable here.

Case 4.8.3: Next we consider a magnetostatic Cauchy problem on a piecewise smooth square $\Omega_2 = \{(x_1, x_2)|0 \leq x_1, x_2 \leq 1\}$ with the measured boundary part

$$\Gamma_1 = \{(1, x_2)|0 \leq x_2 \leq 1\} \cup \{(x_1, 1)|0 \leq x_1 \leq 1\}$$

and the unmeasured boundary part

$$\Gamma_2 = \{(0, x_2)|0 \leq x_2 \leq 1\} \cup \{(x_1, 0)|0 \leq x_1 \leq 1\}.$$

The exact solution is given by $u(\mathbf{x}) = 5x_1^2/6 - x_1x_2/2 - x_2^2/3$, the forcing term $f(\mathbf{x}) = 1$, and the annihilating operator of this case in Eq. (4.52) is Δ. $\mathbf{B} = (\partial u/\partial x_2, -\partial u/\partial x_1)$ represents the magnetic flux density.

Figure 4.12 shows the BPM solution of both the potential $u(\mathbf{x})$ and the flux $q(\mathbf{x})$ on the inaccessible boundary Γ_2, estimated by using 80 measurement points with 1 % noisy data for the Case 4.8.3 on the accessible boundary Γ_1, in comparison with the analytical solution $u_e(\mathbf{x})$ and $q_e(\mathbf{x})$, respectively. Unlike the DR-BEM [99], it should be noted that the present BPM can obtain the satisfactory results without using any interior points and additional corner treatment, which is especially attractive to solve the inverse and optimization problems in high-dimensional
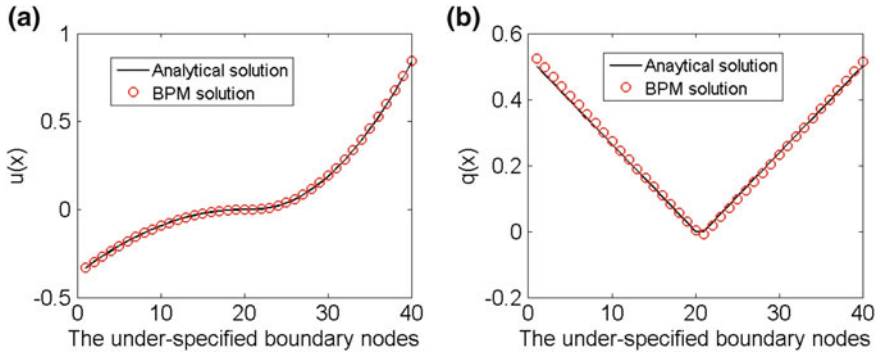
Fig. 4.12 The analytical solution $u_e(\mathbf{x})$ and $q_e(\mathbf{x})$ compared with the BPM solution $u(\mathbf{x})$ and $q(\mathbf{x})$ with 1 % noisy data for Case 4.8.3 by using 80 measurement points
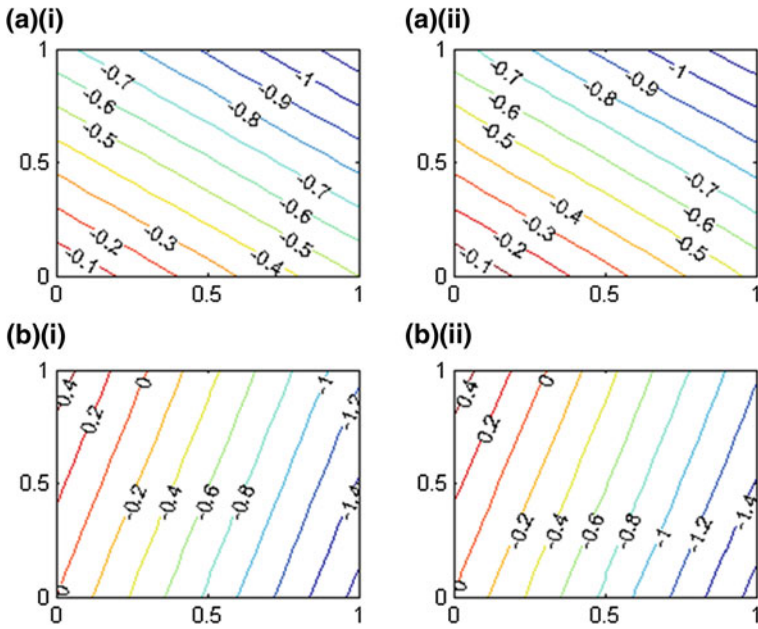

Fig. 4.13 (**a**) The component $\mathbf{B}_x$ of the analytical magnetic flux density (i) and the numerical one (ii) and (**b**) the component $\mathbf{B}_y$ of the analytical magnetic flux density (i) and the numerical one (ii) by using 80 measurement points for case 4.8.3 with 1 % noisy data. Reprinted from Ref. [83] by permission of Taylor & Francis Ltd

domains. Figure 4.13 displays the components of the analytical magnetic flux density $\mathbf{B}$, compared with the BPM numerical components. It can be seen from Fig. 4.13 that the BPM results agree with the analytical solution very well.

References

1. V.D. Kupradze, M.A. Aleksidze, The method of functional equations for the approximate solution of certain boundary value problems. USSR Comput. Math. Math. Phys. **4**(4), 82–126 (1964)
2. W. Chen, M. Tanaka, A meshless, integration-free, and boundary-only RBF technique. Comput. Math. Appl. **43**(3–5), 379–391 (2002)
3. D.L. Young, K.H. Chen, C.W. Lee, Novel meshless method for solving the potential problems with arbitrary domain. J. Comput. Phys. **209**(1), 290–321 (2005)
4. D.L. Young, K.H. Chen, J.T. Chen, J.H. Kao, A modified method of fundamental solutions with source on the boundary for solving laplace equations with circular and arbitrary domains. CMES Comput. Model. Eng. Sci. **19**(3), 197–221 (2007)
5. D.L. Young, K.H. Chen, T.Y. Liu, L.H. Shen, C.S. Wu, Hypersingular meshless method for solving 3D potential problems with arbitrary domain. CMES Comput. Model. Eng. Sci. **40**(3), 225–269 (2009)
6. C.S. Chen, A. Karageorghis, Y.S. Smyrlis, *The Method of Fundamental Solutions—A Meshless Method* (Dynamic Publishers, Atlanta, 2008)
7. W. Chen, Z.J. Fu, X. Wei, Potential problems by singular boundary method satisfying moment condition. CMES Comput. Model. Eng. Sci. **54**(1), 65–85 (2009)
8. W. Chen, F.Z. Wang, A method of fundamental solutions without fictitious boundary. Eng. Anal. Boundary Elem. **34**(5), 530–532 (2010)
9. P.W. Partridge, C.A. Brebbia, L.C. Wrobel, *The Dual Reciprocity Boundary Element Method* (Computational Mechanics Publications, Southampton, 1992)
10. A.J. Nowak, A.C. Neves, *The Multiple Reciprocity Boundary Element Method* (Computational Mechanics Publication, Southampton, 1994)
11. K.K. Prem, in *Fundamental Solutions for Differential Operators and Applications* (Birkhauser Boston Inc., Cambridge, 1996)
12. W. Chen, Z.J. Shen, L.J. Shen, G.W. Yuan, General solutions and fundamental solutions of varied orders to the vibrational thin, the Berger, and the Winkler plates. Eng. Anal. Boundary Elem. **29**(7), 699–702 (2005)
13. W. Chen, Z.J. Fu, B.T. Jin, A truly boundary-only meshfree method for inhomogeneous problems based on recursive composite multiple reciprocity technique. Eng. Anal. Boundary Elem. **34**(3), 196–205 (2010)
14. G.H. Koopmann, L. Song, J.B. Fahnline, A method for computing acoustic fields based on the principle of wave superposition. J. Acoust. Soc. Am. **86**(6), 2433–2438 (1989)
15. C. Yusong, W.S. William, F.B. Robert, Three-dimensional desingularized boundary integral methods for potential problems. Int. J. Numer. Meth. Fluids **12**(8), 785–803 (1991)
16. K. Amano, A charge simulation method for the numerical conformal mapping of interior, exterior and doubly-connected domains. J. Comput. Appl. Math. **53**(3), 353–370 (1994)
17. C.S. Chen, The method of fundamental-solutions for nonlinear thermal explosions. Commun. Numer. Methods Eng. **11**(8), 675–681 (1995)
18. S. Chantasiriwan, Methods of fundamental solutions for time-dependent heat conduction problems. Int. J. Numer. Meth. Eng. **66**(1), 147–165 (2006)
19. L.L. Cao, Q.H. Qin, N. Zhao, An RBF-MFS model for analysing thermal behaviour of skin tissues. Int. J. Heat Mass Transf. **53**(7–8), 1298–1307 (2010)
20. P.S. Kondapalli, D.J. Shippy, G. Fairweather, Analysis of acoustic scattering in fluids and solids by the method of fundamental-solutions. J. Acoust. Soc. Am. **91**(4), 1844–1854 (1992)
21. J. Antonio, A. Tadeu, L. Godinho, A three-dimensional acoustics model using the method of fundamental solutions. Eng. Anal. Boundary Elem. **32**(6), 525–531 (2008)
22. K. Balakrishnan, P.A. Ramachandran, The method of fundamental solutions for linear diffusion-reaction equations. Math. Comput. Model. **31**(2–3), 221–237 (2000)
23. S.P. Hu, D.L. Young, C.M. Fan, FDMFS for diffusion equation with unsteady forcing function. CMES Comput. Model. Eng. Sci. **24**(1), 1–20 (2008)

24. A. Karageorghis, G. Fairweather, The method of fundamental solutions for axisymmetric elasticity problems. Comput. Mech. **25**(6), 524–532 (2000)
25. D.L. Young, C.L. Chiu, C.M. Fan, C.C. Tsai, Y.C. Lin, Method of fundamental solutions for multidimensional Stokes equations by the dual-potential formulation. Eur. J. Mech. B Fluids **25**(6), 877–893 (2006)
26. D.L. Young, S.J. Jane, C.M. Fan, K. Murugesan, C.C. Tsai, The method of fundamental solutions for 2D and 3D stokes problems. J. Comput. Phys. **211**(1), 1–8 (2006)
27. P.P. Chinchapatnam, K. Djidjeli, P.B. Nair, Radial basis function meshless method for the steady incompressible Navier-Stokes equations. Int. J. Comput. Math. **84**, 1509–1526 (2007)
28. D.L. Young, Y.C. Lin, C.M. Fan, C.L. Chiu, The method of fundamental solutions for solving incompressible Navier-Stokes problems. Eng. Anal. Boundary Elem. **33**(8–9), 1031–1044 (2009)
29. J.T. Chen, I.L. Chen, K.H. Chen, Y.T. Lee, Y.T. Yeh, A meshless method for free vibration analysis of circular and rectangular clamped plates using radial basis function. Eng. Anal. Boundary Elem. **28**(5), 535–545 (2004)
30. J.T. Chen, I.L. Chen, Y.T. Lee, Eigensolutions of multiply connected membranes using the method of fundamental solutions. Eng. Anal. Boundary Elem. **29**(2), 166–174 (2005)
31. C.J.S. Alves, P.R.S. Antunes, The method of fundamental solutions applied to the calculation of eigensolutions for 2D plates. Int. J. Numer. Meth. Eng. **77**(2), 177–194 (2009)
32. Y.S. Smyrlis, A. Karageorghis, A linear least-squares MFS for certain elliptic problems. Numer. Algorithms **35**(1), 29–44 (2004)
33. Y.S. Smyrlis, A. Karageorghis, A matrix decomposition MFS algorithm for axisymmetric potential problems. Eng. Anal. Boundary Elem. **28**(5), 463–474 (2004)
34. G. Fairweather, A. Karageorghis, Y.S. Smyrlis, A matrix decomposition MFS algorithm for axisymmetric biharmonic problems. Adv. Comput. Math. **23**(1–2), 55–71 (2005)
35. Y.S. Smyrlis, The method of fundamental solutions: a weighted least-squares approach. Bit Numer. Math. **46**(1), 163–194 (2006)
36. A. Karageorghis, C.S. Chen, Y.S. Smyrlis, A matrix decomposition RBF algorithm: approximation of functions and their derivatives. Appl. Numer. Math. **57**(3), 304–319 (2007)
37. T.W. Drombosky, A.L. Meyer, L.V. Ling, Applicability of the method of fundamental solutions. Eng. Anal. Boundary Elem. **33**(5), 637–643 (2009)
38. L. Marin, An alternating iterative MFS algorithm for the cauchy problem in two-dimensional anisotropic heat conduction. CMC Comput. Mater. Con. **12**(1), 71–99 (2009)
39. J. Lin, W. Chen, F. Wang, A new investigation into regularization techniques for the method of fundamental solutions. Math. Comput. Simul. **81**(6), 1144–1152 (2011)
40. G. Fairweather, A. Karageorghis, The method of fundamental solutions for elliptic boundary value problems. Adv. Comput. Math. **9**(1–2), 69–95 (1998)
41. G. Fairweather, A. Karageorghis, P.A. Martin, The method of fundamental solutions for scattering and radiation problems. Eng. Anal. Boundary Elem. **27**(7), 759–769 (2003)
42. C.S. Liu, Improving the ill-conditioning of the method of fundamental solutions for 2D Laplace equation. CMES Comput. Model. Eng. Sci. **28**(2), 77–93 (2008)
43. W. Chen, Symmetric boundary knot method. Eng. Anal. Boundary Elem. **26**(6), 489–494 (2002)
44. F. Wang, W. Chen, X. Jiang, Investigation of regularized techniques for boundary knot method. Int. J. Numer. Methods Biomed. Eng. **26**(12), 1868–1877 (2010)
45. W. Chen, Y.C. Hon, Numerical investigation on convergence of boundary knot method in the analysis of homogeneous Helmholtz, modified Helmholtz, and convection-diffusion problems. Comput. Methods Appl. Mech. Eng. **192**(15), 1859–1875 (2003)
46. Y.C. Hon, W. Chen, Boundary knot method for 2D and 3D Helmholtz and convection–diffusion problems under complicated geometry. Int. J. Numer. Meth. Eng. **56**(13), 1931–1948 (2003)
47. X.P. Chen, W.X. He, B.T. Jin, Symmetric boundary knot method for membrane vibrations under mixed-type boundary conditions. Int. J. Nonlinear Sci. Numer. Simul. **6**(4), 421–424 (2005)

48. J. Shi, W. Chen, C. Wang, Free vibration analysis of arbitrary shaped plates by boundary knot method. Acta Mech. Solida Sin. **22**(4), 328–336 (2009)
49. Y.C. Hon, Z. Wu, A numerical computation for inverse boundary determination problem. Eng. Anal. Boundary Elem. **24**(7–8), 599–606 (2000)
50. R.C. Song, W. Chen, An investigation on the regularized meshless method for irregular domain problems. CMES Comput. Model. Eng. Sci. **42**(1), 59–70 (2009)
51. L.L. Sun, W. Chen, C.Z. Zhang, A new formulation of regularized meshless method applied to interior and exterior anisotropic potential problems. Appl. Math. Model. **37**(12–13), 7452–7464 (2013)
52. K.H. Chen, J.T. Chen, J.H. Kao, Regularized meshless method for solving acoustic eigenproblem with multiply-connected domain. CMES Comput. Model. Eng. Sci. **16**(1), 27–39 (2006)
53. D.L. Young, K.H. Chen, C.W. Lee, Singular meshless method using double layer potentials for exterior acoustics. J. Acoust. Soc. Am. **119**(1), 96–107 (2006)
54. K.H. Chen, J.T. Chen, J.H. Kao, Regularized meshless method for antiplane shear problems with multiple inclusions. Int. J. Numer. Meth. Eng. **73**(9), 1251–1273 (2008)
55. K.H. Chen, J.H. Kao, J.T. Chen, Regularized meshless method for antiplane piezoelectricity problems with multiple inclusions. CMC Comput. Mater. Con. **9**(3), 253–279 (2009)
56. W. Chen, Z.J. Fu, A novel numerical method for infinite domain potential problems. Chin. Sci. Bull. **55**(16), 1598–1603 (2010)
57. Y. Gu, W. Chen, C.-Z. Zhang, Singular boundary method for solving plane strain elastostatic problems. Int. J. Solids Struct. **48**(18), 2549–2556 (2011)
58. X. Wei, W. Chen, Z.J. Fu, Solving inhomogeneous problems by singular boundary method. J. Marine Sci. Technol. Taiwan **21**(1), 8–14 (2013)
59. W. Chen, Y. Gu, Recent advances on singular boundary method. *Joint international workshop on Trefftz method VI and method of fundamental solution II* (Taiwan 2011)
60. W. Chen, Y. Gu, An improved formulation of singular boundary method. Adv. Appl. Math. Mech. **4**(5), 543–558 (2012)
61. Z.J. Fu, W. Chen, C.S. Chen, Singular boundary method for radiation and wave scattering: numerical aspects and applications. Paper presented at the 23rd international congress of theoretical and applied mechanics (ICTAM2012), Beijing
62. Z.J. Fu, W. Chen, J. Lin, Improved singular boundary method for various infinite-domain wave applications. Paper presented at the global Chinese workshop in conjunction with 10th national conference on computational methods in engineering, Changsha
63. Y. Gu, W. Chen, X.Q. He, Singular boundary method for steady-state heat conduction in three dimensional general anisotropic media. Int. J. Heat Mass Transf. **55**, 4837–4848 (2012)
64. Y. Gu, W. Chen, J. Zhang, Investigation on near-boundary solutions by singular boundary method. Eng. Anal. Boundary Elem. **36**(8), 1173–1182 (2012)
65. Y. Gu, W. Chen, Infinite domain potential problems by a new formulation of singular boundary method. Appl. Math. Model. **37**(4), 1638–1651 (2013)
66. C.S. Chen, Y.C. Hon, R.S. Schaback, Radial basis functions with scientific computation. Department of Mathematics, University of Southern Mississippi, USA (2007)
67. Z.J. Fu, W. Chen, A novel boundary meshless method for radiation and scattering problems, ed. by C.Z. Zhang, M.H. Aliabadi, M. Schanz. Advances in Boundary Element Techniques XI, Berlin, Germany (EC Ltd, United Kingdom, 12–14 July 2010), pp. 83–90.
68. Y. Gu, W. Chen, X.Q. He, Singular boundary method for steady-state heat conduction in three dimensional general anisotropic media. Int. J. Heat Mass Transf. **55**(17–18), 4837–4848 (2012)
69. W. Chen, Z.J. Fu, Y. Gu, Burton-Miller-type singular boundary method for acoustic radiation and scattering. J. Sound Vib. submitted (2013)
70. K.E. Atkinson, The numerical evaluation of particular solutions for Poisson's equation. IMA J. Numer. Anal. **5**, 319–338 (1985)
71. M.A. Golberg, The method of fundamental solutions for Poisson's equation. Eng. Anal. Boundary Elem. **16**(3), 205–213 (1995)

72. M.A. Golberg, C.S. Chen, S.R. Karur, Improved multiquadric approximation for partial differential equations. Eng. Anal. Boundary Elem. **18**(1), 9–17 (1996)
73. C.S. Chen, C.A. Brebbia, H. Power, Dual reciprocity method using compactly supported radial basis functions. Commun. Numer. Methods Eng. **15**(2), 137–150 (1999)
74. M.A. Golberg, C.S. Chen, M. Ganesh, Particular solutions of 3D Helmholtz-type equations using compactly supported radial basis functions. Eng. Anal. Boundary Elem. **24**(7–8), 539–547 (2000)
75. S. Chantasiriwan, Cartesian grid methods using radial basis functions for solving Poisson, Helmholtz, and diffusion-convection equations. Eng. Anal. Boundary Elem. **28**(12), 1417–1425 (2004)
76. C.J.S. Alves, C.S. Chen, A new method of fundamental solutions applied to nonhomogeneous elliptic problems. Adv. Comput. Math. **23**(1–2), 125–142 (2005)
77. C. Erdonmez, H. Saygin, Conduction heat transfer problem solution using the method of fundamental solutions with the dual reciprocity method. HT2005: *Proceedings of the ASME Summer Heat Transfer Conference 2005*, vol. 3 (2005), pp. 853–858
78. C.C. Tsai, The method of fundamental solutions with dual reciprocity for thin plates on Winkler foundations with arbitrary loadings. J. Mech. **24**(2), 163–171 (2008)
79. W. Chen, L.J. Shen, Z.J. Shen, G.W. Yuan, Boundary knot method for Poisson equations. Eng. Anal. Boundary Elem. **29**(8), 756–760 (2005)
80. W. Chen, J. Lin, F. Wang, Regularized meshless method for nonhomogeneous problems. Eng. Anal. Boundary Elem. **35**(2), 253–257 (2011)
81. W. Chen, Meshfree boundary particle method applied to Helmholtz problems. Eng. Anal. Boundary Elem. **26**(7), 577–581 (2002)
82. W. Chen, Z.J. Fu, Boundary particle method for inverse cauchy problems of inhomogeneous Helmholtz equations. J. Marine Sci. Technol. Taiwan **17**(3), 157–163 (2009)
83. Z.J. Fu, W. Chen, C.Z. Zhang, Boundary particle method for Cauchy inhomogeneous potential problems. Inverse Probl. Sci. Eng. **20**(2), 189–207 (2012)
84. Z.J. Fu, W. Chen, A truly boundary-only meshfree method applied to kirchhoff plate bending problems. Adv. Appl. Math. Mech. **1**(3), 341–352 (2009)
85. Z.J. Fu, W. Chen, W. Yang, Winkler plate bending problems by a truly boundary-only boundary particle method. Comput. Mech. **44**(6), 757–763 (2009)
86. R. Gospavic, N. Haque, V. Popov, C.S. Chen, Comparison of two solvers for the extended method of fundamental solutions, ed. by L. Skerget. Boundary Elements and Other Mesh Reduction Methods XXX, vol. 47, pp. 191–199 (2008)
87. D.L. Young, M.H. Gu, C.M. Fan, The time-marching method of fundamental solutions for wave equations. Eng. Anal. Boundary Elem. **33**(12), 1411–1425 (2009)
88. L. Marin, D. Lesnic, The method of fundamental solutions for nonlinear functionally graded materials. Int. J. Solids Struct. **44**(21), 6878–6890 (2007)
89. Z.J. Fu, W. Chen, Q.H. Qin, Boundary knot method for heat conduction in nonlinear functionally graded material. Eng. Anal. Boundary Elem. **35**(5), 729–734 (2011)
90. Z.J. Fu, W. Chen, Q.H. Qin, Three boundary meshless methods for heat conduction analysis in nonlinear FGMs with Kirchhoff and Laplace transformation. Adv. Appl. Math. Mech. **4**(5), 519–542 (2012)
91. J.T. Katsikadelis, The analog equation method: a boundary-only integral equation method for nonlinear static and dynamic problems in general bodies. Theor. Appl. Mech. **27**, 13–38 (2002)
92. H. Wang, Q.H. Qin, Y.L. Kang, A new meshless method for steady-state heat conduction problems in anisotropic and inhomogeneous media. Arch. Appl. Mech. **74**(8), 563–579 (2005)
93. Z.-J. Fu, W. Chen, H.-T. Yang, Boundary particle method for Laplace transformed time fractional diffusion equations. J. Comput. Phys. **235**, 52–66 (2013)
94. S.P. Timoshenko, S. Woinowsky-Krieger, *Theory of Plates and Shells* (McGraw-Hill, New York, 1959)

95. D. Lesnic, L. Elliott, D.B. Ingham, An iterative boundary element method for solving numerically the Cauchy problem for the Laplace equation. Eng. Anal. Boundary Elem. **20**(2), 123–133 (1997)
96. L. Marin, Relaxation procedures for an iterative MFS algorithm for two-dimensional steady-state isotropic heat conduction Cauchy problems. Eng. Anal. Boundary Elem. **35**(3), 415–429 (2011)
97. J. Hadamard, *Lectures on cauchy problem in linear partial differential equations* (Yale University Press, New Haven, 1923)
98. P. Hansen, REGULARIZATION TOOLS: A Matlab package for analysis and solution of discrete ill-posed problems. Numer. Alg. **6**(1), 1–35 (1994)
99. A. Farcas, L. Elliott, D.B. Ingham, D. Lesnic, The dual reciprocity boundary element method for solving Cauchy problems associated to the Poisson equation. Eng. Anal. Boundary Elem. **27**(10), 955–962 (2003)

Chapter 5
Open Issues and Perspectives

Abstract The RBF collocation schemes provide attractive alternatives to traditional mesh-based methods in engineering and science community, particularly, for solving high dimensional, irregular, or moving boundary problems. This chapter discusses some open issues and gives a potential perspective of the RBF collocation methods.

It has been shown throughout this book that the RBF collocation schemes have great potential for solving a wide variety of engineering and science problems. They are integration-free, easy to implement, accurate, and do not require mesh generation. Therefore, the RBF collocation schemes seem attractive as an alternative to the traditional mesh-based methods, particularly, for solving high dimensional, irregular, or moving boundary problems.

Since the RBF collocation schemes are a class of relatively new numerical methods, there are many open issues, which are still under intensive investigation. The following topics are of particular interest

1. The theoretical foundation of the RBF collocation schemes for solving partial differential equations is yet to be established. For example, the Kansa method has been successfully applied to a wide variety of physical and engineering problems. However, the rigorous mathematical proof of the solvability and convergence of the Kansa method are still not available. Moreover, in the singular boundary method, the fundamental assumption is the existence of the origin intensity factors upon the singularities of the corresponding fundamental solutions at the coincident source-collocation nodes. The numerical experiments show that the origin intensity factors do exist and are in a finite value. However, the mathematical proof of their existence is still an open issue.

2. Most of the research in the RBF collocation schemes remains at the phase of the development and improvement, and verifies these methods to the benchmark examples. The next research focus should be turned to practical science and engineering applications.

3. Fast and efficient numerical simulation of large-scale science and engineering problems is a new trend of numerical methods. The undesired ill-conditioned and dense matrix is a major challenge in most of the RBF collocation schemes. It is a serious impediment to apply these methods to large-scale problems. In the last decade, great efforts have been made to alleviate this difficulty, and more research is expected in this regard.

   (a) Instead of global RBF schemes, localized RBFs are constructed to avoid the ill-conditioning matrix, and the corresponding localized approaches are successfully applied to the large-scale engineering problems with millions of interpolation points. Further advancement of the localized RBFs will continue to be a major research direction in the near future.

   (b) The iterative algorithm with preconditioned matrix is introduced to alleviate the difficulty of ill-conditioning, and helps the RBF collocation methods to solve the moderate engineering problems.

   (c) The fast matrix computation algorithms, such as, Fast Multipole Methods (FMM), H-matrix, pre-corrected Fast Fourier Transform (pFFT), and Adaptive Cross Ap-proximation (ACA), are implemented to alleviate the ill-conditioning dense matrix, and make the RBF methods more applicable to the large-scale engineering problems which often require millions of interpolation points. These fast matrix computation techniques can greatly reduce computing cost to $O(Nlog(N))$. Recently, the authors implemented the FFT-BKM and FFT-MFS to successfully solve PDEs with 200 million knots in a single desktop PC. Nevertheless, such fast solution techniques have drawbacks in that they lack the flexibility, e.g., basis function dependency, and require intensive programming. Some kernel-independent fast matrix algorithms should be developed to overcome this drawback.